UNIVERSITÀ POLITECNICA DELLE MARCHE

SCUOLA DI DOTTORATO DI RICERCA DELLA FACOLTÀ DI MEDICINA E CHIRURGIA

Curriculum: Scienze biomediche

XXXIV ciclo

DOWN-REGULATION OF PARAOXONASE-2 ENHANCES CHEMOSESITIVITY IN MELANOMA AND ORAL CANCER CELL LINES.

Dottorando

Dott.ssa
Salvucci Alessia

Relatore

Chiar.ma Prof.ssa
Emanuelli Monica

Correlatore

Chiar.mo Prof.
Sartini Davide

Coordinatore

Chiar.mo Prof.
Catassi Carlo

Triennio 2018-2021

Table of contents

2 Materials and methods

3 Results

Introduction

1.1 Oral squamous cell carcinoma

1.1.1 Epidemiology

Oral squamous cell carcinoma (OSCC) represents the most common malignant neoplasm in oral cancer, arising from the squamous cells of oral cavity. The high-risk oral areas are the floor of the mouth and the ventrolateral tongue, while the low-risk regions lie in the palatal mucosa and the tongue dorsum. In 2020, GLOBOCAN estimated a worldwide incidence of 377,713 cases (2% of total cases) and a mortality of 177,757 (1.8% of total cases) for oral cancer. OSCC is the 18th most common tumor in the world, but it reaches the 13th place when only male incidence is considered. In fact, oral cancer has a sex-related prevalence, but also a geographical-correlated distribution, with an incidence around 70% in low/medium human development index countries. It is highly frequent in South Central Asia (e.g. India, Sri Lanka, and Pakistan), as well as Melanesia (Papua New Guinea displays the highest incidence rate worldwide in both sexes). It is the leading cause of cancer death in Indian men but the incidence rates are high in Eastern and Western Europe and in Australia/New Zealand too (Figure 1) (1). The risk of developing oral cancer increases with age, and the majority of cases occurs after the age of 40 years, with a peak at 60 years. Whether or not young and old patients with OSCC have a different prognosis remains a controversial issue. In the last years, OSCC incidence has increased both in younger age groups and in women (2). The survival rate is strictly related to the time of diagnosis. When OSCC is confined to the primary site, the 5-years relative survival rate is about 85.1%, but it dramatically decreases to 66.8% and to 40.1% for tumors spread to regional lymph nodes and to distant sites, respectively. Despite a general decrease in the mortality rate for the majority of cancer types, because of the delayed detection, the OSCC overall 5-years survival rate has remained stable over time at approximately 50%. Finally, according to a recent analysis of Surveillance, Epidemiology, and End Results (SEER) database, the tongue is the most common OSCC subsite and is associated with higher mortality than forms in other subsites (e.g. floor of mouth, gingivae, and retro molar trigone) (3).

(a)

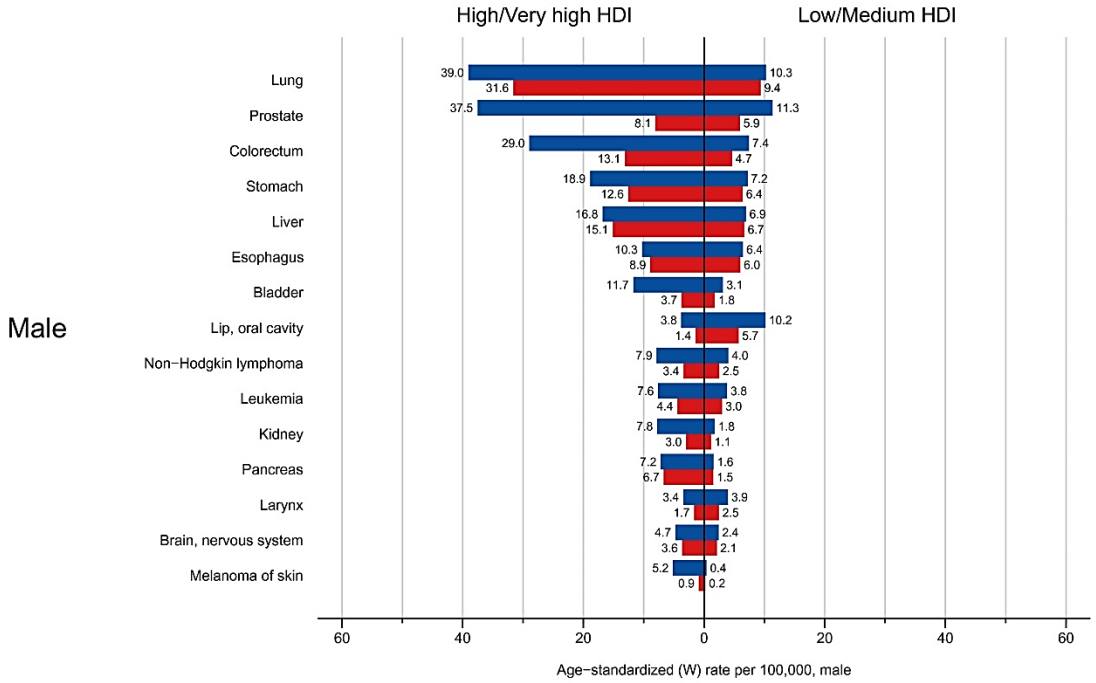

(b)

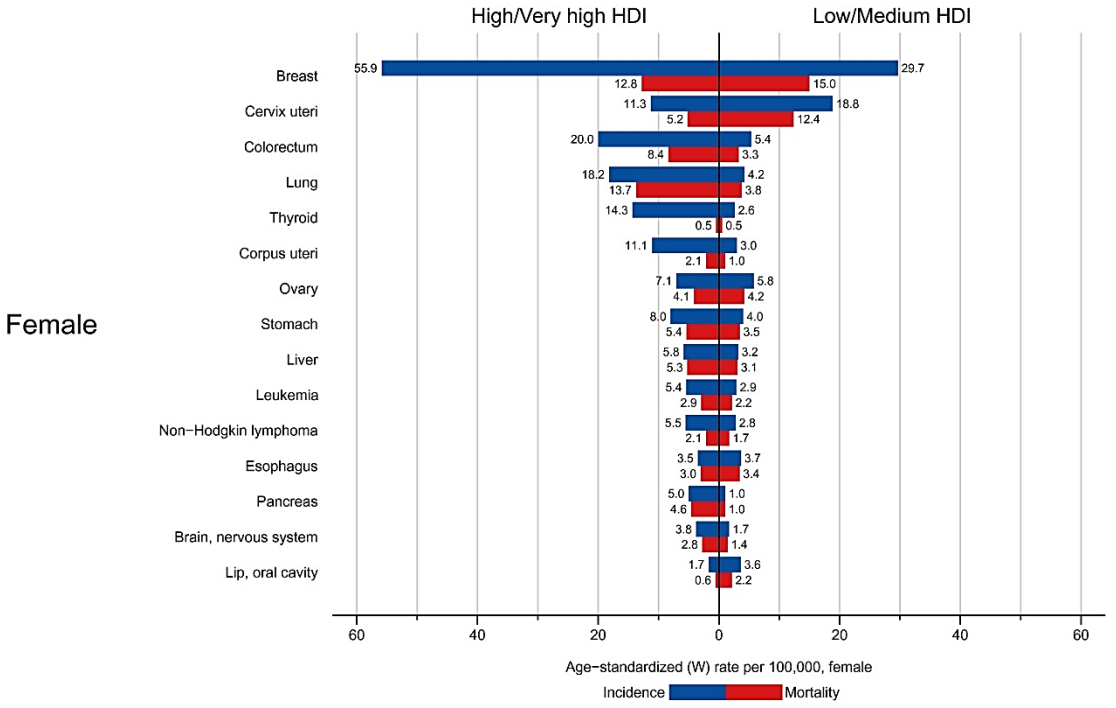

Figure 1. GLOBOCAN estimations of cancer incidence and mortality age-standardized rates in high/very high Human Development Index (HDI) countries versus low/medium HDI countries among men (a) and women (b) in 2020.

1.1.2 Risk factors

The aetiology of OSCC is strongly related to lifestyle habits and behaviour; hence, it is often a preventable disease. The main OSCC risk factors include tobacco smoking, alcohol abuse, human papillomavirus (HPV) infection, ultraviolet (UV) radiation, betel nut chewing, male gender, economic status, oral microbiome, dietary habits, and oral hygiene. Alcohol consumption and smoking are the major risk factors with a synergic effect when used together (4).

Tobacco smoking is responsible for about one-fourth of total oral cancer cases. The risk for developing oral cancer is 3 times higher in smokers when compared with non-smokers. In people who quit smoking four years before, the risk is 35% lower than in smokers, whereas in people who have stopped smoking for over 20 years the risk is the same of people who never smoked. However, involuntary smoke plays an important role too: non-smokers exposed to an environment rich in cigarette smoke have 87% higher risk than those never exposed. This is because cigarette smoke contains several carcinogens, such as nitrosamines, benzopyrenes and aromatic amines. These chemicals affect enzymatic and non-enzymatic antioxidant defence mechanisms promoting cancer. Elevated levels of free radicals of oxygen and nitrogen are found in pre-cancer and cancer lesions (5).

Alcohol consumption is also associated with an increased risk of oral cancer, in a dose- and time-dependent manner. Indeed, in subjects consuming four to five drinks daily, the risk is two- to threefold higher than in non-drinkers. Ethanol increases oral mucosa permeability, dissolves lipids components of the epithelium and is responsible for epithelial atrophy. It also affects salivary flow and hepatic ability to deal with toxic and mutagenic compounds (4).

Human papillomavirus 16 infection is classified as a risk factor and human papillomavirus 18, as a possible cause of oral cancer. In the oral cavity, the most common site of HPV infection is the base of tongue. Two virus-encoded proteins contribute to carcinogenesis: E6 protein promotes degradation of the tumor suppressor p53, whereas E7 facilitates the degradation of the tumor suppressor retinoblastoma protein, initiating finally a deregulation of the cell cycle control.

Ultraviolet radiation, mostly UVB, is involved in carcinogenesis, mainly in lip cancer that is the most sun-exposed area. UV rays are responsible for DNA damage, gene mutations, immunosuppression, oxidative stress, and inflammatory responses, promoting both tumorigenesis and development.

According to the International Agency for Research on Cancer (IARC) classification, betel nut chewing represents one of the main risk for the development of OSCC. Prevalence of betel quid usage among adults in South-East Asia reflects the

geographic distribution of OSCC cases. Several findings support that frequent and long-lasting betel quid consumption increases oral cancer risk. The production of carcinogenic nitrosamines, the generation of ROS due to auto-oxidation of polyphenols contained in areca nut and the alkaline pH are the main responsible for carcinogenicity (6).

Periodontal pathogenic bacteria have been recently associated with a higher risk for OSCC and, among them, *Fusobacterium* showed the most verified alterations in cancerous lesions. These bacteria contribute to an inflammatory state, secreting pro-inflammatory substances such as lipopolysaccharide (LPS), which may induce DNA damage in epithelial cells. Moreover, bacterial compositional differences are recorded among cancer patients, subjects with pre-cancer lesions and healthy individuals (7).

Approximately 10–15% of OSCC cases are attributable to low fruit and vegetable intake, even though the mechanisms of action and the relative roles of various micronutrients are not still completely clear. Probably the antioxidant and anti-carcinogenic properties of substances contained in plant foods counteract the OSCC development.

Lastly, several studies demonstrate a correlation between oral hygiene index and oral cancer, suggesting that poor hygienic conditions can increase OSCC risk (6).

1.1.3 Carcinogenesis

OSCC is a multistep invasive neoplasia that develops over many years involving highly complex multifactorial processes. It occurs when the growing accumulation of genetic and epigenetic changes in epithelial cells influence protein expression, thus altering a variety of signalling pathways. Starting from non-aberrant keratinocytes, an epithelial hyperplasia could precede dysplasia, carcinoma *in situ* and finally an invasive carcinoma, leading to the generation of distant metastases. OSCC can be preceded by potentially malignant disorders, such as oral leukoplakia, oral lichen planus, oral erythroplakia, and oral submucous fibrosis. These premalignant lesions are histologically detectable and can be clear signs of epithelial transformation. The key genetic alterations that initiate carcinogenesis occur in p53 (TP53), notch homolog 1, translocation-associated (Drosophila) (NOTCH1), epidermal growth factor receptor (EGFR), cyclin-dependent kinase inhibitor 2a (CDKN2A), signal transducer and activator of transcription 3 (STAT3), cyclin D1, and retinoblastoma (Rb) (6).

The tumor microenvironment (TME) of OSCC comprises cancer-associated fibroblasts (CAFs), immune cells and other supporting cells. Oncogenic changes in gene expression profiles determine events that lead to ROS accumulation, cytokines

overproduction and epithelial mesenchymal transition (EMT). This chronic inflammatory state is characterized by the presence of immunosuppressive cells with pro-tumor activity, such as regulatory T lymphocytes, M2 macrophages, N2 neutrophils and myeloid-derived suppressor cells. Cancer-associated fibroblasts are also some of the most critical elements of this environment contributing to proliferation, invasion, and metastasis. The suppression of the adaptive immune response is achieved through the overexpression of cytokines and interleukins, such as transforming growth factor-β (TGF-β), tumor necrosis factor-α (TNF-α), interleukin-1 (IL-1), and interleukin-8 (IL-8). Other factors secreted by tumor cells that promote EMT and spreading include matrix metalloproteinase 2 (MMP2), matrix metalloproteinase 9 (MMP9), matrix metalloproteinase 13 (MMP13), ROS, vascular endothelial growth factor (VEGF), chemokine (CXC motif) ligand 1 (CXCL1), chemokine (CXC motif) ligand 8 (CXCL8), platelet-derived growth factor (PDGF), E-cadherin, vimentin, and N-cadherin. This microenvironment permits an uncontrolled cell proliferation, invasion and migration properties (8).

1.1.4 Histopathological classification

Histopathological grading of OSCC, introduced by Broders, is merely based on differences in differentiation between tumors. Although later more complex grading systems were suggested, the current edition of Classification of Head and Neck Tumors drawn up by the World Health Organization (WHO) defines a simple grading system. Based on the Borders' criteria, tumors are classified in well, moderately, and poorly differentiated variants (GX-G3), even though grading alone does not correlate well with prognosis (9). In fact, several studies indicate minor or even no prognostic value of the WHO grading system. On the contrary, the new aforementioned grading systems comprehend features of the tumor per se (e.g. differentiation), but also tumor host interface (invasion patterns), and host reactions (inflammatory response). Therefore, they do not focus only on tumor per se, but also on the microenvironment including stroma and host responses. These multifactorial systems show a better prognostic value than the conventional WHO system, but further validation in large cohorts of OSCC would be desirable (10) (Table 1).

HISTOLOGIC GRADE	
GX	Can not be assessed
G1	Well differentiated
G2	Moderately differentiated
G3	Poorly differentiated

Table 1. Oral cancer histological grading.

1.1.5 Staging

OSCC is classified according to the tumor-node-metastasis (TNM) system of the Union for International Cancer Control (UICC) and of the American Joint Committee on Cancer (AJCC). This system is based on assessment of the size of the primary tumor (T), the involvement of loco-regional lymph nodes in terms of number, size and location (N) and the potential presence of distant metastasis (M) (Table 2). T, N and M are combined to form different stage groups (Table 3). The TNM classification is important for treatment planning, estimating risk of recurrence, and assessment of overall survival. The latest version was published in 2017 (8^{th} version) and introduced two major changes for OSCC, namely incorporation of the tumor depth of invasion (DOI) in the T stage and incorporation of extranodal extension (ENE) in the N stage. The current philosophy is to shift from the more traditional "population-based" approach to a more contemporary "personalized" approach incorporating biologic and molecular markers (10-12).

PRIMARY TUMOR (pT)	
TX	Primary tumor can not be assessed
TIS	Carcinoma in situ
T1	Tumor ≤ 2 cm with depth of invasion (DOI)* ≤ 5 mm
T2	Tumor ≤ 2 cm with DOI > 5 mm and ≤ 10 mm or tumor > 2 cm and ≤ 4 cm with DOI ≤ 10 mm
T3	Tumor > 2 cm and ≤ 4 cm with DOI > 10 mm or tumor > 4 cm with DOI ≤ 10 mm or any tumor
T4	Moderately advanced or very advanced local disease
-T4a	Moderately advanced disease. Tumor > 4 cm with DOI > 10 mm or tumor invades adjacent structures only (e.g. through cortical bone of the mandible or maxilla or involves the maxillary sinus or skin of the face)
-T4b	Very advanced disease. Tumor invades masticator space, pterygoid plates or skull base or encases the internal carotid artery

PATHOLOGICAL REGIONAL LYMPH NODES (pN)	
NX	Regional lymph nodes can not be assessed Carcinoma in situ
N0	No regional lymph node metastasis
N1	Metastasis in a single ipsilateral lymph node, ≤ 3 cm in greatest dimension and ENE-
N2	Metastasis in a single ipsilateral lymph node, ≤ 3 cm in greatest dimension and ENE+ or > 3 cm but ≤ 6 cm in greatest dimension and ENE-; or metastases in multiple ipsilateral lymph nodes, none > 6 cm in greatest dimension and ENE-; or in bilateral or contralateral lymph nodes(s), none > 6 cm in greatest dimension and ENE-
-N2a	Metastasis in either single ipsilateral lymph node that is ≤ 3 cm and ENE+ or single ipsilateral lymph node that is > 3 cm but ≤ 6 cm in greatest dimension and ENE-
-N2b	Metastasis in multiple ipsilateral lymph nodes, none > 6 cm in greatest dimension and ENE-
-N2c	Metastasis in bilateral or contralateral lymph node(s), none > 6 cm in greatest dimension and ENE-
N3	Metastasis in a lymph node > 6 cm in greatest dimension and ENE-; or in a single ipsilateral node > 3 cm in greatest dimension and ENE+; or multiple ipsilateral, contralateral or bilateral nodes, any with ENE+; or a single contralateral node of any size and ENE+
-N3a	Metastasis in a lymph node that is > 6 cm in greatest dimension and ENE-
-N3b	Metastasis in either single ipsilateral lymph node, > 3 cm and ENE+ or multiple ipsilateral, contralateral or bilateral lymph nodes, any with ENE+ or single contralateral lymph node of any size and ENE+

DISTANT METASTASIS (M)	
M0	No distant metastasis
M1	Distant metastasis

Table 2. Oral cancer TNM staging.

AJCC PROGNOSTIC STAGE			
Stage 0	TIS	N0	M0
Stage I	T1	N0	M0
Stage II	T2	N0	M0
Stage III	T3	N0	M0
	T1-3	N1	M0
Stage IVA	T4	N0-1	M0
	T1-4a	N2	M0
Stage IVB	Any T	N3	M0
	T4b	Any N	M0
Stage IVC	Any T	Any N	M1

Table 3. Oral cancer stage groups based on T, N, and M.

1.1.6 Clinical manifestation and diagnosis

Clinical manifestations vary depending on the stage and primary site of the tumor. In oral cancer patients, the most common symptom is pain. Although it represents 30-40% of the main complaints, it arises only when the lesions have reached a remarkable size. In fact, early carcinomas remain unnoticed because they are often asymptomatic. In general, symptoms may vary from mild discomfort to severe pain, especially on the tongue where the pain can arise earlier. Other symptoms include ear pain, bleeding, mobility of teeth, problems in breathing, difficulty in speech, dysphagia and problems using prosthesis, trismus, and paraesthesia (13).

Hence, regardless of the accessibility of the oral cavity during clinical examination, oral cancer is usually diagnosed in advanced stages, dramatically decreasing the chances of survival, despite the therapeutic strategies. For this reason clinicians should always make an accurate clinical examination of the oral mucosa; in fact, changes in surface texture, loss of surface integrity, colour, and size may be suspicious for oral cancer or premalignant lesions. Together with the oral cavity, it is recommended to palpate the lymphoid tissue of the neck (cervical lymph nodes) to look for neck masses, which can represent metastases. Although its high sensitivity, clinical inspection has a low grade of specificity because of its limited ability to differentiate between benign and precancerous lesions, hence it must be accompanied by a biopsy and histopathological examination that are the gold standard to establish the correct diagnosis. Unfortunately, these techniques are time-

consuming and surgery may be associated with adverse reactions or postoperative complications. All these reasons lead clinicians to apply novel adjunctive non-invasive imaging techniques, able to add information to shorten the time for biopsy and guide it by identifying and targeting only highly suspicious lesions. Among them, the most used techniques are vital and virtual staining, narrow-band imaging (NBI), optical coherence tomography (OCT), cross-sectional computed tomography (CT), nuclear magnetic resonance imaging (RMN), high-frequency ultrasonography (HF-US), and *in vivo* reflectance confocal microscopy (RCM). Briefly, the main vital stainings are toluidine blue (TB) and Lugol's iodine. The first one, on the basis of its acidophilic properties, selectively stains tissues rich in nucleic acids such as neoplastic/highly dysplastic lesions, whereas the second one marks the healthy tissues reacting with cytoplasmic glycogen whose normal cells are rich of. The tissue autofluorescence (AF), during the virtual staining, is based on the detection of the intensity of the fluorescence that decreases with the progress of the dysplasia. Through the narrow-band imaging clinicians are able to distinguish tumor vascular patterns from other non-neoplastic affections, whereas by optical coherence tomography they can evaluate the macroscopic characteristics of epithelial, sub-epithelial, and basement membrane structures, with resolutions close to those of microscopy. Both cross-sectional computed tomography and magnetic resonance imaging are robust tools to clarify submucosal spread and involvement of deep layers: the first one permits an accurate detection of incipient cortical bone invasion, whereas the second technique is preferred in the evaluation of medullary bone involvement and in delineating tumor borders in soft tissues. High-frequency ultrasound is useful in determining the interface between tumor tissue and the surrounding myo-architecture, although the use of this tool is less frequent. Finally, the *in vivo* confocal microscopy allows performing a proper virtual biopsy of tissues in their living context, offering real-time cytological and histological details, without complications, such as anaesthesia, surgery, or adverse reactions (14) (Figure 2).

Recently, several studies have focused on the analysis of saliva for the detection of OSCC diagnostic and/or prognostic biomarkers. This new liquid biopsy is very attractive due to its proximity to cancer cells, accessibility, non-invasive collection, and cost-effective sampling. So far, potential biomarkers reporting on proteomic or metabolic activity, as well as on genomic and epigenetic alterations of malignant cells have been identified, thus favouring the early detection and diagnosis of a possible pathological state. The most promising biomarkers include cytokines, DNA and RNA molecules, circulating and tissue-derived cells, and extracellular vesicles. Although only at the beginning, salivary liquid biopsy seems to have a great potential for OSCC

diagnosis and management, improving prognosis, but also therapy and follow-up (15, 16).

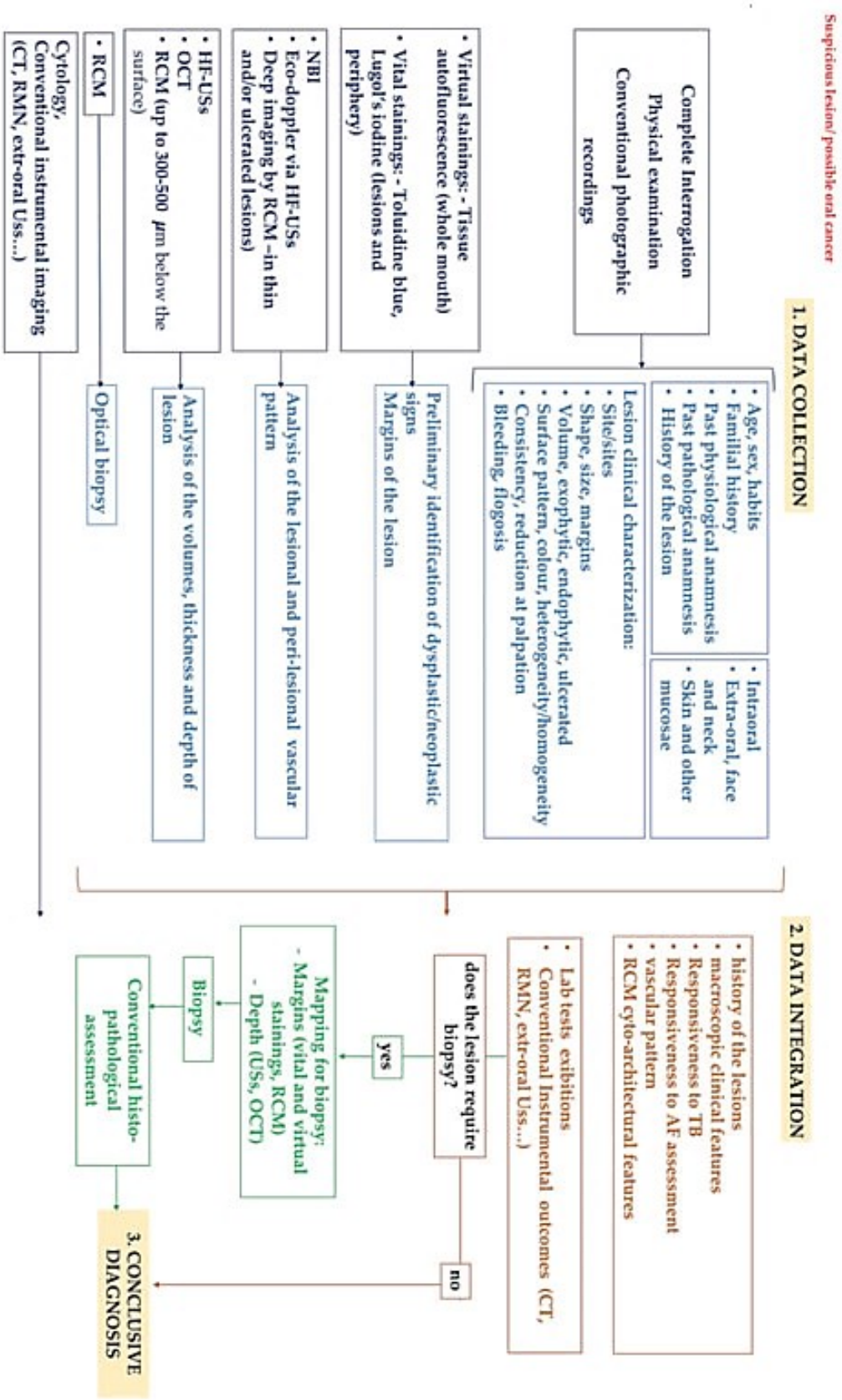

Figure 2. Clinical flowchart for the identification and the evaluation of oral cancer.

1.1.7 Therapeutic strategies

Because of poor prognosis for patients with advanced OSCC, early diagnosis and treatment are the key elements to improve the overall survival. Early detection is critical for a more efficient treatment and prevention and for avoiding extensive surgical resections, necessary in advanced stages. Moreover, it is essential for patients to limit the recovery period and the impact of side effects including facial disfigurement and problems in speech, swallowing, breathing, drinking, and eating that they can face after that. The mainstays of OSCC treatment are surgery, chemotherapy, radiotherapy or a combination of these modalities, depending mainly on location and stage of tumor and patient co-morbidity factors.

Most patients with early stage disease are treated with a single modality therapy that can be surgery or radiotherapy. Surgery is the main treatment (in resectable tumors, surgery is superior to all alternative therapies) and can be supported by lymph node dissection to check cancer spread. Radiation can be used instead of surgery, as the main treatment for unresectable diseases, high operative risk due to patient poor performance status, or recurrent diseases. If the neoplasm is detected at advanced stage, surgery is followed by adjuvant radiation or chemoradiotherapy. For unresectable cases, concurrent chemoradiotherapy is the treatment of choice. Patients with recurrent and metastatic disease are generally treated with palliative intent. The most common chemotherapeutics are cisplatin, carboplatin, 5-fluorouracil, paclitaxel and docetaxel. The combinational treatment cisplatin and 5-fluorouracil shows a higher antitumor potency and a low level of toxicity (4).

Cisplatin (cis-Diammineplatinum(II) dichloride or CDDP) consists platinum bound to two different types of ligands, a stable amine group and a readily exchangeable or leaving chloride (Figure 3a). CDDP enters cells, by diffusion and/or by transporter proteins located in the membrane, where its chlorine ions are replaced with two water molecules forming the active and positively charged species that can covalently bind to DNA. The most reactive regions in DNA are the N7 atoms in the imidazole rings of adenine and guanine bases. Binding to DNA, it produces adducts in three ways: monoadducts, intrastrand and interstrand crosslinks. Monoadduct occurs when cisplatin loses a water molecule, but most of them (90%) react to form crosslinks. A large part of the crosslinks is intrastrand between two guanine molecules, while their advanced forms are observed as crosslinks between chains. Its antitumoral activity is due to the disruption of the double helix structure, thus influencing cell cycle and replication arrests, apoptosis, transcription inhibition, and DNA repair. Moreover, cisplatin is responsible for changes in cytoskeletal pattern of tumor cells binding to free sulfhydryl groups in tubulin and thus causing a partial depolymerisation of

microtubules. On the other hand, aquated cisplatin also binds to cytoplasmic molecules, including reduced glutathione (GSH) and metallothionein (MT), which results in the generation of ROS that also trigger mitochondrial outer membrane permeabilization (MOMP) and DNA damages. Resistance and toxicity are the major problems that limit the usage of cisplatin in clinics. The main resistance mechanisms of cisplatin lead to overexpression of copper transporter 1 (CTR1) and P-glycoprotein, transmembrane proteins that mediate platinum drugs transports. Cisplatin concentration in the proximal tubular epithelial cells can reach five times more cisplatin concentration than in the serum. Hence, nephrotoxicity represents the most frequent dose-limiting toxicity correlated with cisplatin treatment, followed by ototoxicity (17, 18).

5-fluorouracil (5-FU) is an analogue of uracil with a fluorine atom at the C5 position in place of hydrogen (Figure 3b). It rapidly enters the cells, using the same facilitated transport mechanism as uracil, where it is converted to several active metabolites. Up to 80% of administrated 5-FU is broken down by dihydropyrimidine dehydrogenase in the liver. 5-FU exerts its anticancer effects through inhibition of thymidylate synthase (TS) and incorporation of its metabolites into RNA and DNA. Forming a stable ternary complex with TS, 5-FU blocks the *de novo* source of thymidylate, which is necessary for DNA replication and repair. In addition, TS inhibition results in accumulation of dUTP and 5-FU misincorporations that eventually lead to DNA strand breaks and cell death. Moreover, 5-FU metabolite is extensively incorporated in RNA, disrupting its normal processing and function. DNA/RNA damage repair by mismatch repair (MMR) and base excision repair (BER) is one of the acquired tools used by cancer cells to resist 5-FU. Another important resistance mechanism exerted by OSCC cells is inhibition of apoptosis. 5-FU treatment can be associated with the long-term side effects of cognitive impairment since its ability to enter the brain by passive diffusion (18, 19).

(a) (b)

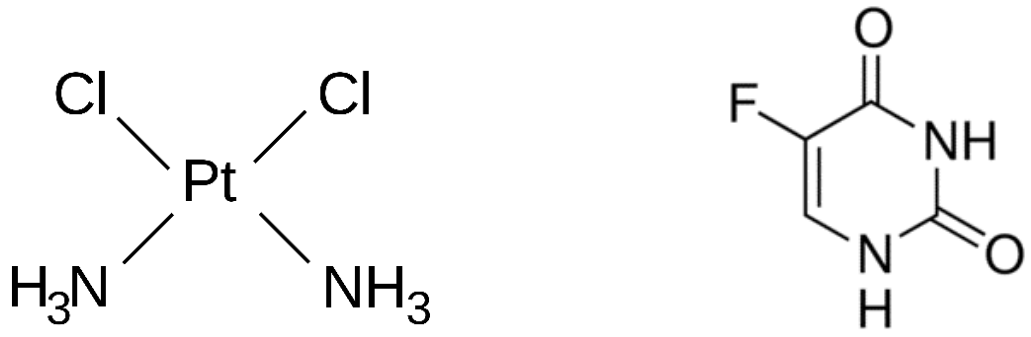

Figure 3. Chemical structure of cisplatin (a) and 5-fluorouracil (b).

Targeted therapy and immunotherapy may be other options, alone or in combination with chemo- or radiotherapy. Cetuximab is a chimeric (mouse/human) monoclonal antibody targeting the EGFR protein that is upregulated in most of OSCC cases. Cetuximab prevents the activation of KRAS gene, that promotes proliferation and survival of cancer cells, and pro-angiogenic factors. Use of Cetuximab is approved both in combination with radiotherapy, for locally or regionally advanced disease, and as a single agent for recurrent or metastatic diseases, where platinum-based therapy has failed. More recently, studies have demonstrated the responsiveness of head and neck squamous cell carcinomas to checkpoint inhibitor-based immunotherapies. Hence, the use of anti-PD1 therapies (pembrolizumab and nivolumab) has been approved for the treatment of recurrent and metastatic OSCC in patients who experienced disease progression after or during platinum-based chemotherapy (20).

1.2 Skin cancers

1.2.1 Epidemiology

Skin cancers represent a heterogeneous group of neoplasms. They are primarily divided into cutaneous melanoma and non-melanoma skin cancers (NMSCs). Melanoma originates from malignant transformation of melanocytes, whereas NMSCs from keratinocytes. NMSCs include basal cell carcinoma (BCC) and squamous cell carcinoma (SCC), as the major subtypes. Skin cancers are a pre-eminent global public health problem, representing the most common malignancies in humans (21, 22).

Cutaneous melanoma is the most aggressive form of skin neoplasm and its incidence is rising. Indeed, although accounting for only 5% of all skin cancers, it is responsible for more than 75% of deaths associated with these tumors. The last GLOBOCAN version (2020) estimated 324,635 new cases (1.7% of all sites) responsible for 57,043 deaths (0.6% of all sites) globally (Figure 4). Incidence rates of malignant melanoma in Whites are five times higher than in Hispanics and 20 times higher than in African Americans. It shows a considerable variation in incidence worldwide between continents and countries, with Australian patients having the highest rates of diagnosis followed by white-skinned United States people versus the lowest rates in Central Asia. European populations have less incidence rate, but it varies considerably based on latitude. Among European countries, Scandinavian peninsula, Switzerland, and Great Britain record the highest rates, whereas Balkan countries, Moldova, and Bosnia and Herzegovina the lowest ones, although the difference might also be attributed, in part, to the weaknesses and the discrepancies of national registration systems. Incidence of cutaneous melanoma is growing worldwide at a fast and dramatic rate. The most alarming element is the median age at diagnosis that for cutaneous melanoma is just 57 years. With regard to gender, females aged 20-24 years are more likely to be diagnosed with malignant melanoma than males (4:10); however, as age increases, males become much more likely to develop melanoma (17:10, aged greater than 65 years). Moreover, men have poorer clinical outcomes than their female counterparts owing to higher rates of disease recurrence, disease progression, and mortality. Melanoma can occur in any tissues that contain melanocytes but most of them arise on the skin surface (1, 23).

(a)

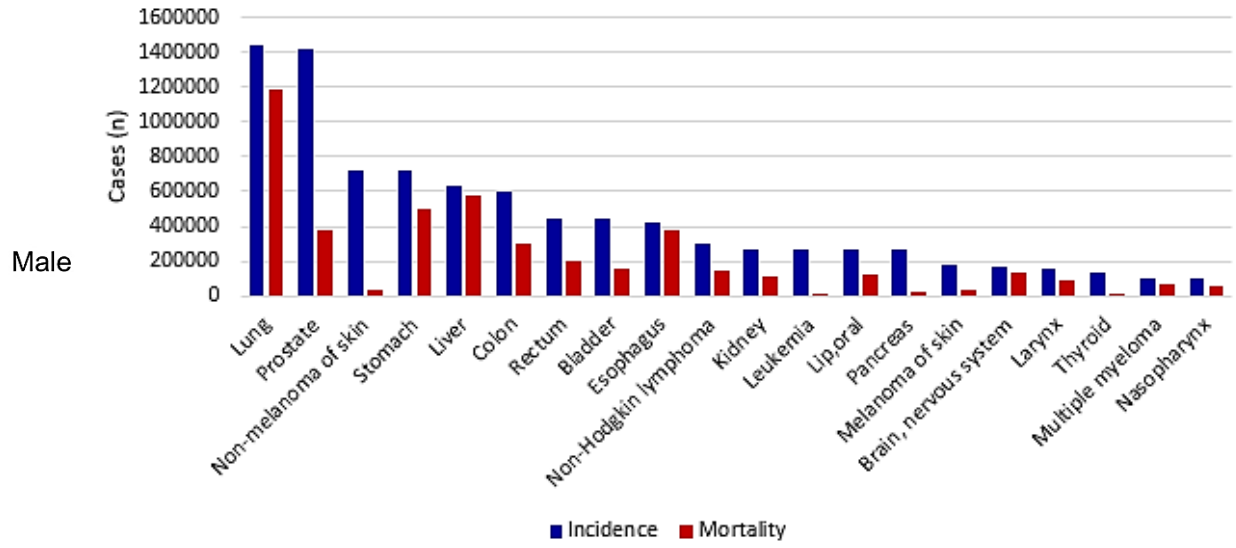

(b)

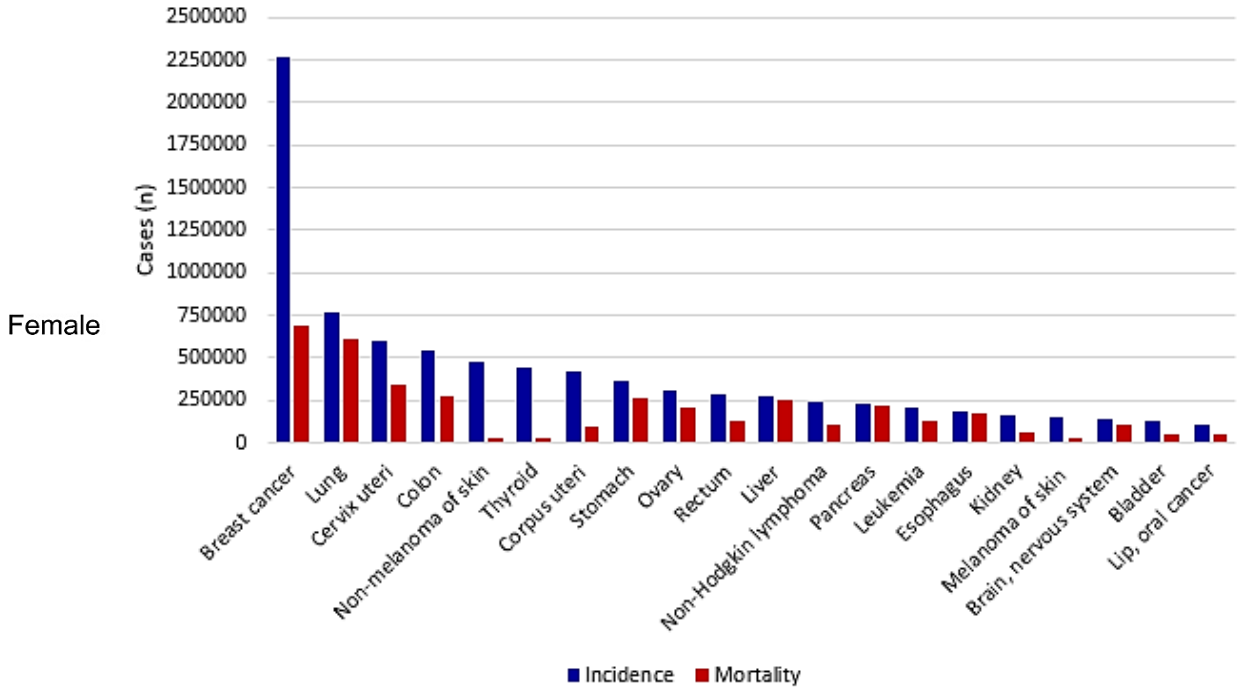

Figure 4. GLOBOCAN worldwide estimations of the 20 most common cancers incidence and mortality expressed as number of cases among men (a) and women (b) in 2020. Incidence excludes BCC, whereas mortality inclueds all types of non-melanoma skin cancer.

The actual number of NMSCs is difficult to estimate because BCC and SCC cases are not required to be reported to national cancer registries. NMSC is one of the most prevalent tumor but the majority is highly curable. In 2020, GLOBOCAN estimated a worldwide incidence of 1,198,073 cases (6.2% of total cases) excluding BCC and a mortality of 63,731 cases (0.6% of total cases). However, despite its low metastatic potential and mortality rate, NMSC is associated with a remarkable morbidity and substantial cost. Incidence rates are approximately 2 times higher among men than among women. Also regarding NMSC, there is a geographical distribution of cases. In fact, NMSC is the most common type of cancer in Australia and New Zealand in both sexes and in the United States among men. In this incidence rank, Europe is in the second place, followed by the United States. The overall incidence in Australia has been decreasing since 2005 (−0.7% per year) thanks to successful mass media campaigns, policies, and access to quality sun-protection products. Incidence rates increased until the early 2010s in New Zealand, but they are expected to decrease in few years reflecting birth cohort effects in younger generations. In the United States, after introduction of new therapies, a rapid decline in death rates has been reported since 2013 (Figure 5). Risk for development of a keratinocyte carcinoma increases with age too. BCC is the most common subtype with approximately 75% of cases, but it is a slow growing and locally invasive form. Approximately 80% of all BCCs occurs on the head and neck and clinical diagnosis is straightforward. In men, incidence is higher than in women and it increases with age and proximity to the equator. The lifetime risk of developing BCC is 30% and among diagnosed individuals, approximately 40% develops another lesion within 5 years. SCC is the second most common form of NMSC (20% of cases). The overall metastatic rate is estimated to be 3% to 10%, depending on both tumor characteristics (location, cell differentiation, and size) and underlying medical conditions. SCC is mostly associated with an advancing age; indeed, around 80% of cases occurs in people aged 60 years and above. Therefore, the average age at diagnosis is mid-sixth decade of life but in regions such as Australia, Florida, New Zealand, and California is lower (20-30 years). As BCC, SCC has a predilection for males (1, 24).

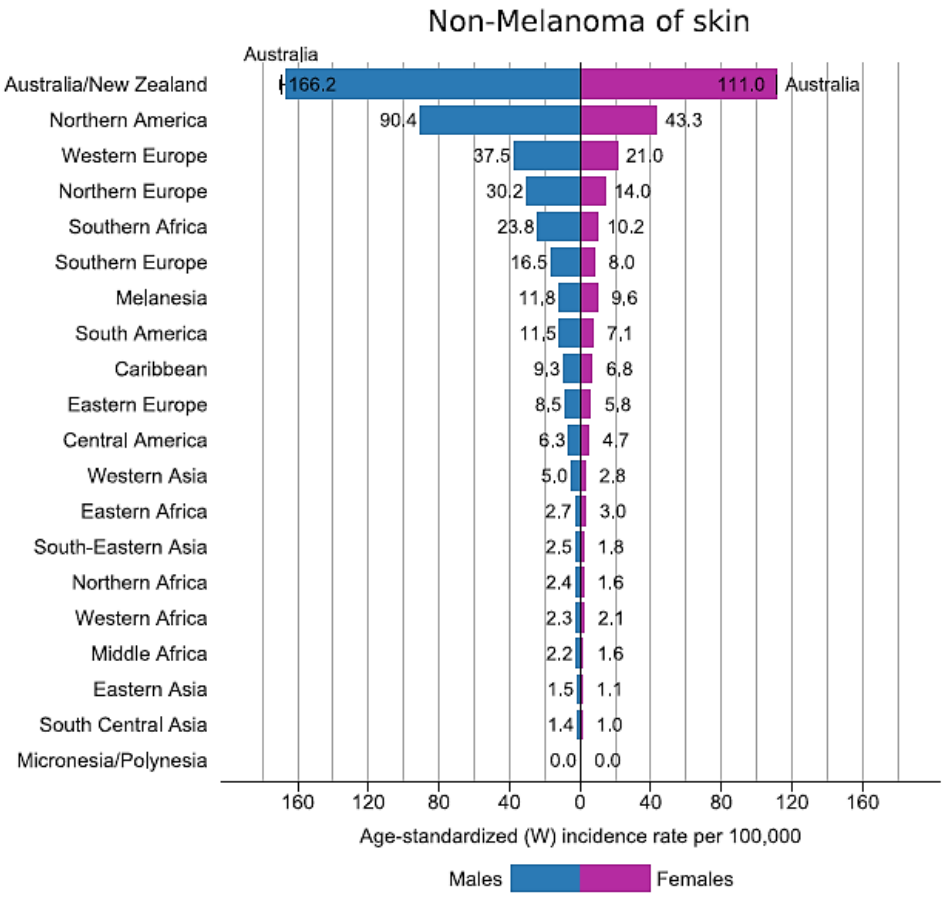

Figure 5. Region-specific incidence rates for non-melanoma skin cancer (excluding BCC) estimated by GLOBOCAN. Rates are shown in descending order of the world age-standardized rate among men.

1.2.2 Risk factors

A plethora of risk factors has been identified with skin cancer oncogenesis, most of them can be clearly categorized into either hereditary or environmental factors. The main endogenous factors include phototype, skin and eye colour, number of melanocytic nevi, presence of dysplastic nevi, and individual or family history of skin cancer, whereas among exogenous factors, including lifestyle behaviours, type and degree of cumulative sun exposure, history of sunburn, and sun protection behaviour are listed. Although the main risk factors are well known, it remains unclear how they interact to contribute to the development of malignancy.

Among researchers, there is no doubt that solar UV radiation (UVR) exposure is the chief environmental risk factor for developing skin cancer. There are mainly two types of UVR rays: ultraviolet A and ultraviolet B. The first ones can pass deeper into the skin, thus causing deeper damage than UVB, responsible for erythema or sunburn. UV rays produce DNA damage, gene mutations, immunosuppression, oxidative stress, and inflammatory responses, all of which play a pivotal role in photo aging of the skin

and in skin cancer genesis. UVB rays directly damage DNA, while UVA damage is indirect, mediated by free radical formation and disruption of cell membrane integrity. Therefore, UVR is not only responsible for the onset of tumorigenesis, inducing mutations in tumor suppressor genes, but also for cancer development. Thus, there is a positive correlation between cumulative and chronic sun exposure and skin cancer. Timing of sun exposure seems to be a key factor too; a higher risk is associated with an exposure from 10a.m. to 2p.m. The geographic variation in incidence of NMSC is associated with ambient sunlight intensity, providing further strong evidence for the relation between them. Moreover, researchers demonstrated that reducing sun exposure during childhood and adolescence through sun-protective behaviours could decrease the lifetime risk of developing NMSC, by as much as 78%. Finally, total and occupational sun exposure is correlated with the development of SCC, whereas non-occupational or recreational sun exposure with BCC and cutaneous melanoma. Recently, indoor tanning has become a common source of UVR, especially among young people. A study reveals that tanning bed use is associated with a 1.5-fold increase in the risk of BCC and a 2.5-fold increase in the risk of SCC. Results from a meta-analysis suggest that tanning bed use raises the probability of developing skin cancer by 20% arriving to 87% if exposure is before the age of 35 (22, 23).

Skin colour or pigmentation is a non-modifiable risk factor influencing the likelihood of malignant transformation. Thus, people with fair skin, freckles, light coloured eyes and hair, and an inability to tan, have an increased risk. In the 1980s, Fitzpatrick defined a method to classify individual skin types in four categories according to skin colour, burning and tanning responses to UVR exposure. The categories range from type I (always burn, never tan) to type IV (never burn, tan easily), being Fitzpatrick type inversely correlated to the risk of skin cancer (25).

Genetic factors seem to be involved in risk developing malignancy. Approximately 8% to 10% of patients with malignant melanoma have a first-degree relative with malignancy. Familial development of melanoma is passed down in a clear autosomal dominant inheritance pattern in “clusters,” with multiple family members being diagnosed in more than one generation (26).

The presence of atypical and multiple nevi is a sign of higher likelihood of developing skin cancer. An atypical nevus is a dysplasia underlying a benign congenital or acquired nevus. Approximately 29-49% of nonhereditary cases occur in the presence of a pre-existing dysplastic nevus whereas an individual carrying dysplastic nevi and with two family members with malignant melanoma has a 500-fold increase in risk. Families with multiple cases of malignant melanoma often exhibit the dysplastic nevus syndrome, a syndrome characterized by multiple atypical moles that continue to appear in adulthood. In general, having a large number of cutaneous nevi or having larger sized (>5 mm) or giant (>20 mm) ones are all factors associated with a higher risk (27).

Melanoma and NMSC are more common in the immunocompromised population. Xeroderma pigmentosum is a rare autosomal recessive disease that decreases the ability of skin to repair DNA damage caused by sun exposure, due to a deficiency in DNA excision and post-replication repair. As a result, people affected by xeroderma pigmentosum develop skin cancer at an early age, therefore the median age of NMSC onset is eight years and patients aged <20 years have a >1000-fold increased risk for developing SCC. Albinism, a congenital defect in melanin formation, is a further example (28). An individual with basal cell nevus syndrome, a rare genetic condition affecting skin, endocrine, central nervous, and skeletal systems, often develops numerous BCCs over lifetime. The median onset is in puberty and it occurs on body areas not generally exposed to UVR, such as the palms of the hands and soles of the feet (23, 24). Concurrent diseases and treatment can also influence the overall risk of skin cancer. For example, psoriasis treatment consists of taking Psolaren drug followed by skin exposure to long-wave UVA. This combination treatment can increase the risk of developing SCC, and potentially other forms of skin cancer. Subjects who have received radiation treatment for skin conditions, such as eczema and acne, or for solid tumor reduction, such as breast or prostate cancer, may have an increased risk of skin cancer, particularly BCC (23). Infection with certain types of human papilloma virus, particularly HPV6 and HPV11, that affect the anal or genital area, increases verrucous cutaneous SCC (29).
Incidence of skin cancer in transplant patients is much higher than in the general population, mainly due to medically induced immunosuppression. In white patients who undergo transplant, the risk of SCC increases from 65- to 250-fold and the risk of BCC from 10- to 16-fold. Moreover, in this population, SCC tends to grow up more rapidly resulting in higher mortality. These dramatic data can be limited providing quality patient education and dermatologic screening campaigns (24).

1.2.3 Carcinogenesis and histological features

Melanoma is an aggressive malignant neoplasm derived from melanocytes that are in the basal layer of the epidermis. When exposed to UV light, they accumulate genetic mutations that activate oncogenes, repress tumor suppressor genes, and impair DNA repair, leading to uncontrolled melanocytes proliferation and ultimately melanoma. There are four major subtypes of invasive cutaneous melanoma that are grouped for their distinct histologic patterns and clinicopathological characteristics:
- superficial spreading melanoma is the most common subtype (46% of cases). It occurs frequently on the backs in men and the lower extremities in women. At the beginning, it grows radially and then vertically into deeper tissue layers. It appears as a pigmented macule with irregular borders that may progressively evolve into a papule or plaque, as far as invasion occurs;

- lentigo maligna melanoma is the second most common subtype. It is mainly located on sun-exposed areas, as the face of elderly people. It presents as a flat, pigmented, irregular-bordered, and asymmetric macule that is described histologically as a lentiginous proliferation of atypical spindle melanocytes at the dermo-epidermal junction with invasion into the papillary dermis;
- nodular melanoma, accounting for around 16% of cases, is an aggressive and vertically growing melanoma. It usually appears as darkly pigmented pedunculated or polypoid nodules;
- acral lentiginous melanoma, the least common subtype, mainly locates in palmar, plantar, and subungual regions. It is a slow-growing macule/plaque or nodule characterized by a proliferation of atypical, not pigmented, spindle melanocytes throughout the dermis.

Finally, rare histological subtypes of melanoma are desmoplastic melanoma, Spitz melanoma, mucosal melanoma, melanoma arising in a congenital nevus, melanoma arising in blue nevus, uveal melanoma (Table 4) (21, 30).

The initiation and progression of cutaneous melanoma are finely driven by specific genomic alterations. Most of mutations occur in somatic tissues leading to a uncontrolled division whereas germline mutations are less common, but they can pass from one generation to the next, resulting in the so-called hereditary or familial melanomas. The two most frequent activating and mutually exclusive mutations occur in B-Raf proto-oncogene, serine/threonine kinase domain (BRAF) and in neuroblastoma RAS viral oncogene homolog (NRAS) gene, with a frequency of 50-70% and 15-30%, respectively. Specific classes of cutaneous melanoma have been associated to specific genetic alterations. In particular, low-cumulative sun-damaged melanoma located on the trunk or extremities typically carries BRAF mutations, whereas melanoma in chronically sun-exposed skin on the head and neck region shows NRAS and/or other RAS mutations, while non sun-related melanomas carry mast/stem cell growth factor receptor (C-KIT) mutations or amplifications (30).

In physiological conditions, keratinocytes tightly control melanocytes proliferation and activity, through paracrine interactions, and cell-cell contacts, in order to maintain a constant keratinocyte/melanocyte ratio. Stromal fibroblasts, located in the dermis, keep under control melanocyte growth and function too, not through a physical interaction but by releasing soluble factors. During malignant transformation, the structural and functional organization is gradually rearranged. Malignant melanocytes change their location moving vertically up into the epidermidis and then into the dermis. The shift from E-cadherin to N-cadherin expression allows them to escape from keratinocyte control and interact with other N-cadherin expressing cells, such as fibroblasts and endothelial cells, located in the

underlying dermis. The formation of these new cell-cell contacts between malignant melanocytes and fibroblasts facilitates melanoma cell survival and progression. At this time, melanoma cells are able to invade and metastasize to distant organs. In cancer, human fibroblasts, the predominant stromal cell type of the connective tissue, acquire a constitutive activated phenotype resistant to apoptotic stimuli, differentiating into the so-called CAFs with tumor-promoting capability. Extracellular acidification of TME and peritumoral area, and the increased number of tumor endothelial cells, are other important features characterizing melanoma (31).

MAJOR MELANOMA SUBTYPES	MINOR MELANOMA SUBTYPES
Superficial spreading melanoma	Desmoplastic melanoma
Lentigo maligna melanoma	Spitz melanoma
Nodular melanoma	Mucosal melanoma
Acral lentiginous melanoma	Melanoma arising in a congenital nevus
	Melanoma arising in blue nevus
	Uveal melanoma

Table 4. Classification of melanoma subtypes into frequency-based categories.

As already mentioned, NMSCs originate from keratinized epithelial cells and they are mainly divided into two subgroups: BCC and SCC. Other NMSCs include cutaneous lymphoma, Kaposi's sarcoma, Merkel cell carcinoma, and other sarcomas. Together, these account for <1% of NMSCs.

BCC derives from the basal layer of epidermidis and its appendages. It appears without precursor lesions mostly in sun-exposed areas, such as face and backs of hands, due to the accumulation of cell mutations induced by UVR. It presents as a small papule that may enlarge slowly over months or years, as it is a slow-growing cancer that rarely metastasizes. It may be difficult to distinguish this tumor from benign growths and thus patients often mistake for pimples. Metastasis is rare but local growth can be highly destructive. BCC can be further divided into different subtypes:

- nodular basal cell carcinoma makes up 60% of cases. It most commonly presents on the face as a pearly, well-defined, translucent papule that may have ulceration;
- superficial basal cell carcinoma typically appears on the trunk as a pink, scaly, thin plaque that can mimic eczema or psoriasis. The border is usually lined with translucent papules and the centre may appear atrophic;
- infundibolocystic basal cell carcinoma is a well-circumscribed pearly papule com-

monly on the head and neck of elderly subjects;
- fibroepithelial basal cell carcinoma appears as a skin-coloured or erythematous sessile plaque or pedunculated papulonodule with a predilection for the trunk;
- morpheaform basal cell carcinoma occurs approximately 5-10% of cases and has a higher rate of recurrence and perineural invasion. It presents as a depressed and waxy plaque with irregular borders, often accompanied by ulceration;
- infiltrative basal cell carcinoma is a poorly defined, indurated, flat or depressed white, yellow, or pale pink coloured plaque associated with higher rates of perineural invasion and recurrence;
- micronodular basal cell carcinoma looks like a erythematous macule or thin papule/plaque composed by multiple small aggregates of basaloid cells within the dermis;
- basosquamous basal cell carcinoma, representing less than 2% of cases, histologically consists of BCC and SCC in different areas with a transition zone of mixed differentiation and its behaviour is also more similar to SCC (Table 5).
Mutated keratinocyte progenitor cells, predominantly UVB-induced, develop into BCC. Nearly all BCCs show constitutive activation of Hedgehog signalling pathway, critical for cell cycle regulation and in half of BCC cases TP53 inactivation is demonstrated. Surprisingly, sporadic BCCs show the greatest number of mutations of any human cancers, perhaps because the ubiquitous nature of the primary source of mutagenesis is UV light (32, 33).

LOW-RISK BCC SUBTYPES	HIGH-RISK BCC SUBTYPES
Nodular basal cell carcinoma	Morpheaform basal cell carcinoma
Superficial basal cell carcinoma	Infiltrative basal cell carcinoma
Infundibolocystic basal cell carcinoma	Micronodular basal cell carcinoma
Fibroepithelial basal cell carcinoma	Basosquamous basal cell carcinoma

Table 5. Classification of BCC subtypes into risk-based categories.

SCC arises from uncontrolled proliferation of epidermal keratinocytes that invade the dermis. SCC cases are usually preceded by premalignant lesions, most of which are actinic keratosis. Incidence is estimated to be around 25% among all NMSC cases and, similarly to BCC, it is mainly caused by UVR. Local tissue destruction may be extensive, and metastases via lymphatic or haematogenous spread may occur in advanced stages. The overall metastatic rate is 3% to 10%, depending on tumor location,

underlying medical conditions, cell differentiation, and size. SCCs near the ears, the vermilion border of the lip, and in scars are more likely to metastasize, thus requiring extensive surgery. Clinical manifestation is highly variable and includes papules, plaques, or nodules, and smooth, hyperkeratotic, crusty, or erosive lesions. Although the rich diversity of SCC cases, a clear and precise classification has not been drawn up so far. In 2007, Cassarino and colleagues proposed a new classification system based on aggressiveness and metastatic behaviour of each SCC variant. They divided them into three categories (low, intermediate and high risk) and one of indeterminate behaviour, that includes rare forms whose data at disposal are insufficient to classify them with certainty (signet ring cell SCC, follicular SCC, papillary SCC, SCC arising from adnexal cysts, squamoid eccrine ductal carcinoma, pigmented SCC and clear-cell SCC). Briefly, all the subtypes, arranged in ascending order of risk and excluding the rare forms, are described:

- squamous cell carcinoma arising from actinic keratosis has a low malignant potential. The rate of transformation of an actinic keratosis to an invasive SCC is likely about 10% per year;
- verrucous and HPV-related squamous cell carcinomas belong to the low risk category. The verrucous carcinoma appears in the oral mucosa and larynx, anogenital region, plantar surface and, less frequently, other cutaneous sites with a verrucous appearance. More than 50% of HPV-related cases are associated with HPV6 and HPV11 infections;
- spindle cell squamous cell carcinoma is an uncommon tumor which almost always arises on sun-damaged skin or at sites of prior radiation exposure. Clinically, it presents as a raised or exophytic nodule with spontaneous bleeding and central ulceration and histologically it is composed almost entirely of atypical spindle-shaped cells, hence its name;
- tricholemmal carcinoma is an invasive, cytologically atypical clear cell neoplasm of adnexal keratinocytes, arising in continuity with the epidermis or follicular epithelium. It usually arises in sun-exposed areas of elderly patients;
- adenoid (acantholytic) squamous cell carcinoma has a striking male predominance. It presents as a nodular, flesh-coloured, pink, or red lesion in most cases;
- lymphoepithelioma-like carcinoma of the skin is a rare malignancy and it shows a remarkable resemblance to nasopharyngeal lymphoepithelioma. It is a slow-growth dermal nodule, which rarely exhibits surface ulceration. Histologically, it is located in the mid-to-deep dermis, and composed of islands and syncytial sheets of large, palely eosinophilic-to-amphophilic polyhedral cells with oval, vesicular nuclei, and prominent nucleoli;
- intraepidermal epithelioma is one of the most controversial entity in dermatopathology. However, it is clinically described as flat to verrucous, gray-tan scaly plaques on the lower extremities;

- invasive Bowen's disease typically represents a slow-growing tumor which arises in sun-damaged skin of the elderly. Most of them appear as a sharply demarcated, erythematous scaly plaque, with frequent hyperkeratosis, crusting, and fissuring;
- adenosquamous carcinoma is a rare but aggressive form with true glandular differentiation. They usually appear as elevated, indurated, keratotic plaques (1-6 cm) consisting of small-to-large interconnecting nests of anaplastic squamoid cells forming frequent keratocysts;
- proliferating pilar tumor is a lesion related to pilar cysts, characterized by epithelial hyperplasia forming a cystic-to-solid keratinizing squamous tumor. Fortunately, most of the cases behave in a benign fashion;
- desmoplastic squamous cell carcinoma is a rare subtype characterized by infiltrative spindled cells associated with a dense stromal response, which, by definition, occupies at least 30% of tumor volume. Histologically, it is characterized by cords and trabeculae of epithelial cells infiltrating a dense, desmoplastic stroma;
- *de novo* squamous cell carcinoma is so called because it arises without any definitive evidence of a precursor lesion. It has an aggressive behaviour and it presents as a nodule;
- squamous cell carcinoma arising in chronic conditions such as long-standing ulcers, sinus tracts, burns or osteomyelitis and chronic inflammatory disorders. It is a very aggressive form with high rates of invasion, recurrence, and metastatic potential;
- radiation-induced squamous cell carcinoma is caused by prolonged administration of low-dose ionizing radiation. The histologic type is a conventional SCC although spindle cell SCC is common and the biologic behaviour appears to be more aggressive (Table 6) (34, 35).

SCC originates from epidermal keratinocytes and adnexal structures, such as eccrine glands or pilosebaceous units. As other cancers, SCC arises impaired genomic maintenance that facilitates acquisition of new mutations. The mechanism leading to genomic instability in keratinocytes is mainly due to UVB-induced inactivation of p53. Several studies also demonstrate that RAS and EGFR activation promote most of the key tumorigenic phenotypes. Moreover, interactions between tumor cells, their extracellular matrix, and the basement membrane zone play a role in SCC (36). Broders histologic grading system divides SCC cases from grade 1 to grade 4, basing on the ratio of histologically differentiated versus undifferentiated cells. A grade 1 lesion has 75% of cells well-differentiated, a grade 2 50%, a grade 3 25%, and finally a grade 4 <25%. Poor differentiation indicates a poorer prognosis with a local recurrence risk more than triple and a metastatic risk approximately double than the counterpart well-differentiated. In addition to Broder's system, SCC can be histologically categorized by Clark level that is based on the depth of tumor penetration (level I-V). In the first level, lesions are *in situ* cancers confined to the epidermis, in level II lesions invade the papillary dermis, injuries of level III encompass the entire papillary dermis but do not invade the reticular dermis, while level IV

lesions invade the reticular dermis, and finally level V malignancies extend to the hypodermis. (37).

LOW-RISK SCC SUBTYPES	INTERMEDIATE-RISK SCC SUBTYPES	HIGH-RISK SCC SUBTYPES	INDETERMEDIATE-RISK SCC SUBTYPES
Squamous cell carcinoma arising from actinic keratosis	Adenoid squamous cell carcinoma	Invasive Bowen's disease	Signet ring cell squamous cell carcinoma
Verrucous and HPV-related squamous cell carcinoma	Lymphoepithelioma-like carcinoma	Adenosquamous carcinoma	Follicular squamous cell carcinoma
Spindle cell squamous cell carcinoma	Intraepidermal epithelioma	Proliferating pilar tumor	Papillary squamous cell carcinoma
Tricholemmal squamous cell carcinoma		Desmoplastic squamous cell carcinoma	Squamous cell cercinoma arising from adnexal cysts
		De novo squamous cell carcinoma	Squamoid eccrine ductal carcinoma
		Squamous cell carcinoma arising in chronic conditions	Pigmented squamous cell carcinioma
		Radiation-induced squamous cell carcinoma	Clear-cell squamous cell carcinoma

Table 6. Classification of SCC subtypes into risk-based categories.

1.2.4 Staging

The eighth edition of the American Joint Committee on Cancer for melanoma staging is based on T, N, and M categories that are combined to form different stage groups. Main changes in the latest edition concern the thickness measurements that should be recorded (0.1 mm to ensure more precious measurements), the removal of mitotic activity as a reason to upstage a thin melanoma, an implementation of the N subcategories with the presence of microsatellites, satellites, or in-transit metastases, and the addition of lactate dehydrogenase (LDH) level in each M category. Staging is vitally important as it allows clinicians putting together the best treatment regimen. However, a high intra- and inter-variability between pathologists is observed, particularly those with ambiguous histologic features. More objective methods are needed to improve accuracy and reproducibility in melanoma diagnosis (38).
Compared with the previous edition, in the eighth edition for NMSC the pathological

stage categories are now defined by stratification using new numerical divisions of maximum lesion dimensions that should be obtained by clinical measurement. N category is still based on the size, number and location of positive nodes. Finally, the absence or the presence of a distant metastasis is the key factor that distinguishes stage IVA from stage IVB. AJCC-8 includes a revision of the SCC staging system, which was developed within the head and neck committee and therefore only applies to SCCs located on head and neck skin and vermillion lip. It is not specified how SCC cases located elsewhere on the body should be staged. Although these changes, TNM staging seems to have a poor significant prognostic value. Validation of the full tumor-node-metastasis system will require large population-based cohort studies because of the rarity of SCC nodal and distant metastases cases (39).

1.2.5 Clinical manifestation and diagnosis

Early detection of skin cancers remains the key factor in improving prognosis. Compared to other cancers, they have the advantage of the cutaneous location, which permits early detection through non-invasive approaches. Nevertheless, definitive diagnosis of skin malignancy is usually made with skin biopsy and histopathologic examination. Skin biopsy types include punch biopsy for small lesions, shave biopsy, ideal for lesions confined in the epidermis, and excisional biopsy for large lesions, known to be malignant or typical for a malignancy. Excisional biopsy of the entire specimen with narrow margins is the most effective way to facilitate proper diagnosis and treatment planning, since vertical depth of invasion is among the most important prognostic factors in diagnosis. Alternatively, a partial biopsy may be performed. Punch biopsy provides a full-thickness sample but it requires suture-based closure, whereas shave biopsy is easy to execute and it usually does not require cutaneous suturing. However, there are doubts regarding staging accuracy and histologic interpretation due to its ability to transect a segment of the lesion in question. Nevertheless, it is highly recommended performing a biopsy, either excisional or partial, of any lesions suspected to be a skin malignancy. Histologic confirmation involves microscopic findings that are mainly cytological atypia, amplified cellularity, and number of dermal mitotic figures. It is recommended to report Breslow thickness (mm), histologic subtype, dermal mitotic rate, peripheral and deep margin status, presence or absence of histologic ulceration, microsatellitosis, tumor infiltrating lymphocytes, cellular regression, angiolymphatic invasion, vertical growth phase, neurotropism, pure desmoplasia, and, finally, Clark's levels for lesions <1 mm in thickness.

It is clear that routine skin physical examination and history acquire a prominent position in detection of new cases. Moreover, studies of high-risk populations report

that patients routinely screened by dermatologists have thinner mean tumor thicknesses of detected malignant melanoma than that of historical or population-based controls. Benefits associated with early detection are mainly reduced medical costs, better outcomes and less invasive treatments. The effectiveness of skin cancer screening may be improved targeting people with high-risk traits, such as Caucasian race, fair complexion, presence of pigmented lesions, several large non-dysplastic nevi, many small nevi, moderate freckling, familial dysplastic nevus syndrome or history of skin cancer. Another important factor in increasing early detection is skin self-examination; although simple, it has a great potential. Hence, in 1985 Friedman and colleagues developed the "ABCD" criteria aiming to educate physicians and the public to recognize malignant lesions, especially melanomas, in their early clinical presentations. The ABCD acronym stands for Asymmetry, Border irregularity, Colour variegation, Diameter >6 mm. Later the letter "E" was added for Evolving, which is especially important for the diagnosis of nodular melanomas. During years, the validity of this system was demonstrated and the sensitivity of self-skin examination ranged from 57% to 90%. Another effective clinical approach is the Glasgow 7-point checklist, which includes 3 major criteria (change in size, shape, and/or colour) and 4 minor criteria (sensory change, diameter of 7 mm or greater, inflammation, and/or crusting or bleeding). The score is weighted 2 for major features and 1 for the minor ones, with the advice that any lesions with scores ≥3 should be referred for specialist opinion. Because of its sophistication, it has been less widely adopted than the ABCDE criteria. Finally, one of the most successful paradigm is the "ugly duckling" sign, based on the perception that a pigmented lesion "looks different from all of its neighbours". This criterion for revealing suspected lesions has been shown to be sensitive for melanoma detection, even for non-dermatologists (40).

Diagnosis of melanoma and NMSC can be significantly improved through various assistive optical devices, such as dermoscopy, total-body photography (TBP) and reflectance confocal microscopy. Dermoscopy or dermatoscopy or epiluminescent microscopy is a widely used non-invasive diagnostic technique for *in vivo* observation of the skin. The dermatoscope consists of a magnifier, usually set for a 10-fold magnification, and a light source. Polarized light allows for visualization of deeper skin structures, while non-polarized light provides information about the superficial skin; most of dermatoscopes have polarized and non- polarized light to gain complementary information. Through optic magnification, clinicians can visualize morphological structures and signs of disease that are not visible into the naked eye. Using dermoscopic criteria, it facilitates the diagnosis of melanoma and NMSC and their subtypes (41). Total body photography (TBP), also known as full body imaging, is a valuable tool for the early detection of skin cancer, especially for lesions that can be recognizable with neither the naked eye nor dermoscopically. It allows creating images that can be electronically captured and archived to manage and track any potential changes over time. This photographic record can be two-dimensional (2D)

or three-dimensional (3D). In 2D TBP, images are taken and composed together to form a body map, whereas 3D TBP creates, partly also thanks to dermoscopic images, a 3D representation of patient surface, facilitating the localization of lesions for follow-up. A recent systematic review revealed that patients undergoing TBP show a lower Breslow's thickness and a higher proportion of *in situ* melanomas compared to those without TBP analysis. Moreover, it was demonstrated that this imaging technique can improve early melanoma detection in high-risk populations (42). RCM is another non-invasive *in vivo* technique that permits clinicians to examine native skin at a nearly histologic resolution. It emits a near-infrared laser beam that is partially backscattered by micro-anatomical structures. This light is forced to pass through a narrow pinhole, diverted by a semi-reflective mirror system and, finally, directed to a detector. The obtained data are visualized on a computer screen that reveals black-and-white images corresponding to the horizontal sections at a selected depth within the skin. RCM is a very promising and useful technique because it reveals skin changes at a cellular level, although currently it is not used routinely in clinical practise (24, 40).

In order to improve detection and diagnosis of skin cancers, an increased use of non-invasive imaging technology pre-biopsy and more quantitative techniques post-biopsy, such as fluorescence *in situ* hybridization (FISH), comparative genomic hybridization (CGH), sequencing, mass spectrometry (MS) and immuno-histochemistry (IHC) should be encouraged (43).

Most of the melanoma lesions are incidentally discovered during routine skin examination, confirming the relevant role in detection. Only occasionally, in fact, subjects may be alerted by the presence of a persistent itching, bleeding, or crusting of a pigmented lesion. Unfortunately, melanoma is usual asymptomatic and can only be responsible for the aforementioned symptoms of local inflammation after invasive growth. Metastatic spread can be accompanied by seizures, headaches, vision changes, coughing, haemoptysis, shortness of breath, dyspnoea, changes in bowel habits, new-onset back pain, or any systemic symptoms (fevers, chills, night sweats, weight loss, etc.) (40).

Patients affected by BCC often complain about an enlarging non-healing lesion that may bleed. They may also describe pruritus or deny any symptoms. Perineural invasion (PNI) is a primarily microscopic finding, indicator of an aggressive clinical behaviour. Depending on subtype, lesions may show very different clinical features. While differentiating between these subtypes is helpful in management, approximately half of malignancies exhibits more than one histologic pattern, mainly nodular-micronodular. In this case, it is recommended guiding management based on the most aggressive subtype (32).

As for BCC, SCC symptoms and clinical presentation are location-specific and highly

variable. Signs such as numbness, tingling, and muscle weakness may reveal a perineural involvement that adversely influences prognosis. A well-differentiated SCC presents as thick, scaly papule and plaque whereas poor-differentiated one is often soft, non-scaly, ulcerated, or haemorrhagic; hence, clinical appearance is strongly influenced by level of differentiation (24).

1.2.6 Therapeutic strategies

In the early stages, melanoma can be successfully treated with surgery alone and survival rates are high, but after metastasis spreading, they drop significantly. Hence, for localized melanoma, surgical removal of tumor and surrounding healthy tissue is the primary treatment. In patients with tumors thicker than 0.8 mm or thinner but ulcerated, a lymph node biopsy is also performed. Metastatic malignancies can be surgically removed but they will be accompanied by other treatment options as well. Until recently, the only treatment option for patients with metastatic melanoma was chemotherapy. The first chemotherapeutic drug approved by FDA for the treatment of melanoma was dacarbazine in 1975. It is still the gold standard for metastatic melanoma, though the response is partial at best. So far, no other chemotherapeutic drug has been more effective or less toxic (43).

Dacarbazine (DTIC) belongs to the class of alkylating agents, which undergoes activation in the liver by microsomal oxidases. The exact mechanism of action is unknown but it mainly acts inhibiting RNA and DNA synthesis by forming carbonium ions resulting in cell cycle arrest and apoptosis. As it does not cross the blood-brain barrier, it is not effective on cerebral metastasis. The major side effects include nausea and vomiting (44) (Figure 6).

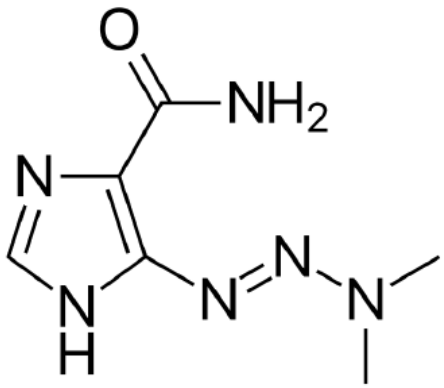

Figure 6. Chemical structure of dacarbazine.

Carboplatin and cisplatin represent further cytotoxic compounds used to treat advanced-stage melanoma. All these chemotherapeutic options can be used alone or in combination. The partial response, cell resistance, and side effects represent the main problems related to chemotherapy that limit its use.

Because of these aforementioned problems, chemotherapy is being gradually replaced by targeted therapies and immunotherapies, which are showing better prognosis for metastatic patients. The most promising target therapies include the BRAF inhibitors, vemurafenib and dabrafenib. Although these drugs are effective for approximately half of subjects with BRAF mutated melanoma, most of them are associated with the development of resistance within a relative short time. Fortunately, some of the resistance mechanisms have been already elucidated and researchers are working to develop new drugs to overcome this problem. One of the first approved immunotherapies developed for metastatic melanoma was an interleukein-2 in 1992. To date the most effective treatments for metastatic melanoma are the immune checkpoint inhibitors. Treatment with antibodies against programed cell death protein 1 (PD-1), PD-1 ligand (PD-L1/2), and cytotoxic T-lymphocyte-associated protein 4 (CTLA-4) effectively block binding to the respective ligands and the corresponding signal that causes tolerance, allowing for stimulation of an immune response (43).

For low-risk BCC tumors, surgical excision is the treatment of choice. Mohs micrographic surgery is the gold standard surgical approach in high-risk and recurrent BCCs, especially in critical anatomic areas, because it offers the highest cure rates. This result is achieved thanks to the complete peripheral and deep margin assessment (approximately 100% of the margins assessed), whereas standard vertical sectioning evaluates approximately only 1% of them. Curettage and electrodessication is a technique recommended for low-risk tumors because it is fast and cost-effective but it cannot assess for histologic margin and it is operator-dependent. Due to the risk of follicular tumor extension, areas with terminal hair growth should be avoided. For the same aforementioned reasons, cryosurgery, that is another treatment option, is reserved to superficial and low-risk lesions. Photodynamic therapy with aminolevulinic acid and methyl aminolevulinate should be considered for patients with superficial BCCs, in particular those with extensive/multifocal disease or diffuse actinic damage. Radiation therapy is the first choice of treatment for subjects whom surgery is contraindicated or for unresectable tumors. Adjuvant radiotherapy is also recommended for any BCCs with large caliber or extensive PNI. Several studies demonstrate that radiation therapy is more effective for treating tumors that are primary, less than 1 cm, and have less aggressive histologic subtypes. It is also associated with poorer cosmetic outcomes and more postoperative complications.

Topical therapies, such as imiquimod and fluorouracil creams, represent other options. However, because of their adverse side effects, they should be limited to superficial and small BCCs in low-risk locations that cannot undergo treatment with more definitive therapies. Although a majority of BCCs is easily cured with local treatment, a subset of patients with locally advanced or metastatic disease requires systemic treatment. The main molecular therapies are the oral medications vismodegib and sonidegib. Both of them are inhibitors of hedgehog pathway that is the most often involved in carcinogenesis. However, main limitations are correlated with the high frequency of adverse effects and development of tumor resistance. PD-1 immunotherapy is a new emerging treatment option for advanced BCC cases (33, 45).

Finally, for well-defined and low-risk SCC tumors smaller than 2 cm in diameter, surgical excision with a minimum margin of 4 mm is expected to remove totally the primary malignancy in 95% of cases. Several studies demonstrate that Mohs micrographic surgery achieves better results in term of cure and recurrence rates than traditional excision. The main disadvantages are that it is a time-consuming and expensive technique and its inability to capture micrometastasis. Electrodessication and curettage is a good choice for treatment of slow-growing tumors <1 cm or for debulking the mass prior to Mohs micrographic surgery. Cryotherapy involves the spraying of liquid nitrogen onto the lesion in two freeze-thaw cycles and shows good short-term cure rates for small SCCs but not for more advanced diseases. In case of recurrence, PNI, and positive margins after excision radiotherapy may represent a valid therapeutic option. This technique is beneficial in regions difficult to close such as lower eyelid, inner canthus of the eye, lip, lip of the nose, and ear. However, it is important to point out that radiation usually produces pallor and telangiectasia in treated skin. Radiotherapy should be avoided in SCC cases involving cartilage because of the risk of necrosis and for SCCs on the back of the hand, the abdominal wall, and the lower limb because excision shows better results. For well-differentiated lesions of Bowen's disease and microinvasive SCCs, use of photodynamic therapy is recommended. There are several variations of this technique but the most used consists in applying a methyl aminolevulinate cream followed by a light-emitting diode three hours later. So far, locally applied treatments, such as topical imiquimod or 5-fluorouracil and intralesional interferon-α are rarely utilized so there is not a conclusive evidence of their effectiveness. Finally, systemic chemotherapy is not widely used for treating SCC and its role remains unclear. As most of lesions are confined to one area of skin, localized treatments are preferred. However, for malignancies that are not amenable to surgery or that spread to other parts of the body, chemotherapy may be a good alternative. For metastatic diseases, the most

efficacious drugs are cisplatin, 5-fluorouracil, doxorubicin, bleomycin, or combinations of these. Clearly, the small amount of patients with high risk SCCs makes more difficult to define an ideal management (24).

1.3 The paraoxonase family

The paraoxonase family includes paraoxonase 1 (PON1), paraoxonase 2 (PON2) and paraoxonase 3 (PON3). The first member to be discovered was PON1, in 1946 by Mazur. It was described as an enzyme capable of hydrolysing diisopropyl fluorophosphate in the plasma and tissues of rabbit and man (46). Because of its capability to hydrolyze the toxic metabolite of parathion (paraoxon), this esterase was named paraoxonase 1 (PON1) (47, 48). In 1996, the other two members were identified and, although neither one hydrolysed paraoxon, they were termed PON2 and PON3 (49). PON2 and PON3 have only recently become the subject of investigation and are less well understood than PON1.

1.3.1 The paraoxonase gene family

The three genes encoding the PON proteins are located in tandem on the long arm of human chromosome 7 (7q21.3-22.1) (49) (Figure 7a). They consist of nine exons of similar length and TATA-less promoters, sharing a considerable structural homology. Between mammalian species, the PON genes share 81-90% identity at the nucleotide level and 79-90% identity at the amino acid level (50). The whole gene cluster may have arisen from the tandem duplication of a common evolutionary precursor. An attractive candidate is the lactonase of the fungus *Fusarium oxysporium*, which shares appreciable structural homology and similar substrates. Based on these findings, PON2 seems to be the oldest member of the family, PON3 arose from it next, and finally PON1 appeared as results of gene duplications (Figure 7b). Moreover, polymorphic variants are common in mammalian PONs. The redundancy and the number of polymorphic forms may suggest that PON enzymes have important physiological roles. The lactonase activity, common in all three members, may protect PON-carrying species against both aromatic and long-chain aliphatic lactones, typical constituents of plants, food products and drugs (51, 52).

(a)

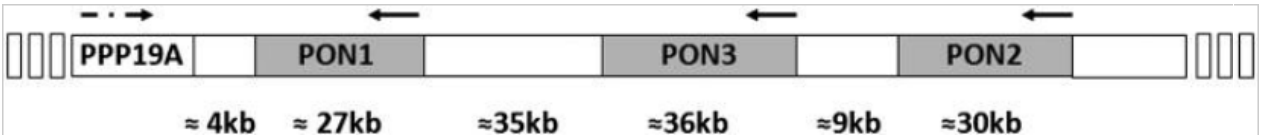

(b)

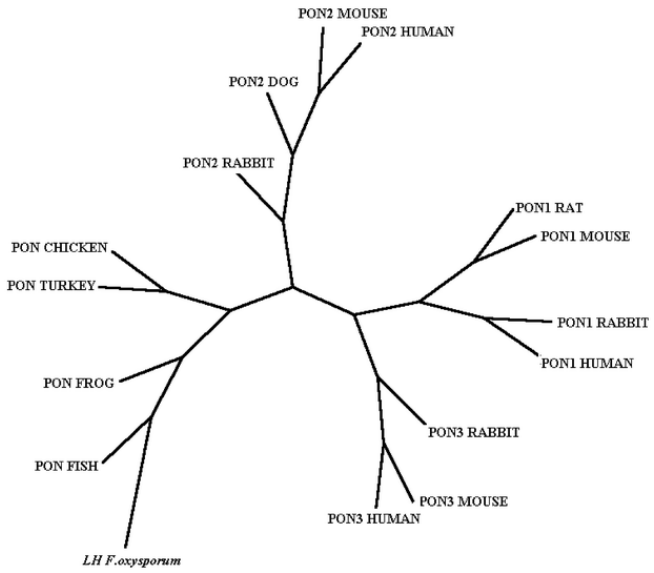

Figure 7. Genetic map of the human PON gene cluster (a). Phylogenetic tree of vertebrate PONs. The fungal lactone hydrolase was used to root the tree (b).

1.3.2 PON2 mRNA

At mRNA level, PON2 has a coding sequence of 1062 nucleotides, which results in the synthesis of a protein consisting of 354 amino acids, approximately 40-43 kDa in mass. Because of the presence of a second transcription start site and events of alternative splicing of the primary transcript, seven PON2 mRNA isoforms have been described (Figure 8). Some of them have significant alterations in the deduced protein, such as the premature truncation after 50 or 84 residues (transcript I.3A and I.3B, respectively), the lack of 86 N-terminal residues (transcript II), or the loss of the second putative Ca^{2+} binding loop (transcripts I.5A and II.5A). It remains to be established which of these PON2 transcripts are translated *in vivo* and what is the biological significance of such variations (53).

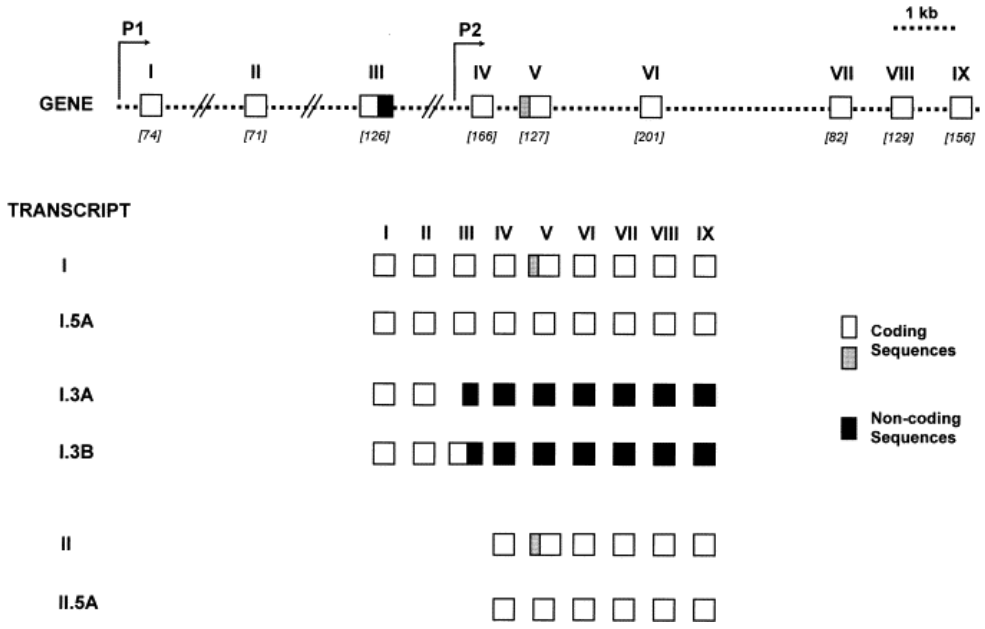

Figure 8. Schematic diagram of the *PON2* gene with exons, shown as boxes with their individual sizes (in base pairs) listed in brackets, and introns as a dotted line. For the first and last exon, only the size of the coding sequence is recorded. The first, second, and third intron are approximately 10.5, 8.1, and 3.8 kb long, respectively. P1 and P2 indicate the first and second transcription start sites, respectively. Underneath is schematic representation of the exon composition of alternative transcripts. Exons contributing to the non-coding portions due to shifts in ORF are indicated in black. The shaded part in exon 5 is a 36-bp section excluded in transcripts I.5A and II.5A by the use of a cryptic splice acceptor site within the coding sequence.

1.3.3 PON2 structure and localization

To date, PON1 is the only member whose structure has been elucidated. The first crystallized PON1 is a recombinant variant derived from rabbit PON1, highly similar to human PON1 in sequence (86%) and function. PON1 is a six-bladed β-propeller, and each blade contains four anti-parallel β-strands twisted so that the first and fourth strands are almost perpendicular to each other. The active site is located in the central tunnel formed by this highly symmetrical structure and the catalytic amino acids reside in the loops that connect the different β-sheets. The stability of the structure is guaranteed by hydrophobic interactions of the β-sheets and implemented by a disulfide bridge between C42 and C353. These two residues, that are located respectively at the N- and C-terminus, are conserved throughout the PON family. In the central tunnel of the propeller, there are also two Ca^{2+} ions, one with catalytic function and one with structural role (53, 54). Starting from PON2 primary structure and the three-dimensional structure of the homologue PON1, a predictive PON2 3D

model has been generated (Figure 9). Except for the regions 18-31 and 92-109, the two models are very similar. The basic folding seems to be enriched, as for PON1, by the presence of three α-helices on the top of its propeller. These helices are distanced from the reaction centre and are characterized by a high content of hydrophobic residues. Likely, these hydrophobic amino acids ensure the anchorage to the lipid bilayer. Two conserved N-linked glycosylation sites D253 and D323 been validated experimentally in PON2 so far, although other two ones have been predicted to be present (D226 and D269) (55).

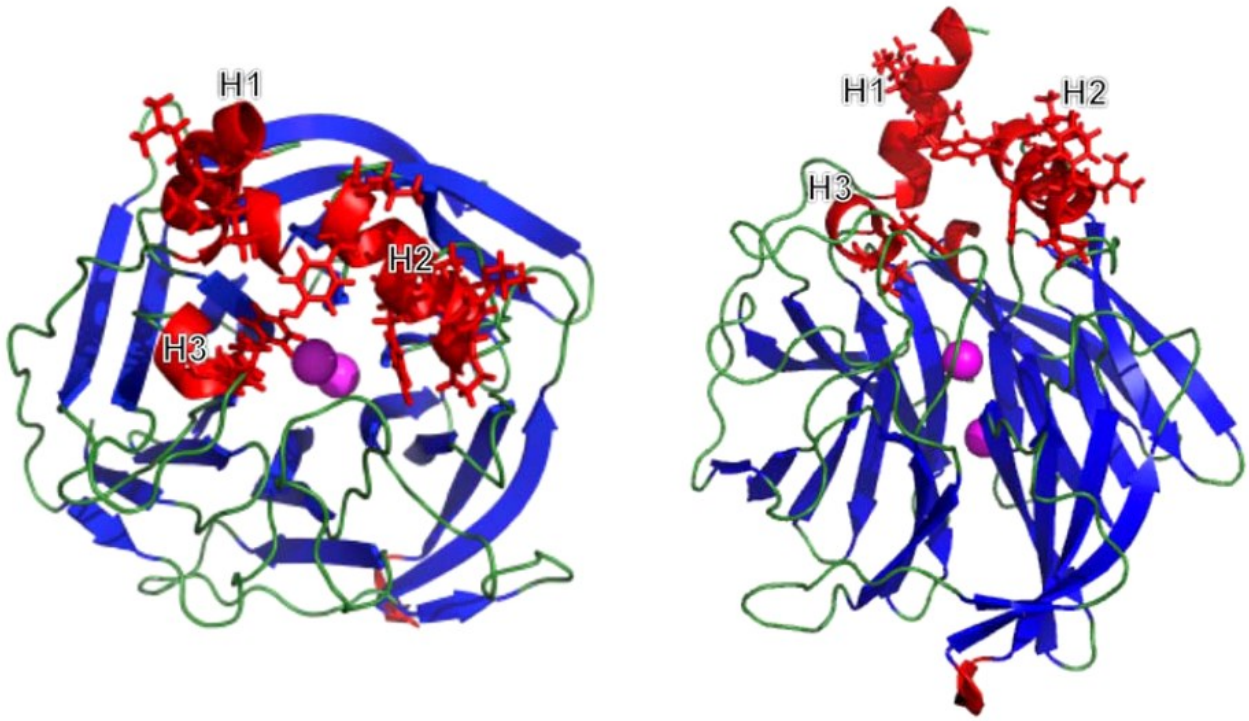

Figure 9. Top and side views of human PON2 structure, characterized as a six-bladed β propeller fold (blue) with three protruded helixes (red, hydrophobic residues within the helices shown as sticks) and loop regions (green). The reactive Ca^{2+} ions (magenta) are in the centre of the propeller fold.

An extensive literature describes the presence of three PON2 isoforms generated by alternative splicing events. In fact, beside the canonical full-length form made of 354 amino acids (39,381 kDa), two other variants have been described: an isoform that differs from the canonical sequence as follows, MGRLVAVGLLGIALAL → MGAWVGCGLAGDRAGF, and another one lacking in the region 123-134 of exon V (342 amino acids; 37,980 kDa). A recent paper demonstrates that this third isoform is disordered and mostly inactive, as missing one residue (H134) of the active site (56).
In the last few years, many papers focused their attention on the post-translational modifications of PON2. In addition to the already mentioned glycosylation, PON2 seems to have many ubiquitination sites. In particular, ubiquitination at position K29,

K144, K156, and K159 were confirmed in cells by Manco et al. (56, 57) and by Akimov and colleagues (58). In the same paper, Manco et al. identified an additional modification: an ADP ribosylation site at D124, also found by Bilan in 2017. Interestingly, this residue belongs to the lacking region 123-134 of the third PON2 isoform (58, 59).
PON1 and PON3 are extracellular proteins synthesized in the liver and secreted into blood flow, where they bind high-density lipoproteins (HDLs). A small amount of PON1 has also been detected in very low-density lipoprotein (VLDL) and postprandial chylomicrons. In addition to the liver, PON3 expression has been identified in the kidney (60). In contrast, PON2 is a ubiquitously expressed intracellular protein. This enzyme is present in many different tissues including heart, liver, lung, testis, placenta, stomach, small intestine, spleen, kidney, vascular endothelial cells, vascular smooth muscle cells (SMCs) and macrophages, but not in the plasma. It localizes in the plasma membrane, in the inner mitochondrial membrane, and in the perinuclear region, where it associates with the endoplasmic reticulum, and the nuclear envelope. It has also been reported an intracellular Ca^{2+}-dependent mechanism of PON2 translocation from endoplasmic reticulum to plasma membrane in response to oxidative stress, where it can inhibit peroxidation of plasma membrane lipids through its enzymatic activity. However, data on the predominant localization inside the cell is rather controversial. PON2 is a type II transmembrane protein, with its N-terminal region identified as a single transmembrane domain and C-terminal one, corresponding to the catalytic domain, located extracellularly in the case of plasma membrane (61).

1.3.4 PON2 activities

Despite their high homology, the different PON family members share some overlapping substrates, but also have distinctive substrate specificities. The catalytic spectrum of all three PON members is defined on their ability of hydrolysing organophosphates, esters and lactones, yielding paraoxonase (PON), arylesterase (ARE), and lactonase (LAT) activities, respectively (Figure 10). However, the range of physiologically relevant substrates remains an open question. As already discussed, PON2 lacks PON activity and displays a moderate arylesterase activity like PON3. All three enzymes are able to hydrolyze both aromatic and long-chain aliphatic lactones, such as dihydrocoumarin and 2-coumaronone, and among them PON2 shows the highest lactonase activity. In addition to this, PON3 can hydrolyze some of the statin lactone drugs (lovastatin and simvastatin) and the diuretic spironolactone. Interestingly, PON2 exhibits the greatest capability to degrade 3-oxo-dodecanoyl homoserine lactone (3OC12HSL), the major player of quorum sensing (QS) in Gram-negative bacteria (62). Accounting for its localization and activity, it has been hypothesized that PON2 can represent the first line defence against Gram-negative

microorganism infections. In addition to these hydrolytic activities, PON2 displays protective effects against lipid peroxidation, intracellular ROS formation and endoplasmic reticulum (ER) stress-induced apoptosis, as confirmed in different *in vitro* and *in vivo* studies. As a consequence, PON2 and its homologs are implicated in the aetiology of several diseases with inflammatory components, including cardiovascular diseases (CVDs), arthritic diseases, cancer, type 2 diabetes, neurological disorders and many more, being important targets in biomedical research.

In conclusion, two main roles have been ascribed to PON2: a Ca^{2+}-dependent hydrolytic activity on lactones, esters and aryl esters and a redox function, which reduces the intracellular levels of reactive oxygen species, thus inhibiting cell apoptosis and protecting cell against inflammatory diseases (51, 61).

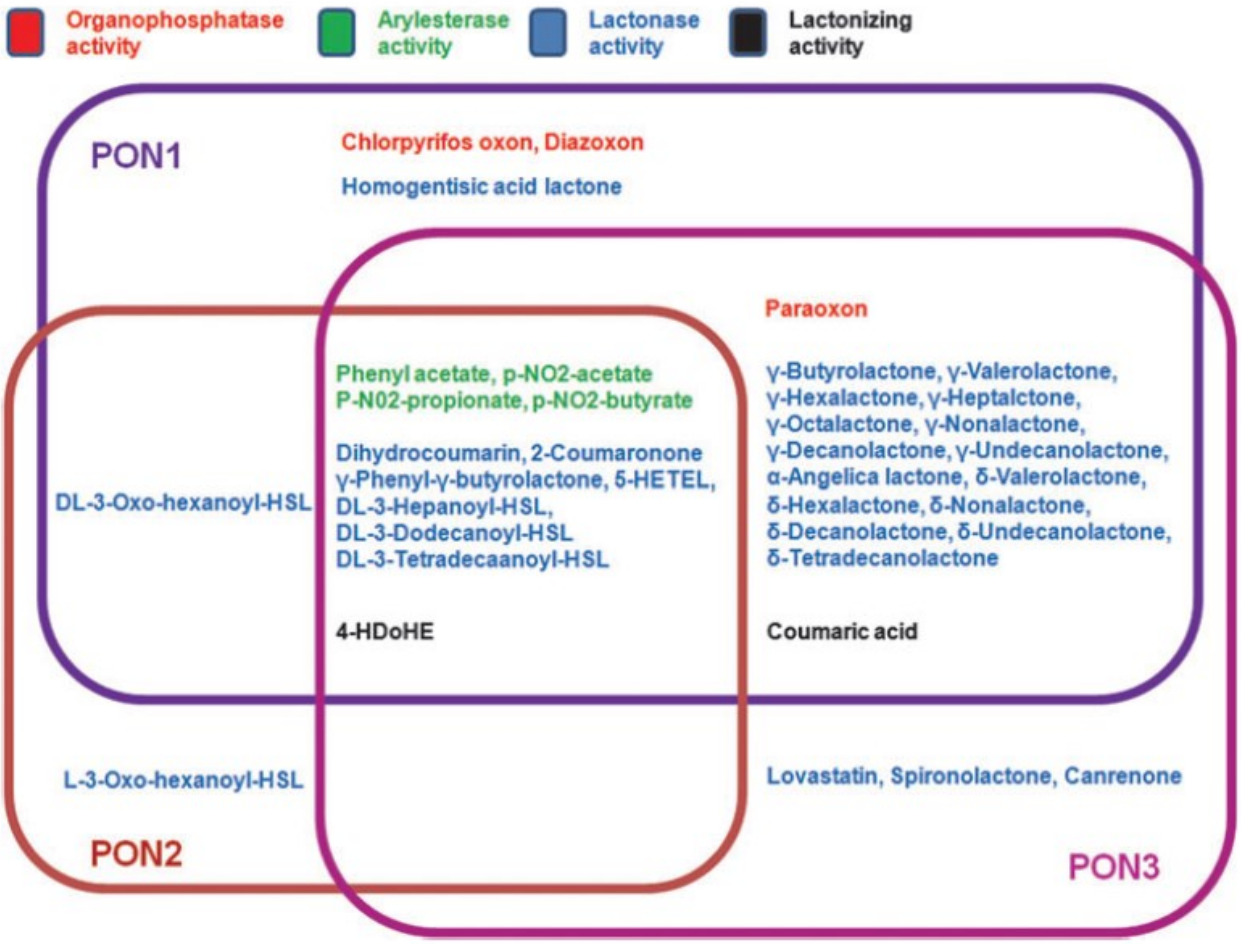

Figure 10. Specific enzymatic activities of the human PONs and relationships among the enzymatic activities of various PONs.

1.3.5 PON2 regulation

In the last two decades, a growing interest in regulation of PON2 expression has emerged, leading to the discovery of several pathways involved in the modulation of expression levels in different normal and cancer cell lines.
Various studies focused their attention on the modulation of PON2 expression by oxidative stress. Two different studies investigated this phenomenon under high glucose conditions, one in macrophages and monocytes (63), and one in human colorectal adenocarcinoma Caco-2 cell line (64). Both of them highlighted a decrease of PON2 expression and lactonase activity under chronic glucose stress. Moreover, lower levels of PON2 mRNA and protein were found in hearts of mice that developed hyperglycaemia after exposure to a high fat diet in their adult life (65). These data are in accordance with other previous studies conducted on Caco-2 cells oxidized in different experimental conditions. In fact, iron-ascorbate-mediated lipid peroxidation in Caco-2 cells induced a significant decrease in the gene expression of all the PON family members, including PON2. Importantly, this effect was attenuated by a pre-incubation of Caco-2 cells with powerful antioxidants, such as butylated hydroxytoluene (BHT) and Trolox (66). Similar results were obtained treating Caco-2 cells with hydrogen peroxide (H_2O_2): oxidative stress decreased PON2 mRNA levels, effect weakened by the additional incubation of the steroid dexamethasone (67).
A great amount of information about PON2 expression regulation comes from studies on macrophages, due to the involvement of this enzyme in aetiology and progression of atherosclerosis. In fact, macrophage foam cells are considered the hallmark of early atherogenesis, that is characterized by cholesterol accumulation, as well as by increased oxidative stress (OS) and production of ROS. Rosenblat and colleagues detected higher PON2 mRNA levels after inducing oxidative stress in mouse peritoneal macrophages, through incubation with buthionine sulfoximine, with angiotensin II, with 7-ketocholesterol, or with oxidized phosphatidylcholine (68). Furthermore, in vascular cells PON2 expression was induced at both mRNA and protein levels by endoplasmic reticulum stress, which stimulates a pathway known as the unfolded protein response (UPR). The UPR, in turn, may induce apoptosis. Concordantly, an ER stress element-like sequence was found in the promoter region of PON2 (69). It has also been demonstrated an increase of PON2 expression and activity in monocytes during their maturation into macrophage, associated to an increase in superoxide anion production and any reactive oxygen species derived from it produced by NADPH oxidase. Probably this process is regulated, at least partly, by the transcription factor activator protein-1 (AP-1), activated by JNK (c-Jun N-terminal kinase). In conclusion, PON2 stimulation may represent a compensatory mechanism against the increase in cellular superoxide anion production observed during macrophage maturation, through the activation of the JNK-AP-1 signal transduction pathway (70). Starting from these results, Aviram et al. examined in

depth PON2 regulation during the last two decades. In macrophages, PON2 activity exhibited a U-shape response curve under oxidative stress. They supposed that under low oxidative stress conditions, below that of control cells, PON2 lactonase activity was inactivated whereas at high range of oxidative stress, macrophage anti-oxidant compensatory mechanism up-regulates PON2, in order to cope with oxidative burden (71). They elucidated that in macrophages PON2 transcription is promoted by urokinase plasminogen activator (uPA) via binding to its receptor, the uPAR, eliciting a cascade of signal transduction pathway, finally culminating in the upregulation of PON2 gene expression. In short, the uPA/uPAR system associates with the cell surface and transmembrane protein platelet-derived growth factor receptor beta (PDGFR- β) that mediates the activation of the downstream phosphatidylinositol 3-kinase (PI3K). PI3K, in turn, activates NADPH oxidase, resulting in intracellular ROS production. The produced ROS activates ERK1/2, which stimulate phosphorylation of sterol regulatory binding protein-2 (SREBP-2), the transcription factor involved in cholesterol biosynthesis. This transcription factor translocates into the nucleus and associates to transcriptional regulatory elements upstream of PON2 gene, promoting its expression. These findings allowed them to clarify the association between ROS production, cholesterol biosynthesis, and cellular PON2 expression in vascular pathophysiology (72).

In 2016, Krüger et al. demonstrated for the first time an enhancement and a decrease of PON2 transcription and translation through Wnt/GSK-3β/β-catenin pathway mediated by Lef-1 and TCF4 activation, respectively, both in leukemia and OSCC cell lines. Remarkably, these preliminary *in vitro* results were supported by western blot analysis on patients affected by OSCC that revealed a considerable correlation between PON2 and β-catenin protein levels. In the presence of Wnt ligands, β-catenin can translocate from the cytoplasm into the nucleus, where it activates the transcriptional factors of the T-cell factor (Tcf)/lymphocyte-enhancer-binding factor (Lef) family that regulates the expression of several genes involved in cell proliferation and survival. In this study, an upregulation of PON2 expression after administration of Wnt3a and Wnt5a ligands was demonstrated, always correlated with an increase of β-catenin levels. Finally, they identified Lef-1 as a positive and TCF4 as a negative PON2 regulator after the identification of binding sites upstream transcription start (73).

At the end, a recent study proposed a model for the control of PON2 expression via a putative mRNA operon involving the Wilms Tumor 1 Associated Protein (WTAP) and the E3-ubiquitin ligase baculoviral IAP repeat-containing (BIRC3). WTAP, which is also an RNA binding protein, binds a conserved dodecameric sequence found in 3'UTR regions of PON2, BIRC3 and other 19 genes. WTAP can control its own splicing and stability and those of PON2 and BIRC3, keeping their mRNA levels low. According to

this model, PON2 increase is regulated by BIRC3, likely via the ubiquitination of WTAP itself, whereas splicing is controlled by via WTAP and interaction with BIRC3 via TAB1. It is worthwhile to notice that BIRC3 inhibits Caspase-3 (CASP3) activity by mono-ubiquitination, preventing CASP3 hyper-activating SREBP-2. Therefore, this model offers a link to different pathways, such as AP-1/JNK signalling, PI3K/PDGFR- β, and ER stress, involved, as already discussed, in the regulation of PON2 expression (56).

1.3.6 PON2 and the innate immunity

It has been hypothesized that one of the most important physiological role of PON2 is attenuating pathogens infection through its lactonase activity. In particular, among all PON members family, this enzyme has the greatest capability to degrade 3OC12HSL, a key factor for the biofilm formation and the virulence factors production in Gram-negative bacteria, including *P. aeruginosa*. Stoltz and colleagues confirmed this hypothesis highlighting an impairment in 3OC12HSL inactivation in lysate of tracheal epithelial cells from PON2 knockout mice compared with wild-type mice (74). Moreover, PON2 knockdown in non-small cell lung cancer (NSCLC) A549 cell line and human umbilical vein EA.hy926 cell line rendered them more sensitive to pyocyanin-induced ROS formation, whereas overexpression of PON2 protected cells from it. Pyocyanin is a *P. aeruginosa* virulence factor positively regulated by 3OC12HSL, capable of inducing an array of damage to various cell types, which could favour bacterial colonization. These findings support a key role of PON2 in the defence against *P. aeruginosa* virulence, but, at the same time, reveal a mechanism by which the bacterium may subvert the protection afforded by this enzyme, via a post-translational modification (PTM) that inactivates PON2. When PON2 hydrolyzes 3OC12HSL, the new generated acid form accumulates in the cells acidifying cytosol and mitochondria within minutes and, finally, triggering Ca^{2+} release. The increase of intracellular Ca^{2+} concentration, in turn, downregulates PON2 mRNA, protein and hydrolytic activity. The decrease of PON2 hydrolytic activity is much more extensive and rapid than protein, indicating a likely post-translational event, which blocks its activity. The nature of this putative PTM appears reversible because the hydrolytic activity begins to rebound over time, whereas protein levels remain low (75). Further studies demonstrated that ubiquitination at position K144 is one change responsible for 3OC12HSL-mediated inactivation (57). On the contrary, a recent study revealed that 3OC12HSL-induced apoptosis is dependent upon PON2 lactonase activity both in mouse and human cells. Consistent with these earlier results, a study showed that 3OC12HSL ability to induce apoptosis in A549 and NCI-H1299 NSCLC cell lines and to block tumor growth *in vivo* is mediated by PON2 (76, 77). These recent findings have

brought PON2 role in the innate immunity into question, opening up a broader scenario that needs more in-depth analysis.

1.3.7 PON2 and the antioxidant activity

Due to its antioxidant activity, PON2, as the other two family members, has a significant role in the aging process and in the development of the diseases associated with a high level of ROS, such as cancer, cardiovascular diseases, neurodegeneration, and diabetes. Mitochondria and ER are a high source of oxidative stress. The predominant localization of this enzyme in these organelles supports the hypothesis of its role in preventing oxidative stress damage at mitochondria level, likely scavenging ROS and reducing these latter generated as a response to ER stress-induced apoptosis.

The primary physiological function of mitochondria is to generate adenosine triphosphate (ATP) through oxidative phosphorylation via the electron transfer chain (ETC). During this event, the unstable intermediate ubisemiquinone or coenzyme Q10 (CoQ10) can donate electrons to molecular oxygen instead of cytochrome c, leading to the production of superoxide and a reduction of ETC activity. In 2011, Devarajan showed, for the first time, that PON2 is localized in the inner mitochondrial membrane, where it binds with high affinity to CoQ10 in a Ca^{2+}-dependent manner. During the Q cycle, CoQ10 is released from the ETC in mitochondria where, in the presence of PON2, it associates to it, preventing the superoxide generation and the subsequent derived reactive oxygen/nitrogen species (RONS). A successive study demonstrated that PON2 capability of binding CoQ10, and thus its antioxidant activity, is independent of its lactonase one (69). PON2 deficiency alters mitochondrial function by decreasing mitochondrial complex I and III activity and total ATP levels and influences mitochondrial oxidative stress by increasing both mitochondrial superoxide production and lipid peroxidation and decreasing reduced glutathione levels. In support of this hypothesis, several studies confirmed that PON2 can modulate ROS formation both *in vitro* and *in vivo* models (61, 78). Because of its capability of binding CoQ10 and thus reducing superoxide levels, this results in both lowered cardiolipin peroxidation and cytochrome C release, finally providing a marked resistance against apoptosis. In fact, the intrinsic apoptotic program is mainly controlled by the balance of pro- and anti-apoptotic B-cell lymphoma-2 (Bcl-2) protein family members that regulate mitochondrial pore opening and cytochrome C release. Importantly the liberation of cytochrome C from its membrane attaching molecule, cardiolipin, requires intramitochondrial redox signalling, without which the cascade is inactivated. Thus, an increase in PON2 expression may help cell to escape from

mitochondrial redox dependent cell death. Another important stress and cell death pathway is the UPR. As already discussed, PON2 protein expression is enhanced by ER stress caused by stimulation of PON2 promoter activity, via an ER stress element-like sequence located in the promoter region of the above mentioned enzyme. The UPR is an integrated intracellular signalling pathway that transmits information about the protein folding status in the ER lumen to the cytoplasm and the nucleus. Accumulation of unfolded or misfolded proteins in ER leads to ER stress and triggers UPR pathway. Although its primary goal is to assist cell survival by translational attenuation and induction of chaperones, in case of insurmountable stress, this pathway can initiate apoptosis in different ways (via IRE1, ATF6, or PERK), resulting in activation of CASP3. PON2 seems to interfere with at least one of these pathways, since enzyme knockdown enhances UPR-derived caspase activity, whereas the opposite effect is observed through PON2 overexpression. In response to ER stress, PON2 overexpression reduces the induction of the very potent pro-apoptotic C/EBP Homologous Protein (CHOP). Lowered CHOP levels, in turn, contribute to cell survival preventing cardiolipin peroxidation, loss of mitochondrial membrane potential, nuclear condensation, and caspase activation. The UPR inositol-requiring transmembrane kinase/endoribonuclease 1α (IRE1α) branch seems to represent the linkage between PON2 and CHOP. IRE1α, briefly, is a transmembrane kinase/endoribonuclease that, upon activation, initiates the nonconventional splicing of X-box binding protein 1 (XBP1u) mRNA into XBP1s mRNA encoding the active transcription factor XBP1s. XBP1s, finally, enters the nucleus and drives transcription of ER quality control genes and ER-associated protein degradation components to remove the excess of misfolded/unfolded proteins in the ER lumen. If ER stress extends, IRE1 actives JNK with the consequent induction of CHOP, through both XBP1s and IRE1/TRAF2/ASK1 signalling cascade. However, CHOP induction derives also from the other two branches of UPR, namely ATF6 and PERK. CHOP induction can also result from ER-associated oxidative stress, which appears upstream of XBP1 and/or JNK pathways. Most likely, owing to its antioxidant role during ER stress, PON2 reduces JNK activation and, thus, CHOP induction. Multiple pathways modulated by redox-sensitive proteins, such as thioredoxin, glutaredoxin, PKD, or 14-3-3/PP5 link ROS with JNK and CHOP activation. Likewise, other studies revealed a reduced CHOP induction by antioxidant interventions. It remains undetermined what particular redox-sensitive pathway PON2 alters to reduce JNK phosphorylation. It is also unknown which ROS sources are activated during ER stress and whether PON2 reduces ROS at the mitochondria only, or at the ER, or perhaps in conjunction (Figure 11) (51, 78, 79).

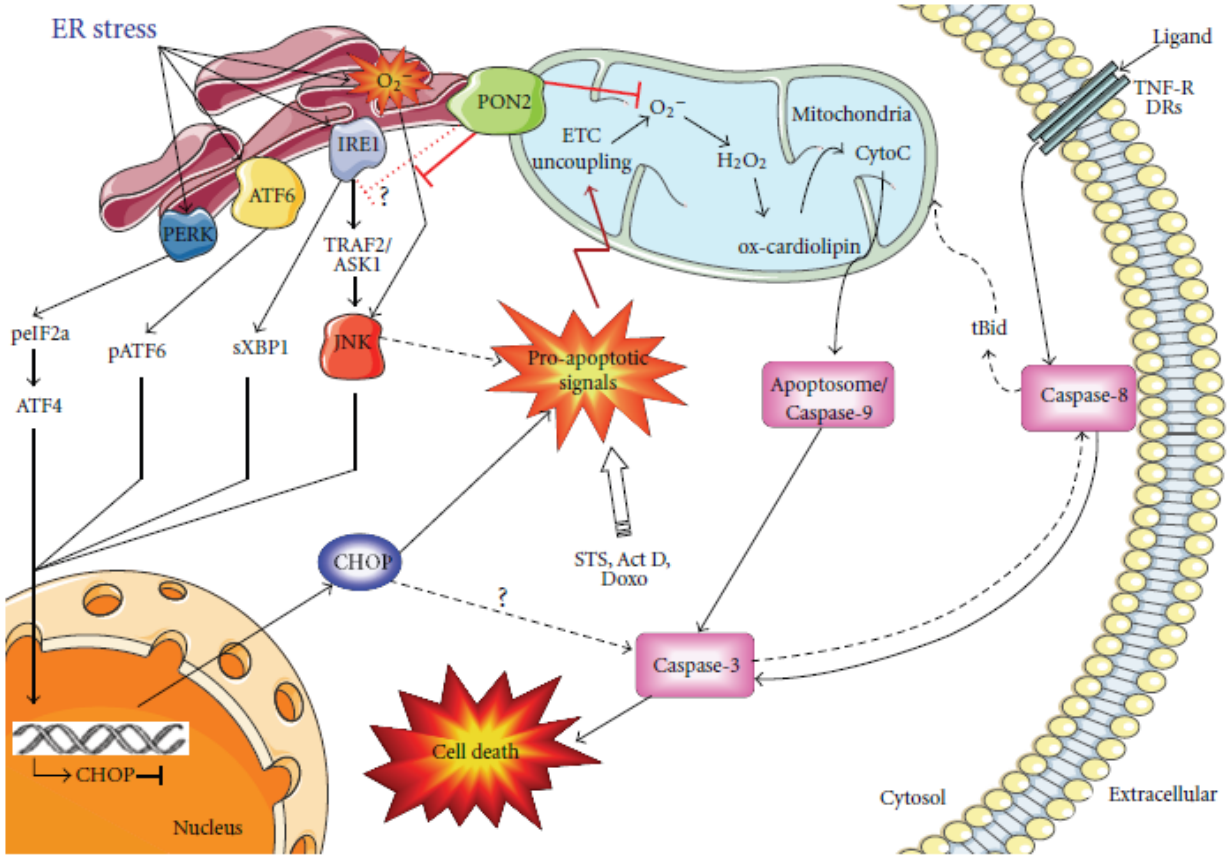

Figure 11. Schematic presentation of the suggested antiapoptotic mechanism of PON2. Its ability to prevent mitochondrial O^2–formation impacts on both ER stress-induced pathways (via acting on JNK and CHOP) as well as mitochondrial pro-apoptotic signalling such as cardiolipin peroxidation and cytochrome C release.

1.3.8 PON2 and cardiovascular diseases

Atherosclerosis is a chronic inflammatory disease characterized by the focal accumulation of numerous cells, lipids, and extracellular matrices in the intima of arteries. Although low levels of HDL and elevated levels of low density lipoprotein (LDL) cholesterol are considered risk factors for this disease, oxidative stress plays a fundamental role too. Half of the inside LDLs contain polyunsaturated fatty acids (PUFAs) that, in physiological conditions, are protected against free radical attack and oxidation by alpha-tocopherol and other antioxidants. Whenever an imbalance in the levels of antioxidants and the amount of PUFAs takes place, LDL is oxidized. Oxidized LDL (OxLDL) is involved in triggering pro-inflammatory events that initiate and exacerbate atherogenesis. PON family members, thanks to their antioxidant activity, act as central regulators of atherosclerosis and could be used as therapeutic targets for its treatment. Most notably, all three enzymes are present in the atherosclerotic plaques, suggesting their involvement in this disease. Indeed, PON1 and PON3 are

associated with HDL, whereas PON2 is synthesized and retained by the major cellular component of the plaques, namely endothelial cells, SMCs, and macrophages (51). In 2001, Ng et al. demonstrated for the first time that cells overexpressing PON2 were less able to modify and oxidize LDL, showing significantly less intracellular oxidative stress if exposed to either H_2O_2 or oxidized phospholipids (80). Subsequent *in vivo* studies confirmed the protective role against cardiovascular disease exerted by PON2, whose expression is strongly reduced in endothelial cells of atherosclerotic patients. Indeed, PON2-knockout and apoE null mice, fed a high-fat diet, developed significantly larger atherosclerotic lesions than their wild-type counterparts, despite lower levels of VLDL/LDL cholesterol. Likewise, they showed enhanced inflammatory properties of LDL, attenuated antiatherogenic capacity of HDL, and, at the end, heightened state of oxidative stress, along with an exacerbated inflammatory response in PON2-deficient macrophages. Conversely, opposite results were pointed out in PON2-overexpressing apoE null mice (81, 82). These antiatherogenic effects of PON2 are mediated, at least in part, by its protection against mitochondrial-related oxidative stress. Indeed, this enzyme is able to prevent superoxide formation that would lead to RONS generation and the subsequent oxLDL. The presence of PON2, thus, avoids foam cells generation by macrophages engulfment and so atherosclerotic lesions. Additionally, oxidized PUFAs could be physiological substrates of PONs because of the similarity of many of these molecules to that of lactones. These studies are sufficient to show that PON2 strongly inhibits the initiation and the development of atherosclerosis.

A new line of research identifies a link between PON2 expression and abnormalities in blood coagulation. Several cellular and molecular pathways regulate blood coagulation, assuring a balance between bleeding and thrombus formation. Oxidative stress and inflammation of the vessel wall contribute to pro-thrombotic states. The overproduction of ROS, in fact, can, in a vicious cycle, induce pro-inflammatory reactions and platelet activity and activate the coagulation cascade. Inflammation may also increase coagulation by stimulating expression of tissue factor (TF), the initiator of the extrinsic coagulation pathway. Enhanced coagulation status can increase, in turn, the risk for cardiovascular diseases. Supporting a direct role for PON2 in cardiovascular diseases, Ebert et al. showed that PON2 deficiency causes vascular inflammation and abnormalities in blood coagulation. PON2-knockout mice display increased circulating interleukin-6 (IL-6) levels, platelet pro-coagulant activity, and TF activity and shortened coagulation times. These experiments, thus, delineate a PON2 redox-dependent mechanism that regulates TF activity in endothelial cells and platelet reactivity, preventing systemic coagulation activation and inflammation (83). In rats under hypoxic-ischaemic conditions, PON2 mRNA and activity are

increased compared with the healthy control group, indicating that this enzyme, through its antioxidant capacity, protected blood vessels and inhibited the release of endothelial TF from blood vessels, thereby acting as a blood coagulant (84). Of note, a very recent study identified PON2 as potentially involved in the pathogenesis of venous thromboembolism in COVID-19 patients (85).

1.3.9 PON2 and insulin sensitivity

Insulin resistance is a pathological condition that occurs when cells fail to respond normally to the hormone insulin. The liver is the primary site of lipid metabolism and a major site for insulin-mediated glucose uptake, production and storage. Hepatic glucose metabolism is strongly influenced by oxidative stress and pro-inflammatory stimuli. That is why, similarly to atherosclerosis, insulin resistance is often associated with dyslipidaemia, oxidative stress, obesity, hypertension, and chronic inflammation. Starting from the previous results indicating that PON2-deficient mice had elevated hepatic oxidative stress coupled with an exacerbated inflammatory response from PON2-deficient macrophages, Bouquardand and colleagues demonstrated that PON2 deficiency is associated with inhibitory insulin-mediated phosphorylation at S307 of hepatic insulin receptor substrate-1 (IRS-1). When insulin binds its receptor, several proteins are phosphorylated, including IRS-1. IRS-1 contains many potential phosphorylation sites that are targeted in response to different signals that modulate its activity positively or negatively. Moreover, they observed that factors secreted from activated macrophages from PON2-def mice could modulate insulin signalling in cultured hepatocytes, consistent with that observed *in vivo*. Modulation of hepatic insulin sensitivity exerted by PON2 seems to be mediated by a shift in the balance of nitric oxide and peroxynitrite formation. To sum up, the antioxidant properties owned by PON2 are able to modulate insulin sensitivity (86).

1.3.10 PON2 and neurodegenerative disorders

PON2 is the only member, among PON family, to be expressed in the nervous system, both central and peripheral one.

Amyotrophic lateral sclerosis is an adult-onset, progressive, and fatal neuro-degenerative disease associated with selective loss of both upper and lower motor neurons in the brainstem and spinal cord. Although its aetiology remains unknown, recent evidence suggests an association between sporadic amyotrophic lateral sclerosis (sALS) and the exposure to toxic environmental factors, such as heavy metals, industrial solvents, and pesticides. In sALS patients, PON2 mRNA levels

detected in brain stem and spinal cord are lower compared with the healthy controls. On the contrary, in the cerebellum and cerebral cortex, PON2 expression levels are similar in the sALS subjects compared with the controls, as well in lymphocytes. Based on these results, pronounced oxidative stress, a condition documented in the ALS pathology, may cause the decrease of PON2 mRNA expression, preventing enzyme to protect cells against neurotoxicity (87).

Parkinson's disease (PD) is a progressive neurodegenerative disorder featured by a strong decrease in the production of dopamine in substantia nigra, due to degeneration of dopaminergic neurons. This slow process affects the motor system but, in more advanced cases, non-motor symptoms can be included. During the progression, there is an increase in lipid peroxidation and altered mitochondrial function and consequent formation of the hydroxyl radical and hydrogen peroxide. These factors together contribute to increased dopamine oxidation in the synaptic cleft and to the neuronal death, leading to the development of dementia. Although the majority of PD cases do not follow a genetic inheritance pattern, in the rare familial forms, the DJ-1 gene, encoding for the deglycase DJ-1, has been identified as one of the causative genes. Proteomic screen by mass spectrometry unveiled PON2 as a novel interacting candidate for DJ-1. DJ-1 interacts with PON2 in neurons promoting its activity. Importantly, PON2 deficiency hypersensitizes neurons to oxidative stress induced by 1-methyl-4-phenylpyridinium, whereas overexpression of PON2 protects neurons in this death paradigm. Taken together, these data suggest that DJ-1 promotes cell survival, at least in part, interacting with and stimulating PON2 activity in response to oxidative stress (88). In the context of PD, neuronal death is determined not only by RONS generation, but also by ER stress. It still remains to be clarified the role of this latter, whose hyperactivation is observed in PD patients and animal models. The contribution of ER stress pathways to neurodegeneration is complex, with the involvement of both pro-survival and pro-death factors. Once its contribution in the disease will be elucidated, PON2 could assume a new and more relevant role too.

Alzheimer's disease (AD) occurs when abnormal amounts of amyloid beta accumulate extracellularly as amyloid plaques and tau proteins, and intracellularly as neurofibrillary tangles, affecting neuronal functioning and connectivity, and resulting in a progressive loss of brain function. AD is responsible for about 80% of dementias diagnosed in the elderly. Although the cause of AD is poorly understood, mounting evidence points to increased oxidative stress and disruption of cholesterol homeostasis, as crucial events implicated in AD etiopathogenesis, being PON family members promising candidates involved in this neurodegenerative disease. Nevertheless, in human post-mortem frontal cortex tissues PON2 mRNA is

upregulated in AD relative to non-demented controls (89). These data were recently confirmed by bioinformatics analysis that candidate PON2 as a potential biomarker and an appropriate AD therapeutic target (90, 91).

1.3.11 PON2 and cancer

Oxidative stress plays an important role in apoptosis leading to premature aging and cancer. There is growing scientific consensus that antioxidant molecules and proteins with the same function can lower the incidence of several diseases. On the other hand, various types of cancers can take advantage of this protection afforded by these enzymes and thus enhance their expression. Here, multiple lines of evidence are presented demonstrating that PON2 is frequently found upregulated in cancer samples although specific regulatory mechanisms remain mostly unknown. The own PON2 antioxidant and antiapoptotic activities may likely favour cancer cell survival and chemotherapeutic resistance. Microarray studies led to observe the overexpression of this enzyme in some both solid tumors and blood cancers and, at the same time, many laboratories investigated PON2 role in the onset and the development of specific cancers. The current understandings allow hypothesizing that PON2 overexpression diminishes the execution of the apoptotic program, most likely through its antioxidant properties.

Several studies reported an upregulation of PON2 in NSCLC (79, 92, 93) and its RNAi-mediated knockdown in A549 cells resulted in increased ROS production and apoptosis rates, through CHOP induction via JNK pathway, a potent pro-apoptotic factor involved in ER stress. This was the first study who verified that PON2 could contribute to tumorigenesis and apoptotic escape (79).

PON2 overexpression was also described in renal cell carcinoma and a stage-specific analysis revealed that its upregulation is in the early stages of the tumor rather than in the late ones. This could indicate that, especially in the early stages of tumor formation, PON2 might play an important and beneficial role allowing to generate the platform for malignant transformation (78). However further studies *in vivo* and *in vitro* are required to explore the role of this enzyme in this type of tumor.

Similarly, PON2 expression levels were higher in bladder cancer tissues compared with normal ones, although this pattern was lost in urine specimens. Surprisingly, among urinary exfoliated cells from cancerous patients, PON2 mRNA is inversely correlated with the tumor stage. Bladder cancer T24 cell line overexpressing PON2 displayed an increase in cell proliferation and resistance to oxidative stress, indicating that tumor cells can benefit from its expression, particularly in the early stages (94). In agreement with these results, Fumarola et al. reported an increase in cell

proliferation and migration in PON2 overexpressing cells and a decrease of both parameters in PON2 silenced cells, respectively. It was also investigated whether PON2 modulation expression could influence T24 sensitivity to treatment with chemotherapeutics (cisplatin and gemcitabine, used alone or in combination). PON2 knockdown led to a significant decrease in proliferative capacity of cells, while enzyme overexpression was responsible for an enhancement of T24 cell proliferation compared with control cells at the 24 h time-point; however, this effect seemed to be lost at higher time points. Moreover, PON2 silenced cells, after treatment, showed higher ROS levels and a greater activation of both caspase-3 and caspase-8. In this light, PON2 overexpression in bladder cancer could represent an adaptive mechanism of tumor cells to escape apoptosis induced by chemotherapy, thus suggesting a potential use of PON2 as molecular target for bladder cancer therapy (95).

Witte et al. reported a moderate overexpression of PON2 mRNA in prostate cancer (79). Higher PON2 mRNA levels were also found in prostate carcinoma compared to benign prostate tissue samples by quantitative RT-PCR. However, statistical analysis did not report any differences between enzyme expression and tumor stage or other clinical parameters (96).

Both Witte and Shakhparonov described an overexpression of PON2 mRNA (79, 92), whereas Devarajan at protein level in ovarian cancer tissues (97). This last work pointed out that PON2 protein expression was higher in early stages compared to the adjacent normal tissue, indicating a specific development-related expression. Moreover, in PON2-siRNA transfected SKOV3 cells, proliferation increased and in PON2-overexpressing mice tumor size and volume reduced. Collectively these results demonstrated that PON2 inhibits ovarian tumor growth in the early stage by reducing insulin like growth factor-1 expression and signalling, and regulating immune function (97).

So far, few studies have focused their attention on the role exerted by PON2 in breast cancer. One of them analysed several genes expression, including PON2, in 69 samples of patients suffering from breast cancer. Concerning paraoxonase 2, there were no significant relationships between clinical stages, tumor characteristics and recurrence within 8 years (98).

Data collected by Precourt and colleagues suggested that PON2 is involved in the antioxidant and anti-inflammatory response in intestinal epithelial cells. In fact, PON2 knockdown in Caco-2/15 cell line was accompanied to an imbalanced primary and secondary antioxidant response with more susceptibility to oxidative stress damages and an exacerbation of inflammatory response, with overactivation of TNF-α, IL-6, and monocyte chemoattractant protein-1 (MCP-1), via NF-κB. However, PON2 deficiency altered neither cellular viability nor integrity (99).

Witte et al. showed a moderate PON2 overexpression at both mRNA and protein level in hepatocellular carcinoma samples (79). This result was later confirmed by bioinformatics analysis of RNA and DNA sequencing data, which observed one of the highest PON2 expression level in liver cancer and revealed a correlation between high PON2 expression and poor prognosis (92). Surprisingly, information arising from *in vivo* studies is very limited: indeed, it is reported only PON2 knockdown in Huh7 and HepG25 cells where any changes in apoptosis rate were observed after 72 h (79).

Overexpression of PON2 in gastric cancer (GC) was confirmed at both mRNA by microarray and Real-Time PCR, and at protein level by western blot and immunohistochemistry (79, 100). In particular, IHC analysis uncovered that high PON2 expression had significantly positive association with several clinicopathological parameters, such as diffuse type, clinical stage, tumor invasion, lymph node metastasis and distant metastasis in GC patients. Moreover, survival analysis suggested that GC patients with high PON2 expression resulted in a remarkably shorter overall survival compared with GC patients with low PON2 expression, being elevated enzyme level an unfavourable predictor for overall survival. Furthermore, transfection with PON2 siRNA suppressed viability, migration and invasion ability of MKN45 and SGC-7901 cell lines, which showed high basal PON2 levels. Taken together, these findings gave evidence that PON2 may act as oncogene in gastric cancer (100).

Several studies confirmed PON2 overexpression both at mRNA and protein level in subjects suffering from pancreatic ductal adenocarcinoma (PDCA) (79, 92, 101). In particular, Nagarajan and colleagues, through modulation of PON2 expression, were able to identify PON2 as a new regulator of PDCA growth and metastasis. Based on these results, PON2 is necessary for tumor growth, at least in part cooperating with KRAS, and for multi-organ metastatic potential, promoting anoikis resistance. PON2 facilitates glucose intake interacting with the glucose transporter (GLUT1), thus preventing the binding with stomatin, a specific GLUT1 inhibitor. In PDCA cells, PON2 inhibits the activation of cellular starvation response that activates the tumor suppressor forkhead box O3A pathway through AMP-activated protein kinase (AMPK) and its downstream pro-apoptotic target gene, thereby inducing anoikis. This new PON2-mediated pathway can be easily targeted by AMPK-activating drugs to inhibit tumor growth. Finally, they demonstrated that in PDCA cells p53 inactivation, due to mutation or genetic deletion, is a key event that promotes PON2 overexpression. In normal pancreatic cells, in fact, p53 repress PON2 transcription directly binding to its promoter (101).

Immunohistochemical analysis revealed PON2 upregulation in brain tissues affected by glioblastoma compared with normal ones. This phenomenon was further

confirmed examining PON2 mRNA expression in two public microarray databases. The ROS level was significantly reduced in PON2-overexpressing glioblastoma cells stimulated with valproic acid compared with controls and an opposite effect was recorded in PON2-silenced glioblastoma cells. These data suggest that PON2 modulates ROS production, and it is involved in valproic acid-mediated tumor cell growth arrest though the recruitment of Bcl-2-like protein 11 (102).

Several studies examined paraoxonase 2 levels in tumors of the hematopoietic and lymphoid tissues. Notably, high PON2 levels were associated with poor prognosis in patients affected by paediatric acute lymphoblastic leukemia (ALL) and with imatinib resistance in chronic myeloid leukemia (CML). PON2-overexpression in K562 cells treated with imatinib prevented cell death, providing apoptotic escape, whereas PON2 deficiency reversed this effect (79). Moreover, two imatinib-resistant CML cell lines expressed significantly higher PON2 levels than their imatinib-sensitive counterparts. This upregulation represented a cell adjustment in response to a chronic exposure to the chemotherapeutic drug; in fact, a short-term treatment had no effect in PON2 level. As mentioned above, Krüger et al. demonstrated that in CML and OSCC cell lines PON2 expression is regulated by Wnt/GSK3β/β-catenin pathway, through both *in silico* and *in vitro* studies (73).

A recent study revealed higher PON2 mRNA levels in thyroid cancer cell lines when compared to a normal one and a putative binding site for miR-376a-3p in PON2 3'-UTR region. The binding of this miRNA to PON2 causes a post-transcriptional suppression, as corroborated by the inverse correlation between PON2 and miR-376a-3p expression (103).

So far two studies only, carried out by Krüger and colleagues, focused on the role exerted by PON2 in OSCC. Firstly, they identified a variable basal PON2 expression in several OSCC cell lines. These data were later confirmed through western blot analysis from extracts of five patients affected by OSCC compared to healthy mucosa. Secondly, they evaluated PON2 levels after a singular irradiation at different time points. Surprisingly PON2 expression induction inversely correlated with basal expression: cells with low PON2 levels showed the strongest response, whereas high levels alleviated this effect. The same trend was recorded when caspase 3/7 activity was measured in the cell lines after irradiation. Interestingly, PON2 knockdown resulted in significantly higher levels of irradiation-induced apoptosis in all cell lines compared with the untreated and control RNAi cells. Taken together these findings suggested a PON2 involvement in the irradiation resistance in OSCC (104). Subsequent studies revealed that PON2 expression was regulated by Wnt/GSK3β/β-catenin pathway, as already mentioned. Extending their cohort to 32 subjects with OSCC, PON2 protein levels were significantly higher in patient group with relapse

compared to those who stayed relapse-free. Considering patients who received radio-/chemotherapy after surgical tumor removal only, PON2 levels remained significantly elevated in the relapse-experiencing group, lower in patients without relapse. Finally, they identified a positive and considerable correlation between PON2 and β-catenin levels corroborating the previous hypothesis (73).

1.4 Aim of the study

PON2 upregulation was reported in a variety of neoplasms, including bladder cancer, prostate carcinoma, hepatocellular carcinoma, gastric cancer, pancreatic ductal adenocarcinoma, glioblastoma, and acute lymphoblastic leukemia (79, 92, 95, 96, 100-102). It is believed that cancer may likely benefit from PON2 antioxidant and antiapoptotic activities. However, to date no further data are available concerning PON2 dysregulation in OSCC and skin cancer. Therefore, the aim of this study is to investigate PON2 role in these neoplasms.

This study will be divided in two parts. In the first part, PON2 expression will be evaluated in two different cohorts of matched tumor and normal tissue samples, obtained from OSCC patients, by immunohistochemistry and western blot. Tumor enzyme levels will be further correlated to clinicopathological parameters. Concerning skin cancers, PON2 levels will be determined in melanoma specimens and nevi used as controls, as well as in BCC samples and adjacent normal-looking tissues. Clinicopathological findings of examined samples will be then taken into account to explore the existence of potential correlations with PON2 intratumor levels. The purpose of this part of the project is to identify whether PON2 could represent a promising diagnostic and/or prognostic biomarker for OSCC and skin cancers. In the second part, shRNA-mediated PON2 knockdown will be achieved in OSCC and melanoma cell lines, and the effect of enzyme silencing will be evaluated in terms of cell viability, proliferation, and sensitivity to chemotherapeutic treatment. Taken together, these *in vitro* analyses will define PON2 contribution to cancer development and response to treatment, thus suggesting the potential use of the enzyme as molecular therapeutic target for these neoplasms.

Materials and methods

2.1 Analyses in tissue sample

2.1.1 Patients and tissue samples collection

30 formalin-fixed and paraffin-embedded (FFPE) OSCC and normal adjacent tissue specimens, collected between February 2020 and January 2021, were analysed by immunohistochemistry. All samples were collected upon surgery from the Department of Biomedical Sciences and Public Health, Section of Pathology, Marche Polytechnic University. Staging was assigned according to the TNM classification of AJCC (8^{th} edition) and histological grading was based on Broder's classification. The group consisted of 12 males and 18 females with an age range of 25-92 and a mean age of 70 (Table 7).
The study also included 11 matched OSCC and normal tissue specimens obtained from the Department of Biomedical Sciences and Public Health, Section of Pathology, Marche Polytechnic University, between 2002 and 2005. After surgery, specimens were snap frozen in liquid nitrogen and stored at -80°C until western blot analysis. The group was composed by 6 males and 5 females and their age ranged from 48 to 91 (mean age was 64) (Table 8).

Overall, 92 tissue specimens, including melanomas, nevi and BCC cases, collected between February 2018 and February 2020, were obtained from the archives of Pathology (Department of Biomedical Sciences and Public Health, Marche Polytechnic University). Melanoma group was composed of 29 primary malignancies (18 males and 11 females with an age range of 28-96 and a mean age of 61) and of 27 age- and gender-matched controls, represented by benign compound and dermal melanocytic nevi. The remaining 36 samples were those of BCC group and included tumor and healthy margin tissues. This group consisted of 23 males and 13 females, whose age ranged from 41 to 83 (mean age was 68), and were divided in two subtypes (17 nodular and 19 infiltrative) (Table 9).

Cases	30
Age	
-mean	70
-range	25-92
Gender	
-male	12
-female	18
Tumor dimension (cm)	
-mean	3.4
-range	0.7-5.5
Margins	
-undamaged	16
-damaged	14
Grading	
-G1	2
-G2	19
-G3	7
Infiltrative front	
-cohesive	8
-incohesive	21
PNI	
-Yes	16
-No	14
Phlogosis	
-+	5
-++	16
-+++	6
pT	
-T1	5
-T2	7
-T3	9
-T4	1
-T4a	8
pN	
-N0	13
-N1	5
-N1a	1
-N2b	6
Stage	
-I	5
-II	6
-III	5
-IVa	14
DOI (mm)	
-mean	1.33
-range	0.3-3.2

Table 7. Clinicopathological findings of 30 OSCC samples analysed through immunohistochemistry.

Cases	11
Age	
-mean	64
-range	48-91
Gender	
-male	6
-female	5
Tumor dimension (cm)	
-mean	2.6
-range	1.2-5
Grading	
-G1	1
-G2	7
-G3	3
pT	
-T1	5
-T2	4
-T3	1
-T4	1
pN	
-N0	7
-N1	1
-N2b	3
Staging	
-I	3
-II	3
-III	1
-IV	4

Table 8. Clinicopathological findings of 11 OSCC specimens analysed through western blot.

	Melanomas	Nevi	BCCs
Cases	29	27	36
Age			
-mean	61	64	68
-range	28-96	37-85	41-83
Gender			
-male	18	15	23
-female	11	12	13
Tumor dimension (cm)			
-mean	N.A.	N.A.	0.7
-range	N.A.	N.A.	0.2-1.3
Breslow thickness (mm)			
-mean	1.6	N.A.	N.A.
-range	0.1-8	N.A.	N.A.
Clark level			
-I	1	N.A.	N.A.
-II	5	N.A.	N.A.
-III	10	N.A.	N.A.
-IV	11	N.A.	N.A.
-V	2	N.A.	N.A.
Mitotic rate (mitoses/mm^2)			
-0	16	N.A.	N.A.
-1-4≤≥	5	N.A.	N.A.
-≥5	8	N.A.	N.A.
Regression			
-Yes	6	N.A.	N.A.
-No	23	N.A.	N.A.
Ulceration			
-Yes	3	N.A.	N.A.
-No	26	N.A.	N.A.
Phlogosis			
-Yes	15	N.A.	N.A.
-No	14	N.A.	N.A.
pT			
-T1	17	N.A.	N.A.
-T2	3	N.A.	N.A.
-T3	6	N.A.	N.A.
-T4	3	N.A.	N.A.
pN			
-N0	23	N.A.	N.A.
-N+	6	N.A.	N.A.
Stage			
-I	17	N.A.	N.A.
-II	6	N.A.	N.A.
-III	6	N.A.	N.A.

Table 9. Clinicopathological findings of 92 samples, including melanomas, nevi, and BCCs, analysed through immunohistochemistry.

2.1.2 Immunohistochemistry

For each case, 5 μm serial sections of representative tumor areas were cut from FFPE blocks, mounted on poly-L-lysine coated glass slides, deparaffinized in xylene, rehydrated in a graded alcohol series and treated with EnVision FLEX Target Retrieval Solution High pH (Dako North America, Inc, Carpinteria, CA, USA). They were then incubated for 7 min in 3% H_2O_2 solution, in order to inhibit endogenous peroxidase activity, and blocked with 5% Normal Goat Serum (Dako North America, Inc, Carpinteria, CA, USA). Samples were washed for 5 min with EnVision FLEX Wash Buffer (Dako North America, Inc, Carpinteria, CA, USA) and incubated with rabbit polyclonal antibody against human PON2 (1:1000 dilution) (Sigma-Aldrich, St. Louis, MO, USA) at room temperature for 1 h. After a washing, they were treated with EnVision FLEX/HRP (Dako North America, Inc, Carpinteria, CA, USA) for 20 min, washed, and incubated with FLEX DAB+ Chromogen (Dako North America, Inc, Carpinteria, CA, USA) for 10 min. Following the counterstaining with Mayer's haematoxylin, sections were permanently mounted on glass slides and examined by light microscopy. Positive controls consisted of human kidney tissue sections whereas negative control slides were obtained by replacing primary antibody with Rabbit IgG Isotype (Thermo Fisher Scientific, Waltham, MA, USA). Two examinators independently evaluated the scores of all cases and cell counting was performed by means of NIS Elements BR 3.22 imaging software (Nikon Instruments, Tokyo, Japan). Stained cells were counted in at least ten fields per sample and quantified as percentage of total counted cells. Each specimen was analysed three times.

2.1.3 Western blot

Oral tissue extracts were prepared with lysis buffer (50 mM HEPES pH 7.9 containing 150 mM sodium chloride, 0.5% Triton X-100, 1 mM phenylmethylsulfonyl fluoride, and 2 μg/ml aprotinin). Aliquots of frozen tissue (20–40 mg) were suspended in 33 volumes of lysis buffer and then homogenized on ice using Ultra-Turrax homogenizer (IKA, Staufen, Germany) at medium speed. After centrifugation at 13000xg for 10 min at 4°C, the supernatants, representing the protein extracts, were collected. Protein concentration was measured by the Bradford method, using bovine serum albumin (BSA) as standard (105).
Samples containing 20 μg protein were subjected to sodium dodecyl sulfate-polyacrylamide gel electrophoresis (SDS-PAGE), according to Laemmli method, using a 12,5% polyacrylamide running gel (106). Proteins were transferred to polyvinylidene fluoride (PVDF) membranes at 250 mA for 40 min, using a wet transfer method. PVDF membranes were blocked for 2 h at room temperature in 1X tris-buffered saline (TBS) solution containing 2% BSA and 0,1% tween-20. After washing three times with 1X TBS with 0,1% tween-20, membranes were incubated with rabbit polyclonal antibody

against PON2 (Sigma-Aldrich, St. Louis, MO, USA) (1:500 dilution) in 1X TBS solution containing 1% BSA and 0,1% tween-20 overnight at 4°C. Membranes were then incubated with horseradish peroxidase (HRP)-conjugated goat anti-rabbit IgG (Thermo Fisher Scientific, Waltham, MA, USA) (1:150000 dilution) for 1 h at room temperature and finally subjected to five washings. PON2 was visualized using enhanced SuperSignal West Femto Maximum Sensitivity Substrate (Thermo Fisher Scientific, Waltham, MA, USA) and the related chemiluminescent signal was acquired using ChemiDoc XRS + System (Bio-Rad Laboratories, Hercules, CA, USA).

2.1.4 Statistical analysis

Data were analysed using GraphPad Prism software version 8.00 for Windows (GraphPad Software, San Diego, CA, USA). Differences between groups and correlations with clinicopathological parameters were determined using Wilcoxon, Mann-Whitney, Kruskal-Wallis test and Spearman's rank correlation. A p-value < 0.05 was considered statistically significant.

2.2 Analyses in cell lines

2.2.1 Cell lines and culture conditions

The human OSCC HSC-2, HSC-3, HSC-4, HOC621, and SAS cell lines were kindly provided by Prof. Lorenzo Lo Muzio, Department of Clinical and Experimental Medicine, University of Foggia. Cell lines were routinely cultured in Dulbecco's Modified Eagle's Medium/Nutrient Ham's Mixture F-12 (DMEM/F-12) medium supplemented with 10% fetal bovine serum and 50 µg/ml gentamicin at 37°C with 5% CO_2 air-humidified atmosphere.

The human malignant melanoma A375 cell line was purchased from the American Type Culture Collection (ATCC) and maintained in DMEM containing 4.5 g/L glucose, supplemented with 2 mM glutamine, 10% fetal bovine serum, and 50 µg/mL gentamicin at 37°C with 5% CO2.

2.2.2 Total RNA extraction and cDNA synthesis

The related cell pellets ($1x10^6$ cells) were homogenized in lysis buffer and total RNA was isolated through the SV Total RNA Isolation System (Promega, Madison, WI, USA), according to the manufacturer's protocol. The quantity of RNA was assessed spectrophotometrically by measuring the absorbance at 260 nm, and the purity was determined by calculating the ratios between the absorbance at 260 nm and 280 nm and at 260 and 230 nm. 2 µg of total RNA were reverse transcribed in a total volume of 25 µl for 60 min at 37°C with M-MLV Reverse Transcriptase (Promega, Madison, WI, USA) using random primers.

2.2.3 Real-Time PCR

In order to evaluate basal PON2 mRNA expression, a Real-Time PCR assay was performed using a CFX96 Real-Time PCR Detection System (Bio-Rad Laboratories, Hercules, CA, USA). cDNA, generated as previously described, was used as template and the primers sequences were 5'-TCGTGTATGACCCGAACAATCC-3' and 5'-AACTGTAGTCACTGTAGGCTTCTC-3' for PON2 and 5'-TCCTTCCTGGGCATGGAGT-3' and 5'-AGCACTGTGTTGGCGTACAG-3' for β-actin. All used primers flank an intron to avoid false-positive results due to amplification of contaminating genomic DNA in the cDNA preparation. Both genes were run in duplicate for 40 cycles at 94°C for 30 sec and

58°C for 30 sec, using SsoFast EvaGreen Supermix (Bio-Rad Laboratories, Hercules, CA, USA) and β-actin as reference gene. EvaGreen dye allowed to monitor real-time PCR product thanks to fluorescence emitted after its binding with the double strand DNA. These measurements were then plotted against cycle numbers and the parameter threshold cycle (Ct) was defined as the cycle number at which the first detectable increase above the threshold in fluorescence was observed. Upon this, PON2 mRNA basal expression for each cell line was calculated using ΔCt method where ΔCt = Ct (PON2) - Ct (β-actin). Hence, a small ΔCt value represented a high PON2 expression whereas a large one was attributable to a low expression level.

2.2.4 Western blot

Cell pellets ($2x10^6$ cells) were suspended in 200µl lysis buffer (phosphate-buffered saline, containing 1% Nonidet P-40, 0.1% sodium dodecyl sulfate, 1mM phenylmethylsulfonyl fluoride, and 2 µg/ml aprotinin) and homogenized by passing 3-5 times through a 30 gauche needle attached to a 1 ml syringe. After centrifugation at 16000xg for 10 min at 4°C, the supernatant containing the protein extract was collected. Protein concentration was estimated by using Bradford method. Samples containing 20 µg protein were subjected to SDS-PAGE and then transferred to PVDF membrane following the above mentioned procedure.

2.2.5 shRNA-mediated PON2 silencing in HSC-3 and HOC621 OSCC cell lines and in A375 melanoma cell line

To assess the role played by the enzyme in oral cancer, HSC-3 and HOC621 cell lines were selected to be further treated to reach PON2 knockdown.

PON2 silencing was also induced in A375 cell line to analyse enzyme contribution to melanoma cell.

To this aim, a set of pLKO.1 vectors (pLKO.1-643 and pLKO.1-647), containing stem-loop cassettes encoding short hairpin RNA (shRNA) targeting human PON2 (Sigma-Aldrich, St. Louis, MO) was used (Figure 12).

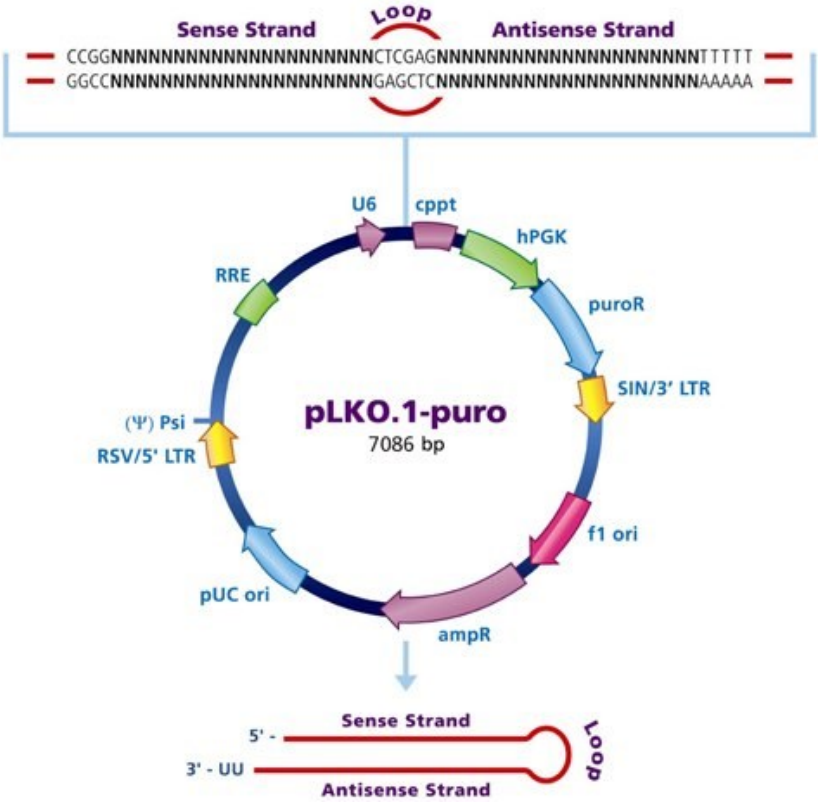

Figure 12. pLKO.1-puro vector map coding a generic shRNA.

2.2.6 Transfection and selection

The day before transfection, 7×10^4 HSC-3 and HOC621 cells/well and 4×10^4 A375 were seeded in 24-well plates in 500 µl complete growth medium, so that cells could achieve approximately 80% of confluence at the time of transfection. Cells were then transfected with two plasmids targeting PON2 (pLKO.1-643 and pLKO.1-647), whereas control cells were treated with empty vector (pLKO.1-puro) or transfection reagent only (mock). Transfection was performed using FuGENE HD Transfection Reagent (Promega, Madison, WI, USA), according to the manufacturer's instructions. Briefly, plasmid DNA (0.5 µg/well) was diluted in 25 µl of serum-free medium without antibiotics in a sterile tube. According to the 3:1 FuGENE HD Transfection Reagent/DNA ratio, 1.5 µl of the transfection reagent was added to the tube, and the resulting mixture was incubated for 15 min at room temperature. At the end of incubation period, the transfection mixture was added to cells in each well containing 500 µl of new complete growth medium. After 48 h, medium was replaced with a new one containing puromycin (0.5 µg/ml for OSCC cell lines and 1 µg/ml for melanoma cells) so that cells harbouring pLKO.1vectors could be selected, with medium changes every 48 h. For all subsequent experiments, puromycin resistant cells were maintained in complete selection medium.

2.2.7 Efficiency of PON2 silencing

To evaluate PON2 mRNA level in HSC-3, HOC621, and A375 cells, total RNA extraction, cDNA synthesis, and Real-Time PCR were performed as described in the paragraphs 2.2.2 and 2.2.3. Fold changes in relative gene expression were evaluated by $2^{-\Delta(\Delta Ct)}$ method, where ΔCt = Ct (PON2)-Ct (β-actin) and Δ(ΔCt) =ΔCt (silenced cells)-ΔCt (control cells) (107). Through western blot, performed as previously described, PON2 protein level was assessed in both OSCC and melanoma cell lines.

2.2.8 MTT assay

Cell viability was evaluated using a colorimetric assay with 3-(4,5-dimethylthiazol-2-yl)-2,5-diphenyl tetrazolium bromide (MTT) at different time points (0, 24, 48, and 72 h). This assay is based on the conversion of the soluble yellow tetrazolium salt to the insoluble purple formazan crystals by mitochondrial NAD(P)H-dependent oxidoreductase enzymes. Hence, the cellular metabolic activity is used as indicator of the cell viability (108).
PON2 silenced and control cells were seeded on 96-well plates ($3x10^3$ cells/well for OSCC cells and $2x10^3$ cells/well for melanoma cells) and allowed to attach overnight. For each time point, 10 µl of MTT reagent (5 mg/ml in phosphate-buffered saline) was dissolved in 110 µl of complete medium and added to the cells (100 µl/well). After incubation for 4 h at 37°C, the medium was discarded and 200 µl of 2-propanol were added to lyse cells and dissolve the formazan crystals. The amount of formazan crystals formed during the incubation is directly correlated to the number of viable and metabolically active cells. The reaction product was quantified by measuring the absorbance at 540 nm, using an ELISA plate reader. Results were expressed as percentage of the control (control equals 100% and corresponds to the absorbance value of each sample at time zero) and presented as mean values ± standard deviation of three independent experiments performed in triplicate.

2.2.9 Trypan blue exclusion assay

Trypan blue assay was used to estimate the cell proliferation ability. It is a simple and rapid method to identify live and dead cells in a given population. The guiding principle is that live cells possess intact membrane that exclude trypan blue. On the contrary, in cells with compromised membranes the dye can enter and bind

intracellular proteins thereby rendering them a bluish colour (109).
Briefly, cells were plated on 6-well plates ($1x10^5$ cells/well for HSC-3 and HOC621 and $3x10^5$ cells/well for A375) in serum-free medium for 24 h. Then the medium was replaced with a complete one. For each time point (0, 24, 48, and 72 h), cells were harvested by 500 µl trypsin and centrifuged at 300xg for 3 min. After resuspension of pellet in 500 µl of complete medium, the dye was added and the cells counted. The number of viable cells was determined using Burker's chamber. Each experiment was performed in triplicate and independently repeated three times.

2.2.10 Chemotherapeutic treatment

Cisplatin and 5-fluorouracil were selected, as representing two of the most used chemotherapeutic drugs in the treatment of OSCC. CDDP was dissolved in 0.9% sodium chloride (NaCl), whereas 5-FU in dimethyl sulfoxide (DMSO).

Regarding skin cancers, cells were treated with dacarbazine and cisplatin. DTIC was dissolved in 1M hydrochloric acid (HCl), while CDDP in 0.9% NaCl, as above reported.

HSC-3 and HOC621 cells downregulating PON2, as well as controls, were seeded in 96-well plates ($3x10^3$ cells/well) and allow attaching overnight. The day after seeding, cells were treated with CDDP or 5-FU or a combination of both drugs, and cell viability was measured at different time points (0, 24, 48, 72, and 96 h). A wide range of concentrations for both compounds was explored prior to use and the selected concentrations were in accordance with previous studies. The final concentrations of cisplatin were 0.75 µM for HSC-3 and 3 µM for HOC621, whereas the concentration of 5-FU treatment was 3.75 µM for both cell lines. In the combined treatment, CDDP was concentrated 0.3 µM and 5-FU 1.875 µM. Effect of both NaCl and DMSO, used to dilute CDDP and 5-FU respectively, was assayed.

Controls and PON2 downregulating A375 cells were seeded in 96-weels plates ($2x10^3$ cells/well) following the same protocol. The final concentrations used in the treatments were 540 µM DTIC and 4, and 8 µM CDDP. Analogously, cells were incubated with medium containing HCl or NaCl, used to dissolve DTIC and CDDP, respectively.

2.2.11 ROS production

2',7'-dichlorodihydrofluorescein diacetate ($DCFH_2$-DA) is one of the most widely used fluorescent probe for the detection of intracellular oxidative stress. The non-fluorescent $DCFH_2$-DA diffuses and crosses the plasma membrane and is deacetylated

by intracellular esterase to form the polar 2',7'-dichlorodihydrofluorescein, which is retained in the cytoplasm. This latter is oxidized into the fluorescent 2',7'-diclorofluorescein by ROS and RNS, providing a general measure of cellular redox state.
A375 cells were seeded on 96-well black plates provided with clear bottoms ($2x10^3$ cells/well) and allowed to adhere overnight. Subsequently, the old medium was replaced with a new one with or without chemotherapeutic drug and oxidative stress was measured at different times (0, 24, 48, and 72 h). At each time point, cells were incubated with 50 µM $DCFH_2$-DA for 45 min at 37°C in the dark. After a phosphate-buffered saline wash to remove extracellular $DCFH_2$-DA, fluorescence was measured by using a plate reader at Ex/Em=485 nm/535 nm. As probe stock solution contained DMSO, the solvent was added to the blank. Each experiment was performed in triplicate and independently repeated three times.

2.2.12 FTIRM measurements and data analysis

In light of MTT results, PON2 knockdown influence on molecular structure and cellular composition was monitored upon CDDP treatment, by using Fourier Transform InfraRed Microspectroscopy (FTIRM) measurements. FTIRM is a vibrational spectroscopic technique that permits to investigate the chemical structure and composition of cells and tissues. Thanks to its spatial resolution of roughly 10-20 µm, it is suitable for the investigation of small cell assemblies or even individual cells. Analysis of infrared (IR) bands in terms of position, intensity and width enables the molecular fingerprints of the most relevant biological molecules such as proteins, lipids, sugars, and nucleic acids. This information can be correlated to biological processes, as well as apoptosis, oxidative stress, dehydration, and DNA fragmentation.
OSCC cells were plated on 6-well plates ($1x10^5$ cells/well) and allow to attach overnight. After 24 h, medium was replaced with a new one containing CDDP, thus starting chemotherapeutic treatment (0.75 µM for 0, 24, 48, 72, and 96 h for HSC-3 and 3 µM for 0, 24, 48, and 72 h for HOC621). At each time point, cells were harvested by trypsinization, centrifuged at 500xg for 3 min, washed with 0.9% NaCl isotonic physiological solution, and centrifuged again. After fixation by adding paraformaldehyde solution (4%), cells were washed with isotonic physiological solution three times and, finally, resuspended in the above mentioned solution for subsequent FTIRM analysis. Each experiment was performed in triplicate and independently repeated three times.

FTIRM measurements were performed by using an INVENIO interferometer, coupled with a Hyperion 3000 Vis-IR microscope and equipped with a HgCdTe (MCT_A) detector operating at liquid nitrogen temperature (Bruker Optics, Ettlingen, Germany). Just before acquisitions, HSC-3 and HOC621 cells were centrifuged, resuspended in MilliQ water and centrifuged twice at 800xg for 10 min. An aliquot of 15 µl for each cellular sample was dropped onto calcium fluoride (CaF_2) optical windows (13 mm-diameter and 1 mm-thick) and let air-dried. For each sample, ~60 microareas (30 × 30 μm^2) containing groups of 3-4 densely packed cells were selected by the television camera and the corresponding IR spectra were collected in transmission mode in the 4000–800 cm^{-1} Mid IR region (512 scans, spectral resolution 4 cm^{-1}, zero-filling factor 2, scanner velocity 40 kHz) and let air-dry. Before each measurement, the background spectrum was acquired by using the same parameters on a clean portion of the CaF_2 window. All raw spectra were pre-processed to avoid atmospheric carbon dioxide and water vapour contribution and then vector normalised on the full spectral range (respectively Atmospheric Compensation and Vector-Normalization routines, OPUS 7.5, Ettlingen, Germany). From each experimental group, the mean absorbance spectrum and the corresponding mean absorbance spectra ± standard deviation were calculated and baseline linear fitted and then curve fitted in the 3050–2800 cm^{-1} (representative of cellular lipids) and 1800–900 cm^{-1} (representing proteins, nucleic acids and carbohydrates) spectral regions. In these two spectral ranges several bands with biological meaning were selected (Table 10). The underlying bands were chosen based on second derivative analysis and fixed before running the iterative process to obtain the best reconstructed curve (residual close to zero; bandwidth 10 to 40 cm^{-1} range) (GRAMS/AI 9.1, Galactic Industries, Inc., Salem, NH, USA).

For each underlying band, position (wavenumbers, cm^{-1}) and integrated area (A) were calculated and used for the following band area ratios: A_{3010}/A_{2960}, A_{2925}/A_{2960}, A_{1740}/A_{1655}, and A_{1170}/A_{1655}. Selected band area ratios represent specific biological processes. A_{3010}/A_{2960} and A_{1740}/A_{1655} ratios, respectively unsaturation and oxidation rate in lipid alkyl chains, are usually representative of oxidative stress processes. A_{2925}/A_{2960} band area ratio, associated to the saturation rate of lipid alkyl chains and hence to the relative amount of lipids, is related to the presence of apoptotic phenomena in cells. Finally, A_{1170}/A_{1655} ratio represents the relative amount of non-hydrogen bonded proteins.

Wavenumbers (cm^{-1})	Biochemical assignment
3010	Unsaturated CH groups in lipid alkyl chains
2960	CH_3 groups in lipid alkyl chains
2925	CH_2 groups in lipid alkyl chains
1740	C=O ester groups in lipids
1655	Amide I in proteins
1170	Non-hydrogen bonding proteins

Table 10. Centre position (wavenumbers) and biochemical assignment of selected bands.

2.2.13 Statistical analysis

GraphPad Prism software version 8.00 for Windows (GraphPad Software, San Diego, CA, USA) was used to statistically analyse the data obtained. One-way and two-way analysis of variance (ANOVA), Tukey's multiple comparisons test, Spearman rank correlation, Wilcoxon signed-rank test and Mann-Whitney U test were adopted to evaluate differences among examined samples and correlations with clinicopathological parameters. Statistical significance was set at $p<0.05$.

Results

3.1 Data obtained in tissue sample

3.1.1 PON2 expression in OSCC

Western blot analysis performed on protein extracts obtained from tissue specimens of 11 subjects affected by OSCC revealed a significant (p=0.001) PON2 overexpression (3.15-fold increase) in cancerous tissue comparing with the normal counterpart (Figure 13).

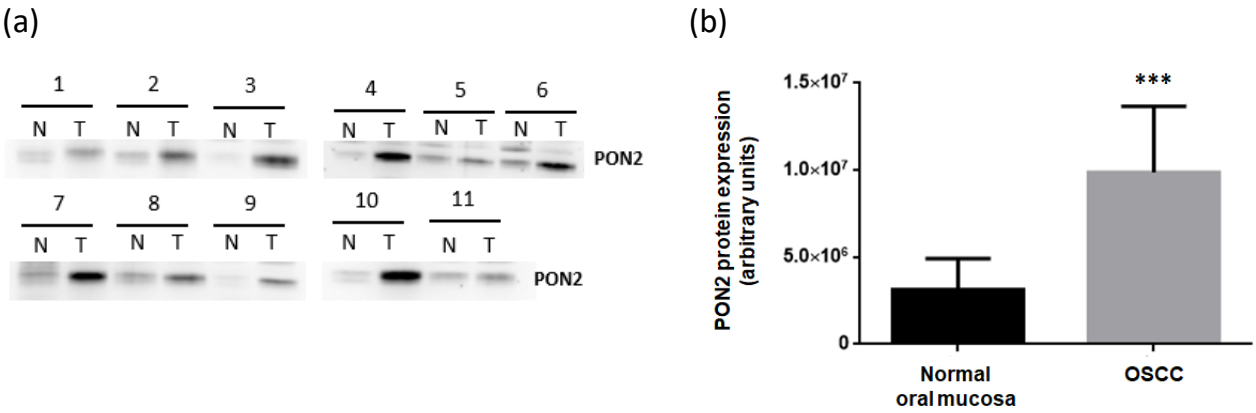

Figure 13. Tumor (T) and matched adjacent normal (N) tissues were analysed by western blot to detect PON2 expression levels (a). Bands intensity was quantified using Image Lab software and data were expressed as mean ± standard deviation. (b).

In order to further explore PON2 role in OSCC cancer, its expression was also analysed in 30 OSCC and normal adjacent tissue specimens by immunohistochemistry. Enzyme immunopositivity was totally absent in normal tissue (00.00 ± 00.00), compared with the cancerous counterpart one (40.87% ± 39.20), where PON2 displayed a cytoplasmic localization ($p<0.0001$) (Figure 14).

(a) (b)

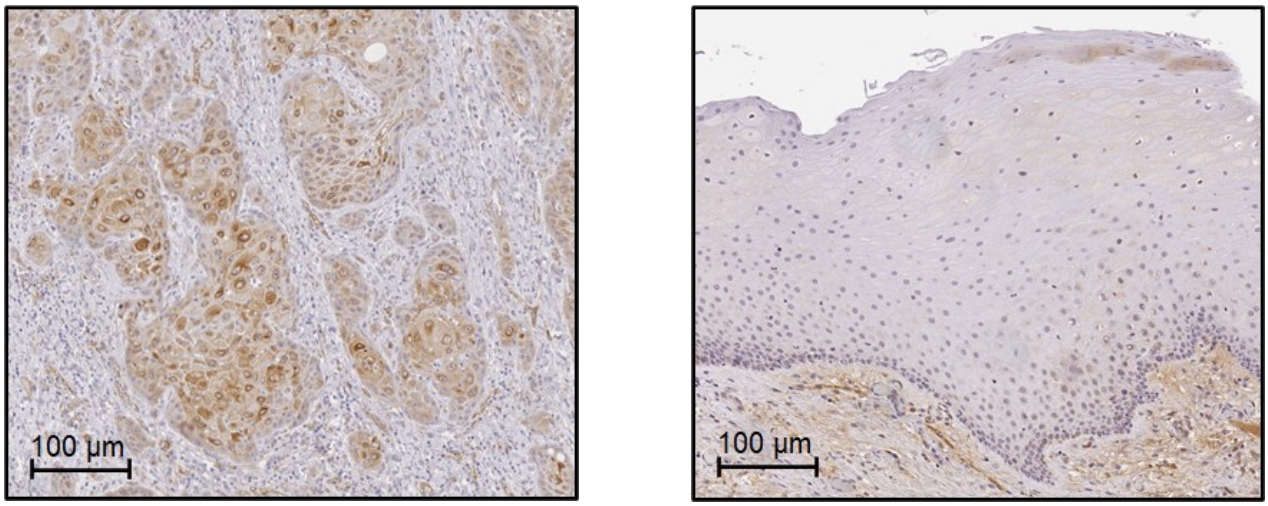

Figure 14. Immunohistochemical PON2 staining in an OSCC section (a) and the respective control tissue (b).

Statistical analysis devoted to explore the presence of correlation between clinicopathological features and tumor protein level (expressed as percentage of PON2 positive cells in tumor specimens) revealed a significant inverse association between PON2 expression and tumor size (r=-0.3799 and p=0.0384) (Figure 15), indicating a potential involvement of this enzyme in the early stages of tumor formation.

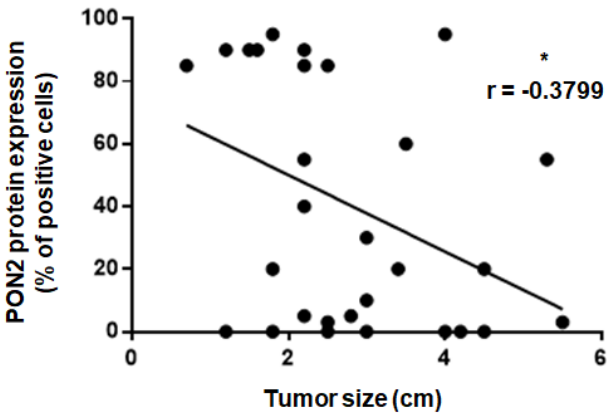

Figure 15. Negative correlation between immunhistochemical PON2 expression and tumor size (*p<0.05).

3.1.2 PON2 expression in skin cancers

PON2 expression was also assessed both in skin cancer tissues (melanoma and BCC) and in their related controls by means of IHC. Significantly ($p<0.0001$) increased PON2 immunopositivity was found in the cytoplasm of melanoma specimens (58.75 ± 29.76) when compared to that of control cases (2.50 ± 1.32) (Figure 16).

(a) (b)

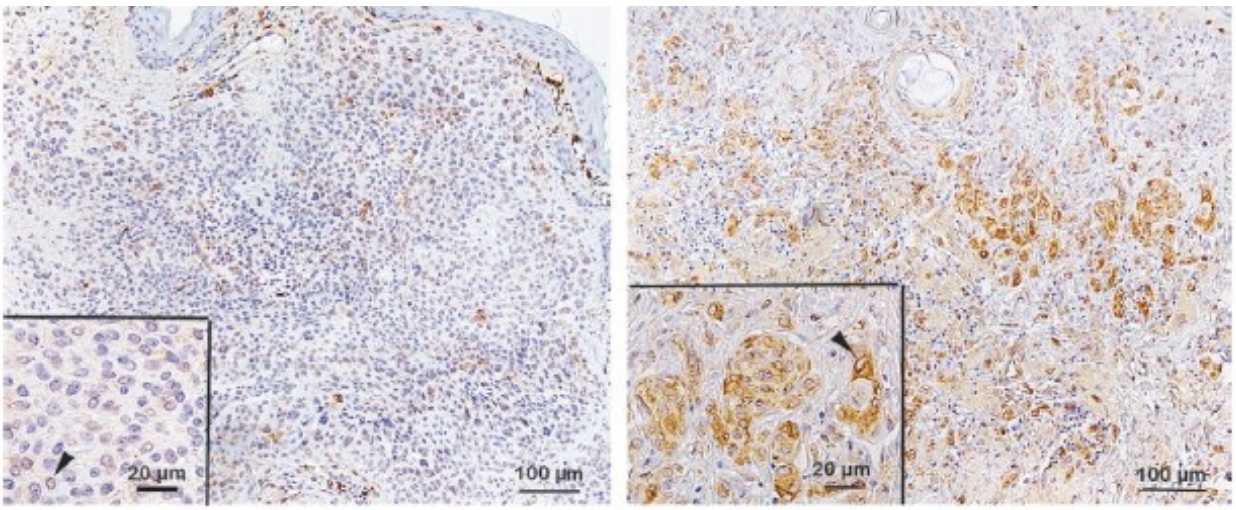

Figure 16. Immunohistochemical PON2 staining in control nevi (a) and melanoma sections (b). Arrow heads in inserts indicate PON2 immunopositivity at nuclear envelope level.

Furthermore, a statistically significant positive correlation was observed between PON2 expression and several clinicopathological features, such as Breslow thickness ($p<0.0001$), Clark level ($p<0.0001$), presence ($p<0.0001$) and number ($p=0.0082$) of mitoses, primary tumour (pT) ($p=0.0061$), and pathological stage ($p=0.0061$). Finally, samples with lymph node metastasis ($p=0.049$) and those without regression ($p=0.047$) showed significant higher PON2 immunopositivity (Figure 17).

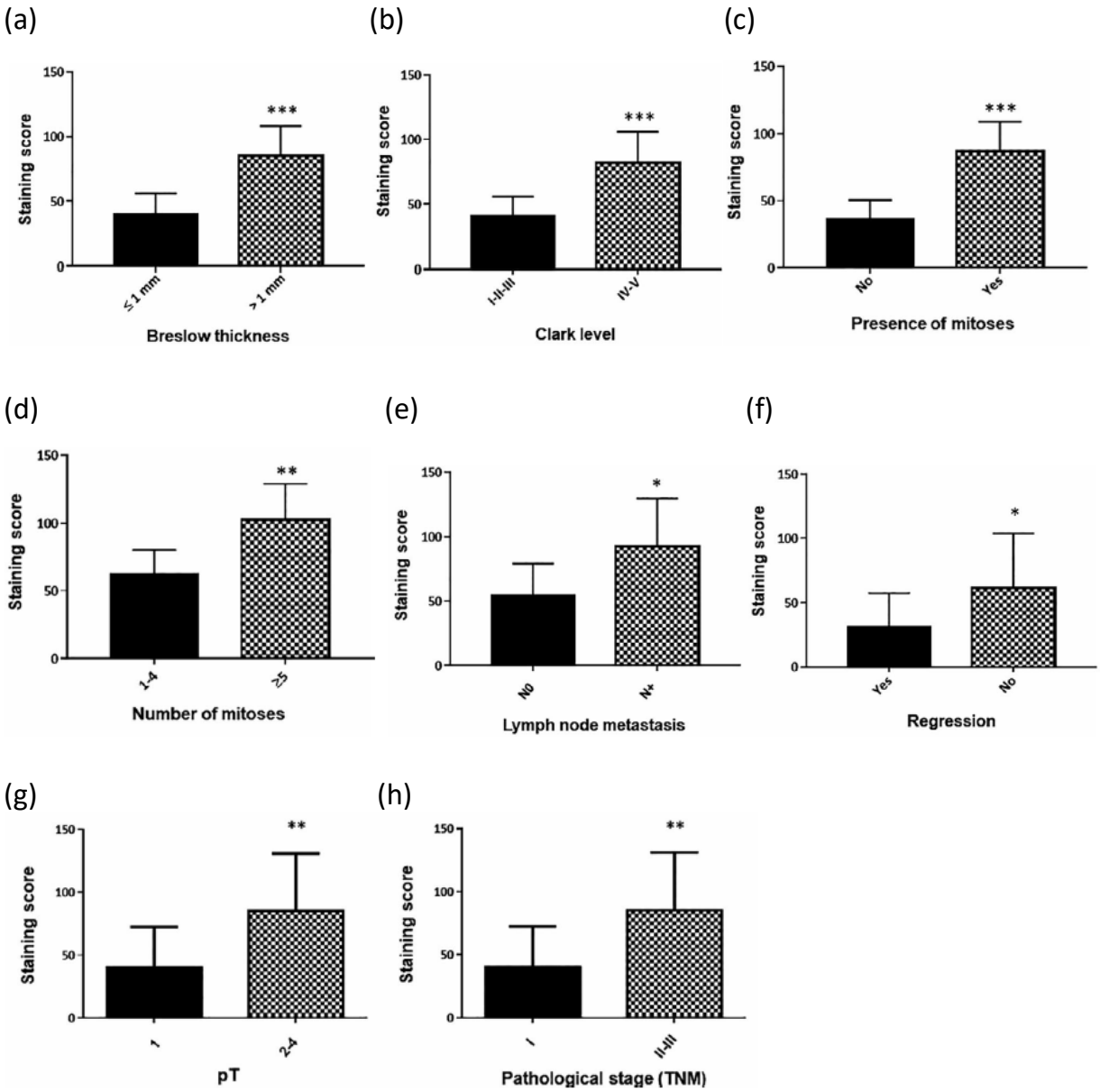

Figure 17. Correlation between PON2 expression by IHC in melanoma specimens and clinicopathological findings: Breslow thickness (***p<0.0001) (a), Clark level (***p<0.0001) (b), presence (***p<0.0001) (c) and number (**p=0.0082) (d) of mitoses, lymph node metastasis (*p=0.049) (e), regression (*p=0.047) (f), pT (**p=0.0061) (g), and pathological stage (**p=0.0061) (h).

PON2 immunopositivity was also significantly (p<0.0001) higher in the cytoplasm of BCC cells (18.33 ± 7.41) than that of control counterparts (7.36 ± 2.46). Interestingly, when distinguishing between BBC subtypes, infiltrative cases (27.37 ± 8.98) only showed a significant (p<0.0001) increase of PON2 level with respect to control (6.57 ± 4.73), while in nodular cases there was no significant ($p \geq 0.05$) difference between tumor (8.24 ± 3.42) and control tissue (8.24 ± 3.33). A significant (p<0.0001) enhanced protein positivity was evidenced in infiltrative (27.37 ± 8.98) compared to nodular BCCs (8.24 ± 3.42) (Figure 18). However, no significant association was found when clinicopathological findings were considered.

Taken together, all these data revealed a positive correlation between PON2 expression and tumor aggressiveness, suggesting the use of this enzyme as a potential prognostic factor for BCC and melanoma.

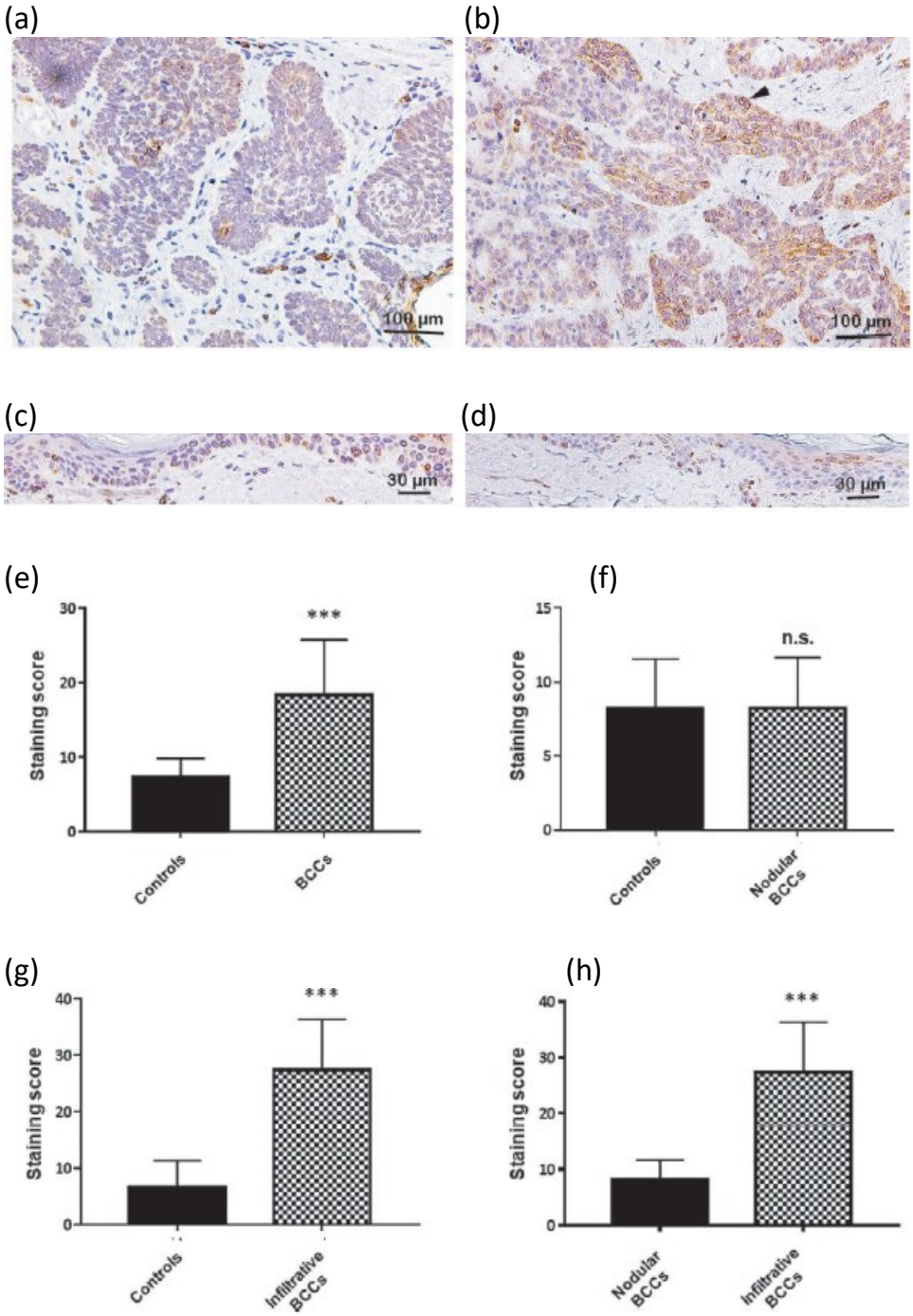

Figure 18. Immunohistochemical PON2 staining in nodular (a) and infiltrative (b) BCC sections and their respective controls (c and d). Arrow heads indicate PON2 immunopositivity at nuclear envelope level. PON2 staining score was evaluated in BCCs and controls (e), in nodular BCCs and controls (f), in infiltrative BCCs and controls (g), and nodular and infiltrative BCC) (h) (***$p<0.0001$; n.s. $p\geq0.05$).

3.2 Data obtained in cell lines

3.2.1 PON2 expression in OSCC cell lines

Basal PON2 expression was evaluated in five OSCC cells lines both at mRNA level, through Real-Time PCR, and at protein level, by western blot. HSC-4 and SAS cell lines showed higher mRNA PON2 levels (Figure 19a), whereas the highest PON2 protein expression was found in HOC621 cells (Figures 19b and c). HSC-2 and HSC-3 cell lines showed lower PON2 levels at both levels (Figure 19). In the light of these results, further experiments were performed on HSC-3 and HOC621 cells, exhibiting the lowest and the highest PON2 basal expression, respectively.

(a)

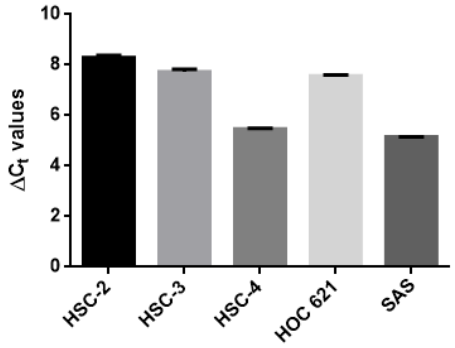

(b)

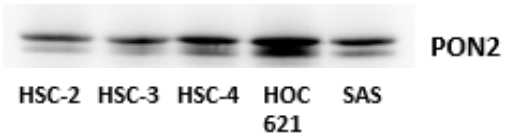

(c)

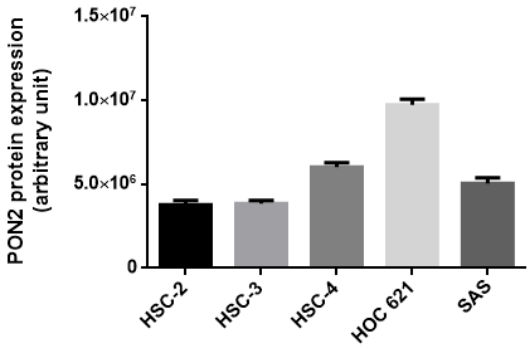

Figure 19. Evaluation of PON2 expression Real-Time PCR (a) and western blot analysis (b) in five OSCC cell lines. Bands intensity was quantified using Image Lab software and data were expressed as mean ± standard deviation.

3.2.2 Efficiency of PON2 silencing

HSC-3 and HOC621 cell lines were transfected with a set of pLKO.1 plasmids (pLKO.1-643 and pLKO.1-647) coding shRNAs targeting human PON2, with empty vector (pLKO.1-puro) or treated with transfection reagent only (mock). At the end of puromycin selection, cells were harvested to verify PON2 knockdown. Data obtained from Real-Time PCR analyses revealed a significant decrease in PON2 mRNA expression ($p<0.05$) in cells transfected with pLKO.1-647 plasmid (0.344 ± 0.001 for HSC-3 and 0.586 ± 0.066 for HOC621) comparing to cells treated with pLKO.1-puro (1.000 ± 0.122 for HSC-3 and 1.000 ± 0.163 for HOC621). On the contrary, cells treated with pLKO.1-643 plasmid showed a significant decrease of PON2 level ($p<0.05$) in HSC-3, but not in HOC621 cell line (0.708 ± 0.158 for HSC-3 and 1.150 ± 0.193 for HOC621) (Figures 20a and 21a).

Western blot data were consistent with Real-Time PCR results. Indeed, densitometric analysis of immunoreactive bands confirmed PON2 silencing in pLKO.1-647 (0.556 ± 0.030 for HSC-3 and 0.493 ± 0.029 for HOC621) respect to controls (pLKO.1-puro) (1.000 ± 0.079 for HSC-3 and 1.000 ± 0.054 for HOC621) ($p<0.05$). On the contrary, PON2 silencing tentatively achieved with pLKO.1-643 cells was not successful in neither HSC-3 nor HOC 621 (0.867 ± 0.073 for HSC-3 and 1.149 ± 0.106 for HOC621) (Figures 20b and c; Figures 21b and c). Mock and pLKO.1-puro samples did not show any significant ($p\geq0.05$) difference in PON2 expression (data not shown). Hence, further experiments were performed in pLKO.1-puro and pLKO.1-647 for both OSCC cell lines.

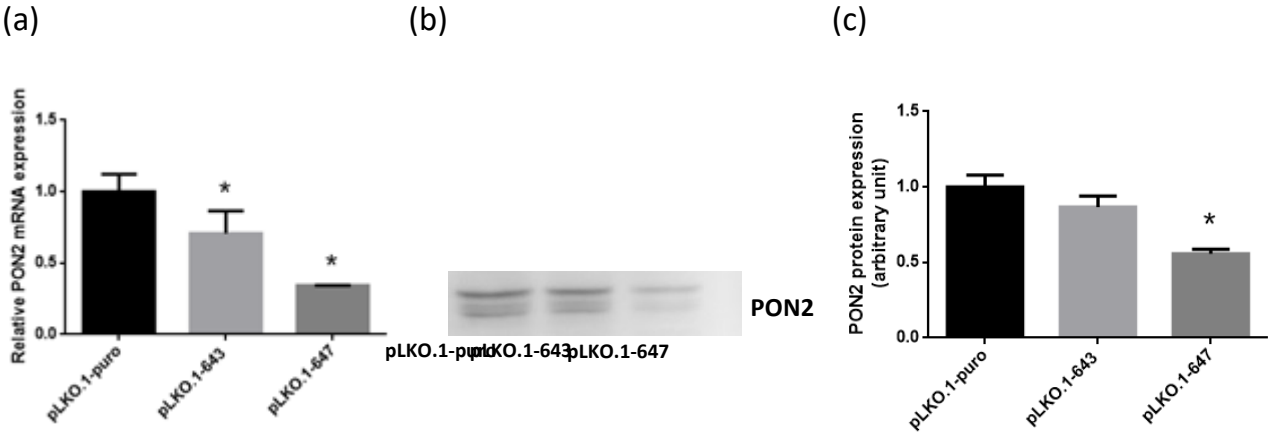

Figure 20. Evaluation of PON2 silencing in HSC-3 cell line Real-Time PCR (a) and western blot (b). Bands intensity was quantified using Image Lab software and values were expressed as mean ± standard deviation (c) (*$p<0.05$).

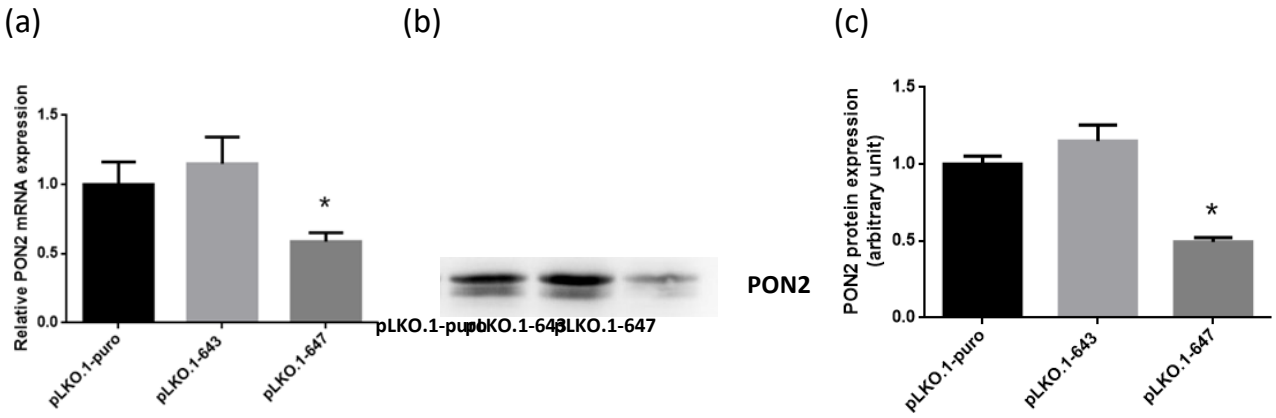

Figure 21. Evaluation of PON2 silencing in HOC621 cell line Real-Time PCR (a) and western blot (b). Bands intensity was quantified using Image Lab software and values were expressed as mean ± standard deviation (c) (*p<0.05).

Similarly to OSCC cells lines, after transfection and puromicyn selection, A375 cells were harvested and analysed through Real-Time PCR and Western blot, to evaluate PON2 silencing efficiency. Data obtained revealed a significant (p<0.05) decrease in PON2 mRNA level in cells treated with pLKO.1-647 (0.24 ± 0.01) with respect to controls (1.00 ± 0.05 for mock and 1.09 ± 0.04 for pLKO.1-puro) (Figure 22a).
Accordingly, a marked (p<0.05) decrease in protein expression was reported for cells transfected with pLKO.1-647 (2.99 ± 0.31) in comparison with those treated with pLKO.1-puro (9.47 ± 1.23) or with mock (9.56 ± 0.76) (Figures 22b and c).

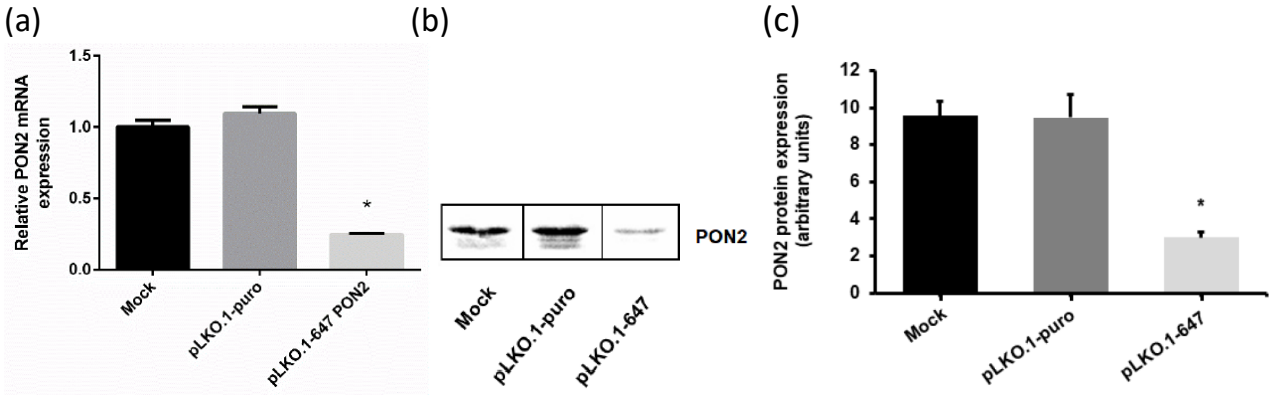

Figure 22. Evaluation of PON2 silencing in A375 cell line Real-Time PCR (a) and western blot (b). Bands intensity was quantified using Image Lab software and values were expressed as mean ± standard deviation (c) (*p<0.05).

3.2.3 Effects of PON2 silencing on cell viability and proliferation

To examine the biological effects of PON2 downregulation in OSCC lines, cell viability and proliferation were evaluated through MTT and trypan blue assay, respectively. In OSCC cell lines, PON2 knockdown significantly ($p<0.05$) affected both cell viability (Figures 23a and 24a) and proliferation (Figures 23b and 24b), starting from 48 h time point compared with control, thus hypothesizing PON2 involvement in oral cancer cell growth.

(a)

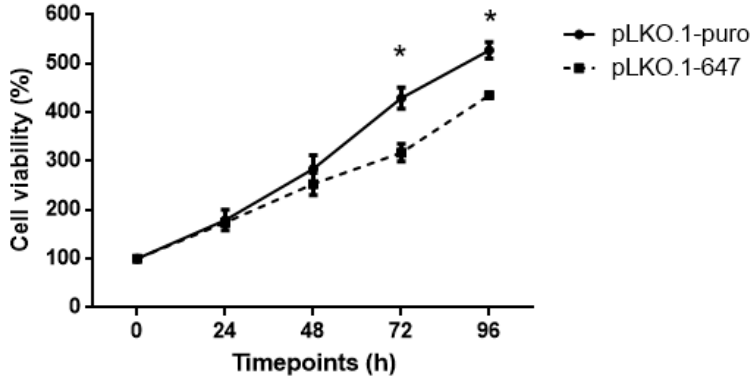

(b)

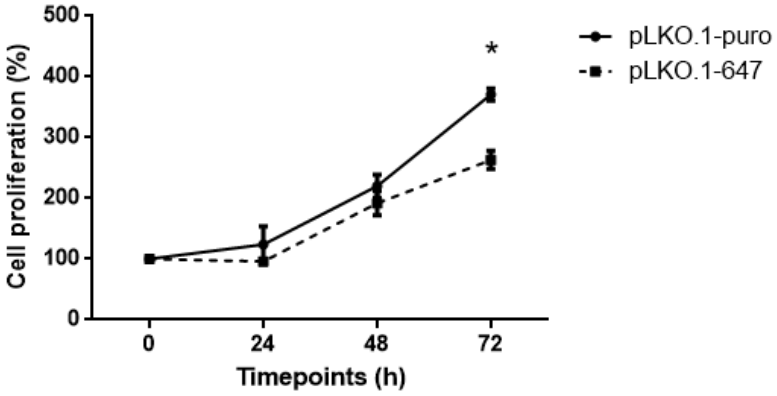

Figure 23. Effect of PON2 silencing on HSC-3 cell viability (a) and proliferation (b), analysed by MTT (a) and trypan blue exclusion (b) assays, respectively. All values were expressed as mean ± standard deviation (* $p<0.05$).

(a)

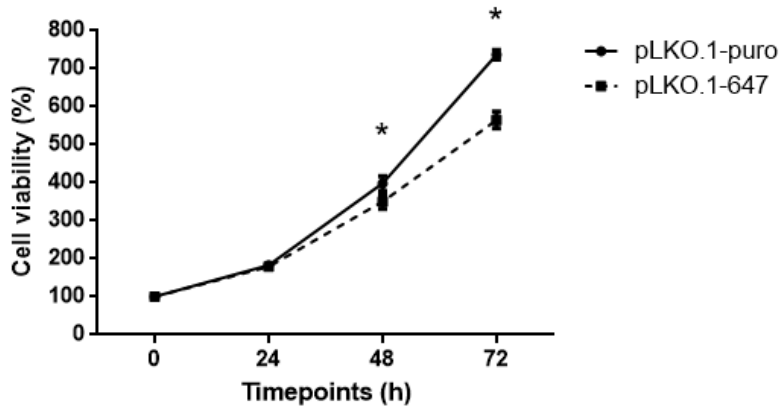

(b)

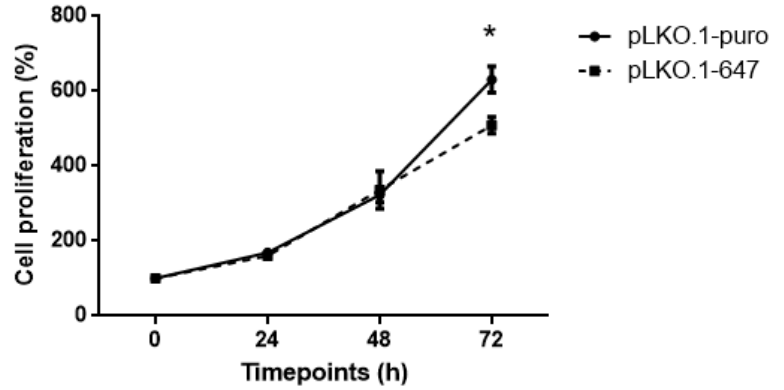

Figure 24. Effect of PON2 silencing on HOC621 cell viability (a) and proliferation (b), analysed by MTT (a) and trypan blue exclusion (b) assays, respectively. All values were expressed as mean ± standard deviation (* $p<0.05$).

Effects of PON2 downregulation on these aspects of tumor cell phenotype were also studied in skin cancer. MTT and trypan blue assays were carried out to evaluate alterations in vitality and proliferation of A375 melanoma cell line. PON2 downregulating A375 showed a significant ($p<0.05$) reduced viability and proliferation at 48 and 72 h respect to controls, being cells transfected with pLKO.1-puro or treated with transfection reagent only (Figure 25).

(a)

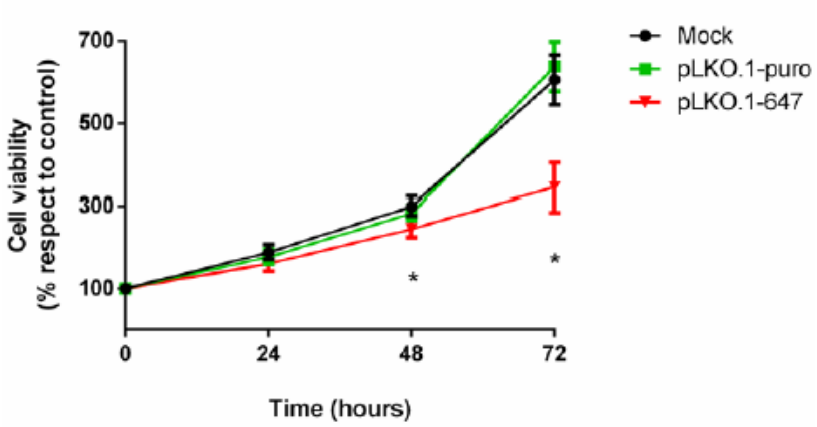

(b)

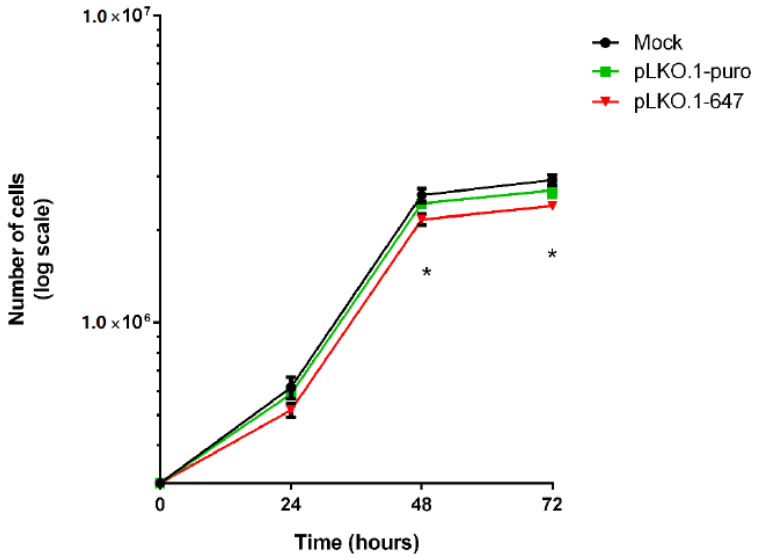

Figure 25. Effect of PON2 silencing on A375 cell viability (a) and proliferation (b), analysed by MTT (a) and trypan blue exclusion (b) assays, respectively. All values were expressed as mean ± standard deviation (* $p<0.05$).

3.2.4 Effect of PON2 silencing on cell sensitivity to chemotherapeutic treatment

A potential PON2 involvement in chemosensitivity was recently reported in different solid and blood tumors. In order to further explore this aspect, PON2 downregulating OSCC cells, as well as controls, were treated with CDDP and 5-FU, alone and in combination, and effects on cell viability were monitored through MTT assay. In particular, HSC-3 cells were treated with CDDP ranging from 0.3 µM and 1.5 µM, 5-FU from 0.75 µM to 3.75 µM, as well as with both drugs for 96 h. HOC621 cells were subjected to chemotherapeutic drugs administration as follows: CDDP (0.3-6 µM), 5-FU (0.75-3.75 µM) and combination of both drugs for 72 h.

CDDP treatment (0.75 µM) induced a significant ($p<0.05$) decrease in cell viability in pLKO.1-647 HSC-3 cells compared with pLKO.1-puro at 48, 72, and 96 h (Figure 26). Similarly, PON2 silencing in HOC621 cells led to a significant ($p<0.05$) decrease in cell viability at time point 48 h under treatment with 3 µM CDDP in comparison to controls cells (Figure 27). For both OSCC cell lines, 5-FU, as well as combined treatment were not responsible for significant changes in cell viability (data not shown). The difference in effects induced by chemotherapeutic drug regimens is likely attributable to the different mechanism of action of single agents.

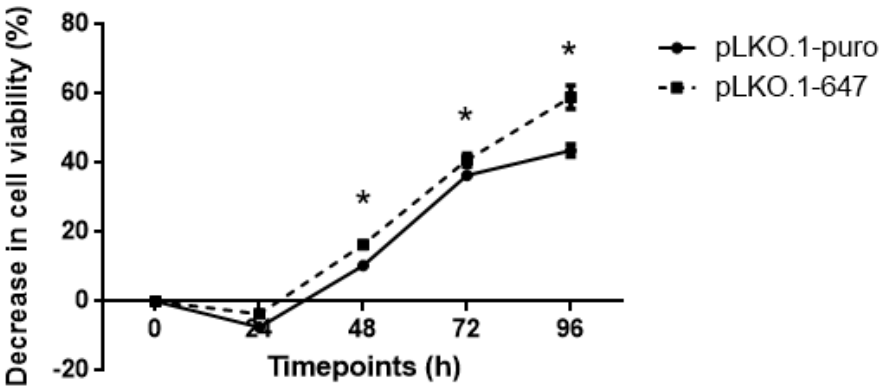

Figure 26. Effect of PON2 silencing on HSC-3 cell viability, analysed by MTT, subjected to treatment with 0.75 µM CDDP. Results were represented as percentage of decrease in cell viability and expressed as mean ± standard deviation (*$p<0.05$).

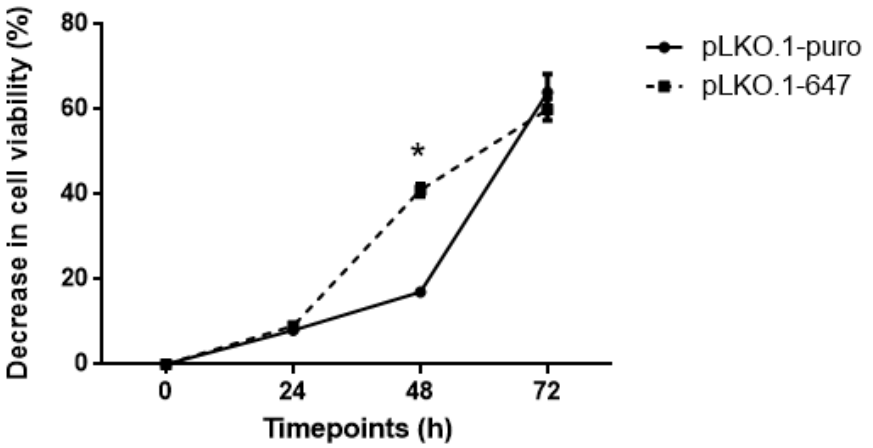

Figure 27. Effect of PON2 silencing on HOC621 cell viability, analysed by MTT, subjected to treatment with 3 µM CDDP. Results were represented as percentage of decrease in cell viability and expressed as mean ± standard deviation (*$p<0.05$).

Similarly, MTT assay was performed to evaluate the effect of chemotherapeutic treatment with CDDP and DTIC (used alone) on cell viability of A375 melanoma cell line. Following CDDP treatment (4 μM), a significant decrease ($p<0.05$) of cell viability was recorded at all different time points in PON2 downregulating cells in comparison with controls (Figure 28a). Treatment with 8 μM CDDP resulted in an excessive cell death that did not allow to observe differences between the two cell groups (Figure 28b). On the contrary, no significant difference in cell viability was noticed after treatment with DTIC (Figure 28c).

(a)

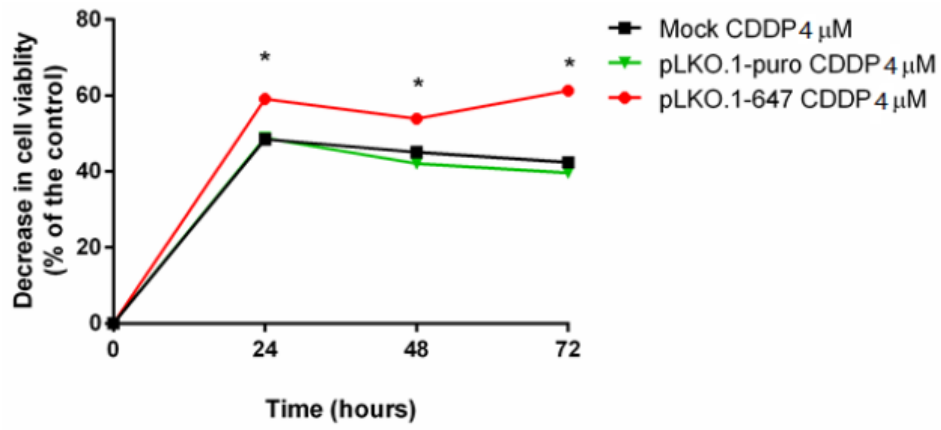

(b)

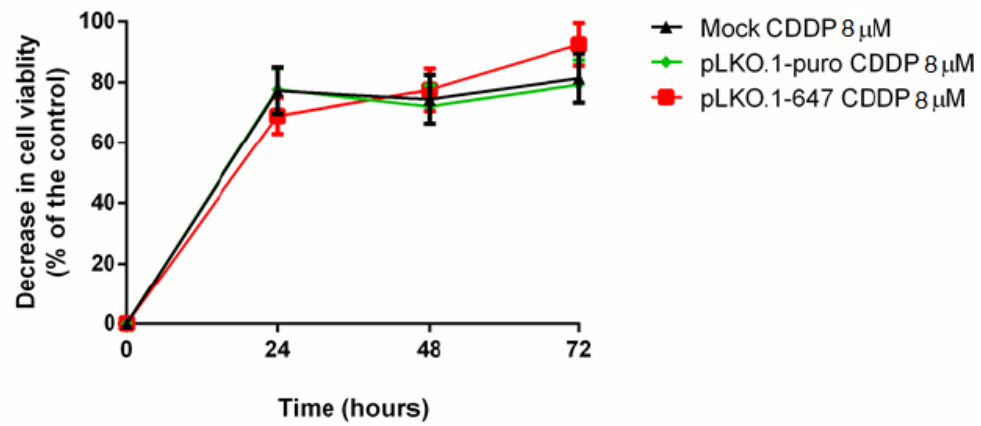

(c)

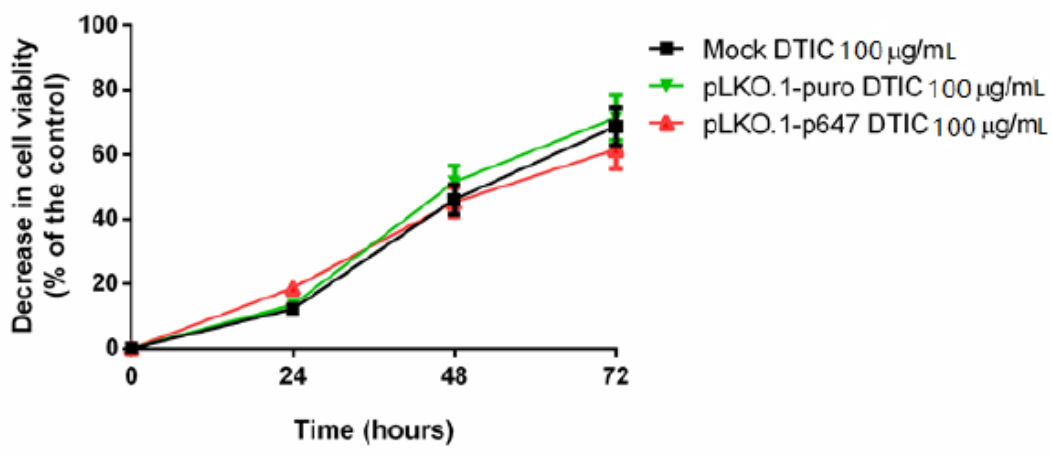

Figure 28. Effect of PON2 silencing on A375 cell viability, analysed by MTT, subjected to treatment with 4 µM CDDP (a), 8 µM CDDP (b), and 100 µg/ml DTIC (c). Results were represented as percentage of decrease in cell viability and expressed as mean ± standard deviation (*p<0.05).

3.2.5 Effects of PON2 silencing evaluated by FTIRM upon chemotherapeutic treatment in OSCC cell lines

The IR spectra of PON2 silenced and control HSC-3 (Figures 29a and b) and HOC621 cells (Figures 30a and b) were reported in the 3050-2800 cm^{-1} and 1800-900 cm^{-1} spectral ranges, representative respectively of cellular lipids and cellular proteins/nucleic acids. In order to evaluate the impact of CDDP treatment on the macromolecular composition of PON2 silenced and control HSC-3 and HOC621 cells, the following band area ratios were statistically analyzed: A_{3010}/A_{2960} (unsaturation rate in lipid alkyl chains); A_{2925}/A_{2960} (saturation rate in lipid alkyl chains and hence related to the relative amount of lipids); A_{1740}/A_{1655} (oxidation rate in lipid alkyl chains), and A_{1170}/A_{1655} (non-hydrogen bonded proteins). Compared with reference samples, both PON2-downregulating cell lines showed a general increase in the spectral parameters related to oxidative stress and apoptosis, following chemotherapeutic administration.

More in detail, in HSC-3 cell lines, (i) higher values of A_{3010}/A_{2960} and A_{2925}/A_{2960} were observed in PON2 silenced cells (pLKO.1-647) respect to not silenced ones (pLKO.1-puro) at all time points (Figures 29c and e); (ii) as regards the band area ratio A_{1740}/A_{1655}, a general increasing time-dependent trend was observed, as result of CDDP treatment, with values markedly higher in PON2 silenced cells compared with those of controls, at 24, 48, and 72 h time points (Figure 29d); (iii) the A_{1170}/A_{1655} ratio presented higher values in pLKO.1-647 compared with pLKO.1-puro at 48 h (Figure

29f).

In HOC621, (i) statistically higher values of the A_{3010}/A_{2960} ratio were observed in pLKO-1-647 compared with reference cells at 72 h, demonstrating an increased CDDP-related unsaturation rate in lipid alkyl chains in cells downregulating PON2 (Figure 30c); (ii) as regards the band area ratios A_{2925}/A_{2960} and A_{1740}/A_{1655}, they showed an increasing time-dependent trend, with higher values in PON2 silenced cells (pLKO.1-647) respect to not silenced ones (pLKO.1 puro) (Figures 30d and e); (iii) both cell groups showed similar values at 24 and 72 h for the ratio A_{1170}/A_{1655}, while a difference was observed at 48 h, with PON2 silenced cells displaying the highest value (Figure 30f).

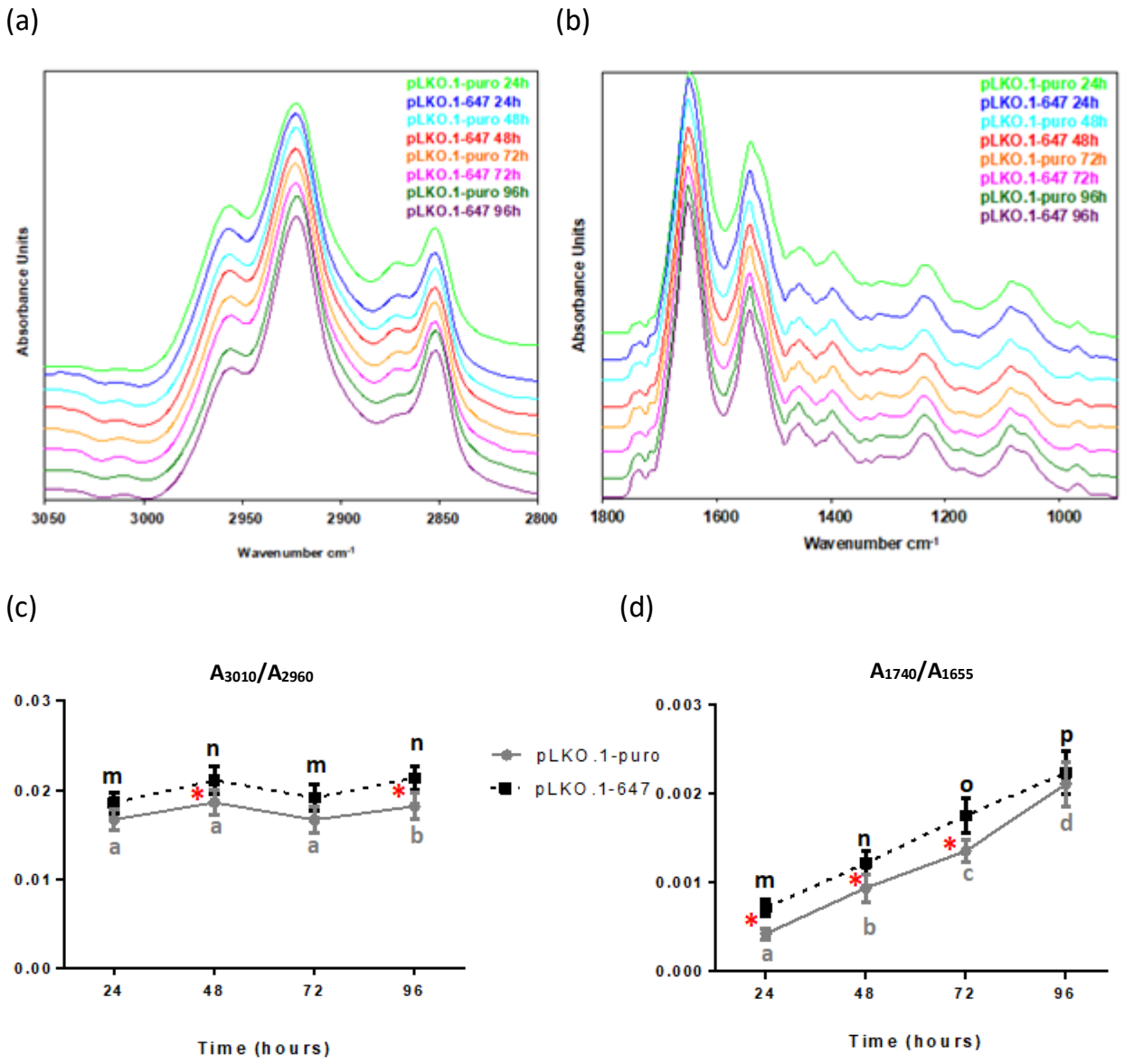

(e) (f)

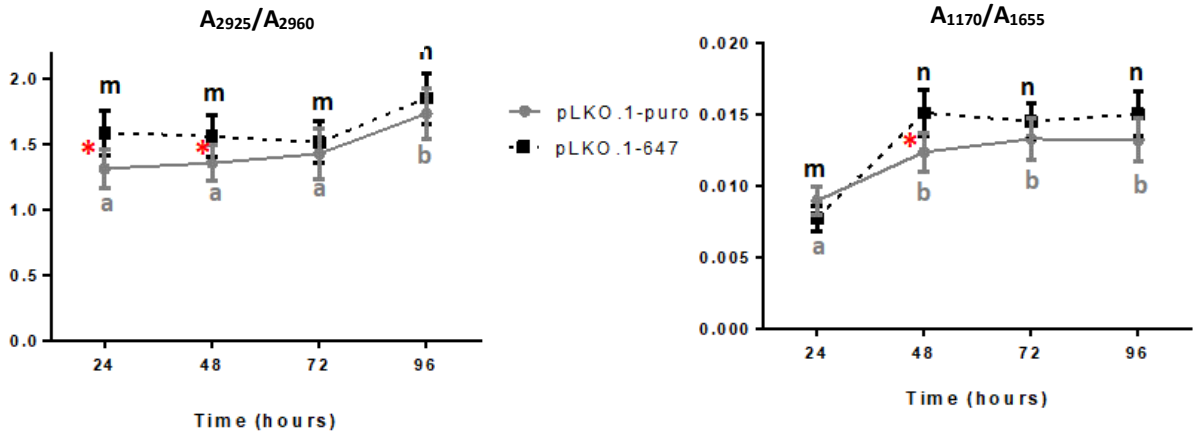

Figure 29. FTIRM analysis to evaluate the effect of 0.75 µM CDDP treatment on macromolecular composition of HSC-3 cells. Mean IR spectra were showed in absorbance mode in the 3050-2800 cm^{-1} (a) and 1800-900 cm^{-1} (b) spectral ranges. Calculated band area ratios, represented as mean ± standard deviation, with biological assignment: A_{3010}/A_{2960} representing unsaturation rate of lipids (c), A_{1740}/A_{1655} oxidation rate of lipids (d), A_{2925}/A_{2960} saturation rate of lipids (e), and A_{1170}/A_{1655} non-hydrogen bonded proteins (f). Different letters were used to indicate statistically significant differences among different time points whereas red asterisks for statistically significant differences between pLKO.1-puro and pLKO.1-647 cells at each time point (*p<0.05).

(a) (b)

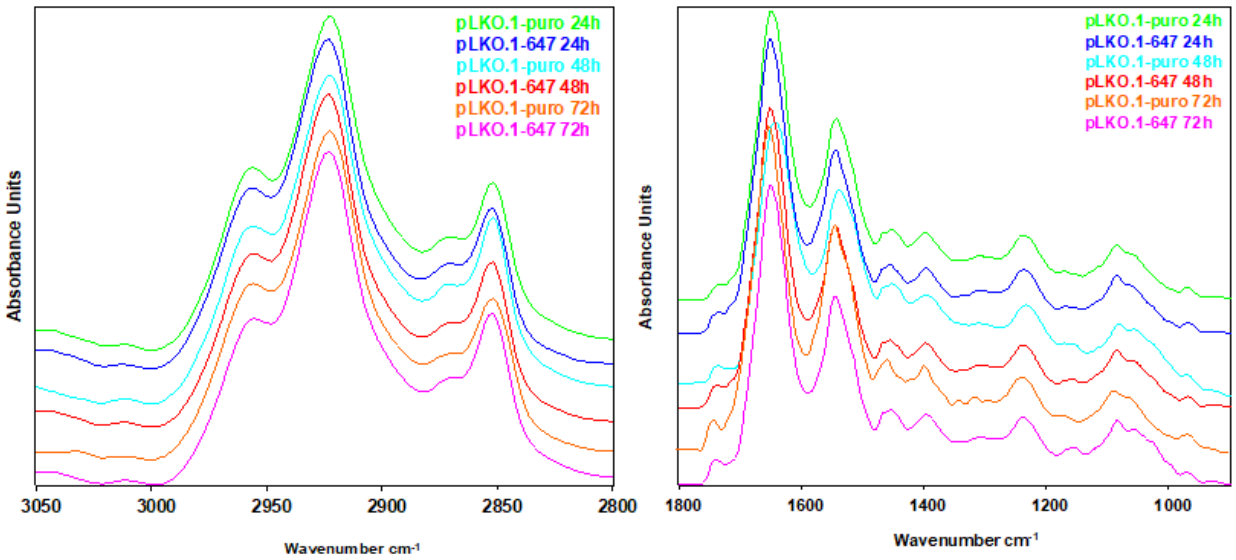

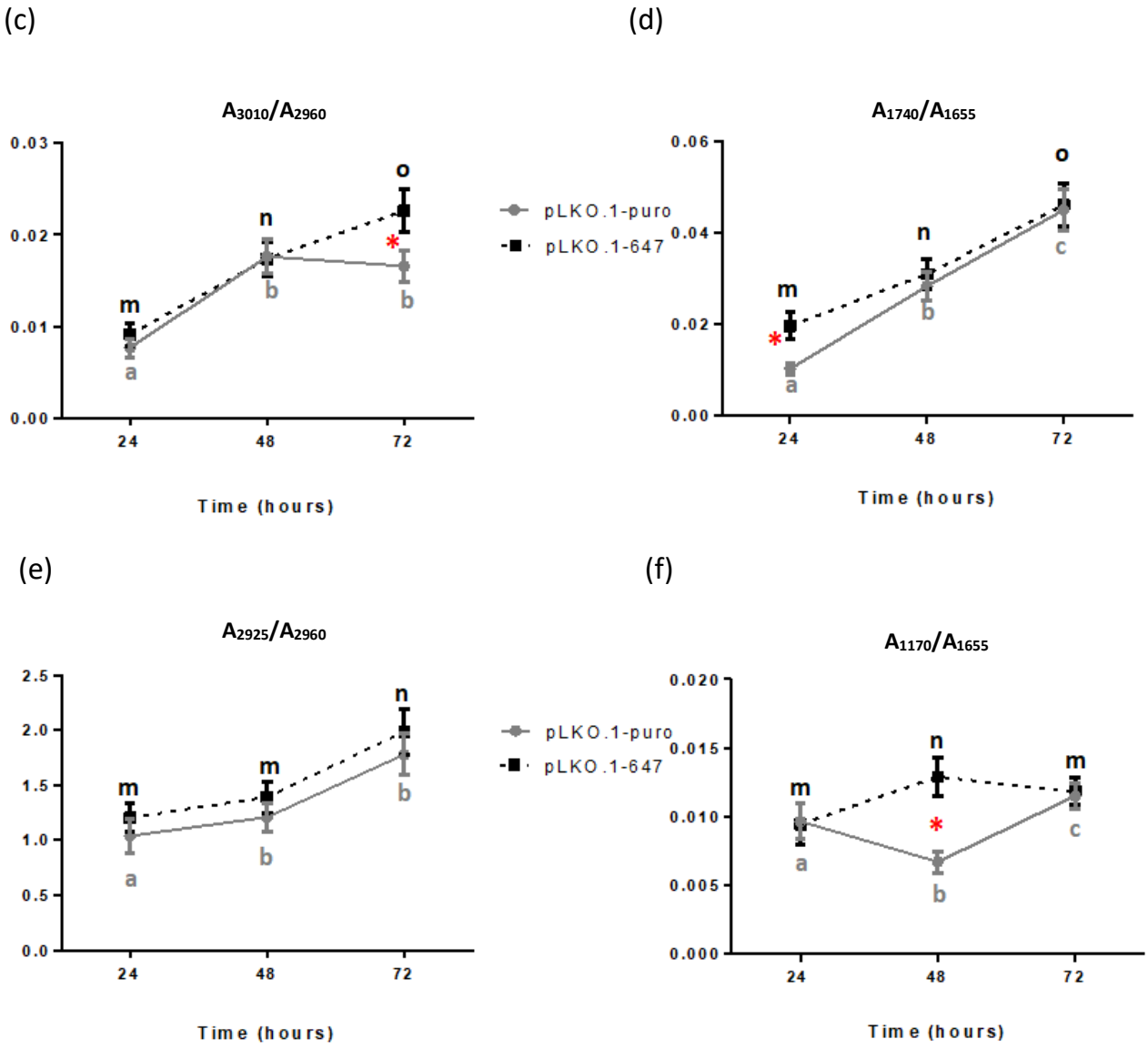

Figure 30. FTIRM analysis to evaluate the effect of 3 µM CDDP treatment on macromolecular composition of HOC621 cells. Mean IR spectra were showed in absorbance mode in the 3050-2800 cm^{-1} (a) and 1800-900 cm^{-1} (b) spectral ranges. Calculated band area ratios, represented as mean ± standard deviation, with biological assignment: A_{3010}/A_{2960} representing unsaturation rate of lipids (c), A_{1740}/A_{1655} oxidation rate of lipids (d), A_{2925}/A_{2960} saturation rate of lipids (e), and A_{1170}/A_{1655} non-hydrogen bonded proteins (f). Different letters were used to indicate statistically significant differences among different time points whereas red asterisks for statistically significant differences between pLKO.1-puro and pLKO.1-647 cells at each time point (*$p<0.05$).

3.2.6 Effect of PON2 silencing on ROS production upon chemotherapeutic treatment in melanoma cell line

In light of these results, 4 µM CDDP treatment was selected to evaluate influence of PON2 knockdown on A375 intracellular ROS formation at different time points (0, 24, 48, and 72 h), by using $DCFH_2$-DA probe. Interestingly, in absence of CDDP, ROS production levels in PON2 downregulating cells were similar to those of control cells (mock and pLKO.1-puro) (data not shown). On the contrary, incubation with the chemotherapeutic agent led to a significant ($p<0.05$) increase of intracellular ROS concentration in pLKO.1-647 cells with respect to reference cells, at both 48 and 72 h, indicating an impairment in oxidative stress regulation (Figure 31).

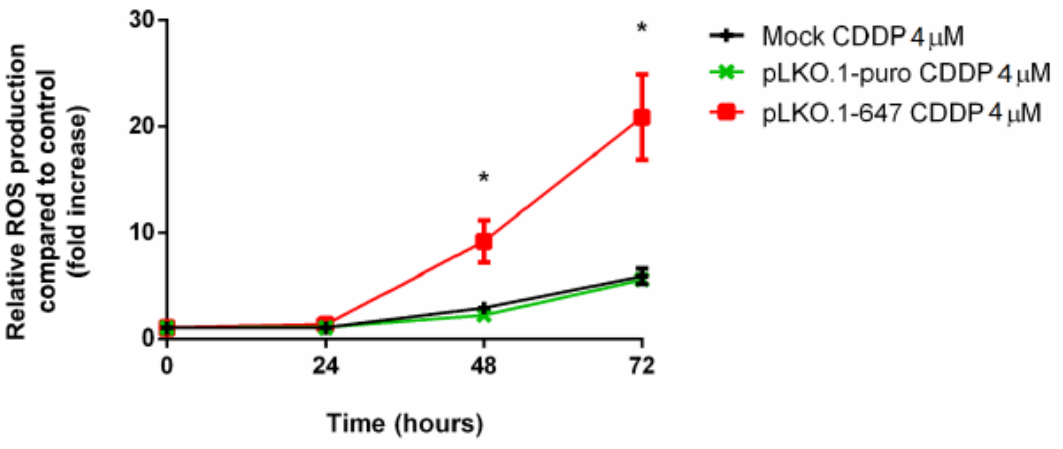

Figure 31. Effect of PON2 silencing on A375 intracellular ROS levels analysed by $DCFH_2$-DA assay, uder treatment with 4 µM CDDP. Results were expressed as mean ± standard deviation (*$p<0.05$).

Discussion and conclusions

Oral squamous cell carcinoma is the most common malignant neoplasm arising from squamous cells of oral cavity. Its incidence is around 378,000 cases worldwide annually and it is expected to reach more than 510,000 cases by 2035 (1). It has both a sex and geographical prevalence. Indeed, it is more common in males than in females, with an incidence around 70% in low/medium human development index countries (2). This geographical distribution is in part ascribable to lifestyle habits such as tobacco smoking, alcohol abuse, and betel nut chewing, constituting the main OSCC risk factors. Thus, mass media campaigns and successful health policies could have a significant impact on OSCC incidence (4). The survival rate is strictly related to the time of diagnosis; the earlier the disease is identified, the lower the morbidity. However, because of the delayed detection, OSCC overall 5-years survival rate is about 50%. This issue exacerbates in Asia where 60-80% of cases are diagnosed at advanced stages comparing to 40% in developed countries. Hence, regardless of accessibility of the oral cavity during clinical examination, oral cancer is usually detected only at advanced stages. The most common reasons include initial painless signs, recurring misdiagnosis, and lack of markers for early identification. For this reason, clinicians should always make accurate clinical examinations of the oral mucosa that can be accompanied by a biopsy followed by histopathological examination and/or novel short-time and non-invasive imaging techniques (13). Early diagnosis is also crucial for an efficient treatment that limits extensive surgical resections, recovery period and relapse. To date, surgical treatment remains the gold standard although for advanced or recurrent cases it is supported by chemo- or radiotherapy. Finally, targeted therapy and immunotherapy may be other valuable options, used alone or in combination with systemic treatments. Hence, despite a general decrease in mortality rate for the majority of cancer types, OSCC is still a lethal malignancy worldwide (4, 14).

Skin cancers assemble different neoplasms that are primarily divided into cutaneous melanoma and non-melanoma skin cancers. Melanoma originates from malignant transformation of melanocytes in the basal layer of the epidermis. NMSCs include basal cell carcinoma and squamous cell carcinoma, as the major subtypes, and they are all caused by keratinocytes malignant transformation (21). Skin cancers represent a pre-eminent public health problem since they classify as the most common malignancies occurring in humans (1). At the base of skin cancer oncogenesis, a

plethora of risk factors have been identified that can be categorized into either hereditary or environmental. Melanoma shows a considerable variation in incidence worldwide, mainly based on latitude and race. Although its incidence is low (5% of all skin cancers), it is responsible for more than 75% of deaths associated with these malignancies, being the most aggressive form of skin neoplasms. Moreover, clinicians are worried by the latest dramatic increment in incidence rate and by the simultaneous reduction of the median age at diagnosis. On the contrary, the majority of NMSC diagnosed cases are curable. Indeed, they are slow growing tumors with low metastatic potential. Incidence is higher in men than in women and they display a geographical distribution, as cutaneous melanoma (22, 23). Early detection of skin cancers remains the key factor in order to improve prognosis. Cutaneous location allows its detection by using non-invasive approaches. Nevertheless, a definitive diagnosis requires skin biopsy and histological examination. Routine skin physical examinations have a prominent role in detection of new cases (40). In the early stages, melanoma can be successfully treated but after metastasis spreading survival rates significantly drop. Hence, early diagnosis is a powerful instrument to obstruct this malignancy. When melanoma is still localized, tumor and surrounding healthy tissues are removed surgically. For late-stage cases, surgical excision is usually accompanied by other treatment options that are mainly chemotherapy, targeted therapy, and immunotherapy (43). Because of its low metastatic potential, surgery is the gold standard for NMSC treatment. However, for malignancies that are not amenable to surgery, or that have already spread to other parts of the body, chemotherapy and immunotherapy may be good alternatives (24, 45).

Paraoxonase 2 belongs to paraoxonase family, along with paraoxonase 1 and paraoxonase 3 (49). Although the three members share high identity at both nucleotide and amino acid level, they have distinctive substrate specificities and locations. Indeed, PON1 and PON3 are mainly synthetized in the liver and secreted into the blood flow where they associate to high-density lipoproteins. On the contrary, PON2 is an intracellular protein expressed in different tissues. Inside cells, it localizes in the plasma membrane, in the inner mitochondrial membrane, and in the perinuclear region where it associates with the endoplasmic reticulum and the nuclear envelope. In case of plasma membrane localization, PON2 is a type II transmembrane protein with its N-terminal region identified as a single transmembrane domain and C-terminus, corresponding to the catalytic domain, placed extracellularly (55). In spite of its nomenclature, PON2 lacks paraoxonase activity but it displays a moderate arylesterase and the strongest lactonase activities, among all PON family members (62). PON2 acts as an antioxidant enzyme, which reduces oxidative stress by inhibiting intracellular reactive oxygen/nitrogen species

formation and ER stress-induced apoptosis.

Modulation of intracellular ROS levels is crucial to maintain cellular homeostasis (51). Different ROS levels induce different biological responses. At low-moderate concentrations, they act as signalling molecules promoting cell proliferation, differentiation, and migration and activating several stress-responsive survival pathways. On the contrary, high intracellular ROS levels can modify structure and function of critical cellular macromolecules including nucleic acids, proteins and lipids, leading to severe damages up to cell death (110). Cancer cells are characterized by increased aerobic glycolysis, known as Warburg effect, and oxidative stress as a consequence of alterations in signalling pathways regulating cellular metabolism. Hence, cancer cells have a basal higher ROS level when compared to normal proliferating cells. Nevertheless, role of ROS in cancer initiation, promotion, and progression remains controversial. On one hand, ROS can contribute to tumor formation by inducing DNA mutations and activating pro-oncogenic signalling pathways, but excessive levels are detrimental to cells. Therefore, cancer cells have adapted to the imbalance redox status, by developing antioxidant defence mechanisms. They have a peculiar high antioxidant capacity that regulates ROS levels, so that they are compatible with cellular biological functions but still higher than in normal cells, especially at early stages of tumor development (111).

PON2, thanks to its antioxidant and antiapoptotic activity, may likely favour initiation and progression of tumorigenesis. In the last two decades, several lines of evidence demonstrated PON2 upregulation in both solid tumors and blood cancers, such as bladder cancer, prostate carcinoma, hepatocellular carcinoma, gastric cancer, pancreatic ductal adenocarcinoma, glioblastoma, and acute lymphoblastic leukemia (79, 92, 95, 96, 100-102).

According to what reported in this study, immunohistochemistry and western blot analysis performed on OSCC and normal adjacent tissue specimens confirmed PON2 overexpression (tumor versus normal tissue). Moreover, statistical analysis revealed an inverse correlation between PON2 expression and tumor dimension. These results suggest that OSCC cell may take advantage of antiapoptotic and antioxidant functions exerted by PON2, especially in the early stages of tumorigenesis, known to have high ROS levels. This data conforms to another study that indicated a PON2 mRNA upregulation in the early stages of RCC compared with late phase disease (78). Similarly, in 2018 Devarajan highlighted a significant increase in PON2 expression in samples affected by stage I and stage II ovarian cancer, when compared to the corresponding adjacent normal tissues, but no changes were detected in stage III and stage IV samples (97). In this work, PON2 overexpression was also identified in skin cancers by using immunohistochemistry. Once clinicopathological findings were

considered in melanoma specimens, PON2 staining score was positively correlated with important prognostic factors such as Breslow thickness, Clark level, presence and number of mitoses, regression, pT, pathological stage, and lymph node metasteses. BCC cases showed higher PON2 levels than controls, but when distinguished in different subtypes, enzyme upregulation was underlined only in infiltrative BCCs and not in nodular cases. Collectively these data point out a correlation between paraoxonase 2 expression and tumor aggressiveness, candidating the enzyme as a promising prognostic factor for skin cancers, as Wang et al. suggested for gastric cancer (100).

Subsequently, the effect of PON2 downregulation on cancer cell phenotype was *in vitro* evaluated, focusing on cell proliferation, viability, and sensitivity to chemotherapeutic treatment, both in OSCC and melanoma cell lines. In both cases, cell viability and proliferation were significantly impaired by PON2 knockdown, while cells became more sensitive to chemotherapy. These results are in line with previous data that suggested a PON2 involvement in promoting proliferation in different solid tumors (95, 97, 100).

Chemotherapy represents one of the main weapon in fighting cancer. Although it can improve the overall survival and prognosis of patients, chemoresistance, severe therapy-related toxicities, and adverse effects remain the leading clinical obstacles that limit its use and that need to be overcome (112). It was estimated that around 90% of failures in chemotherapy is associated with development of multidrug resistance. As already discussed, carcinogenesis is characterized by multistep processes that involve alterations of several cellular pathways during initiation, promotion and progression. Thus, it is improbable that a single-targeting chemotherapeutic agent would be able to inhibit cancer growth effectively. For this reason, combined treatments have been developed in the last decades. In more detail, a promising approach considers the use of an approved chemotherapeutic agent in combination with a dysregulation of a molecule involved in carcinogenesis promotion, in order to increase the efficacy and selectivity of the drug, as well as reduce its toxicity. The main advantage of this strategy lies in targeting various signalling pathways in an additive or even synergistic manner making cancer cells more sensitive to antineoplastic agents (113).

Several recent studies revealed an emerging association between PON2 sensitivity to radio-chemotherapy. In 2006, for the first time, PON2 was identified among a set of 128 genes useful for outcome prediction of chronic myeloid leukemia patients exhibiting primary imatinib-resistance. Microarray analysis highlighted an upregulation of the enzyme in the non-responder group in comparison to tyrosine kinase inhibitor sensitive patients. This signature encompasses genes involved in DNA

repair, apoptosis inhibition, and oxidative stress protection, in line with the concept that resistance to therapy is a multifactorial and multistep pathway (114). Similarly, PON2 overexpression in leukemia cell line prevented imatinib-induced death and enzyme deficiency reversed this effect, enhancing cell susceptibility to chemotherapeutics. This likely explained PON2 contribution to imatinib resistance, previously observed in primary resistant chronic myeloid leukemia patients (79). A recent study shed light on PON2 role in dexamethasone resistance in acute lymphoblastic leukemia. PON2 overexpression was confirmed in ALL patients comparing to healthy subjects and in dexamethasone (DEX)-resistant ALL subgroup compared to the sensitive counterpart. Similarly, DEX-resistant ALL cell lines showed higher PON2 levels than sensitive ones, suggesting that PON2 dysregulation was associated with DEX resistance. PON2 knockdown reduced cell viability and clonogenic capacity and increased apoptotic rates and expression of apoptosis-related proteins upon DEX treatment, contributing to restore glucocorticoid sensitivity in resistant ALL cell lines. Moreover, data obtained from *in vivo* studies suggested that PON2 downregulation inhibited tumor progression and made cells more sensitive to treatment. Altogether, these observations indicated that PON2 inhibition, in combination with DEX treatment, delayed progression of leukemia both *in vitro* and *in vivo,* suggesting that the enzyme might represent a promising therapeutic target for DEX-resistant ALL cells (115). PON2 involvement was also noticed regarding doxorubicin treatment. PON2 upregulation in endothelial cells was responsible for a reduction in dose-dependent activation of caspase-3 and intracellular ATP concentration upon doxorubicin administration (79). Fumarola et al. investigated effect of PON2 dysregulation in bladder cancer cells subjected to single and combined chemotherapeutic treatment with cisplatin and gemcitabine. Lower levels of PON2 expression induced a reduction in cell viability and a simultaneous increase in ROS production and caspases activation upon antineoplastic treatment. Conversely, cells overexpressing the enzyme showed opposite effects. Hence, whole data demonstrated that the enzyme had a great impact in determining susceptibility to chemotherapy (95). Krüger and colleagues were the only ones to report about PON2 protection against radiation-induced cell death in OSCC. In several OSCC cell lines, basal PON2 expression was positively correlated with radiation sensitivity. Moreover, irradiation led to a variable induction of PON2 expression. Cells exhibiting the lowest endogenous PON2 levels showed the strongest response, whereas this effect was markedly reduced in samples displaying constitutive high enzyme expression. Moreover, PON2 knockdown resulted in a significant increase in radiation-triggered cell death rate with respect to controls, revealing enzyme contribution to radiation resistance in OSCC (73).

Results reported in this study confirmed association between PON2 expression level and chemosensitivity, both in OSCC and melanoma. Indeed, in OSCC cell lines, PON2 knockdown induced a greater decrease in cell viability in comparison to control cells following cisplatin treatment. FTIRM analysis showed that molecular alterations affecting lipids and proteins, attributable to oxidative stress and apoptotic processes, were greater in PON2 silenced cells than their respective controls. Interestingly, incubation with 5-fluorouracil or with both drugs did not significantly modify cell viability and sensitivity to chemotherapy. This phenomenon can be explained based on the different mechanism of action of both drugs. In fact, antineoplastic activity exerted by cisplatin is largely ascribable to intracellular ROS generation that triggers cellular damage and apoptosis. Hence, oxidative stress increase induced by PON2 depletion amplifies cisplatin action. Similarly, in melanoma cells a decrease in cell viability was reported in PON2 silenced cells after treatment with cisplatin, but not with dacarbazine. As confirmation, intracellular ROS levels were monitored in control and downregulating cells, indicating a greater oxidative stress in the second group following cisplatin incubation.

Taken together these data suggest a PON2 involvement in cancer chemosensitivity. Combination of PON2 dysregulation and radio- chemotherapy could therefore represent an effective strategy to achieve better outcomes than current therapeutic options. Moreover, inhibiting PON2 could make cells more sensitive to oxidative stress and to apoptosis, enhancing therapy efficacy. However, further detailed studies will be required to better understand mechanisms at the base of PON2 involvement in carcinogenesis and in radio- and chemosensitivity of cancer cells.

List of abbreviations

2D	Two-dimensional
3D	Three-dimensional
3OC12HSL	3-oxo-dodecanoyl homoserine lactone
5-FU	5-fluorouracil
A	Area
AD	Alzheimer's disease
AF	Tissue autoflorence
AJCC	American Joint Committee on Cancer
ALL	Acute lymphoblastic leukemia
AMPK	AMP-activated protein kinase
ANOVA	Analysis of variance
AP-1	Activator protein-1
ARE	Arylesterase
ASK1	Apoptosis signal-regulating kinase 1
ATCC	American Type Culture Collection
ATF6	Activating transcription factor 6
ATP	Adenosine triphosphate
BCC	Basal cell carcinoma
BCL-2	B-cell lymphoma-2
BER	Base excision repair
BHT	Butylated hydroxytoluene
BIRC3	E3-ubiquitin ligase baculoviral IAP repeat-containing
BRAF	B-Raf proto-oncogene, serine/threonine kinase
BSA	Bovine serum albumin
CAF_2	Calcium fluoride
CAFS	Cancer-associated fibroblasts
CASP3	Caspase-3
CDDP	Cisplatin
CDKN2A	Cyclin-dependent kinase inhibitor 2a
CDNA	Complementary DNA
CGH	comparative genomic hybridization
CHOP	C/EBP Homologous Protein
C-KIT	Receptor tyrosine kinase
CML	Chronic myeloid leukemia
COQ10	Coenzyme Q10
CT	Computed tomography
CT	Threshold cycle
CTLA-4	Cytotoxic T-lymphocyte-associated protein 4
CTR1	Copper transporter 1
CVD	Cardiovascular disease
CXCL1	Chemokine (CXC motif) ligand 1

CXCL8	Chemokine (CXC motif) ligand 8
$DCFH_2$-DA	2',7'-dichlorodihydrofluorescein diacetate
DEX	Dexamethasone
DJ-1	Parkinsonism associated deglycase
DMEM/F-12	Dulbecco's Modified Eagle's Medium/Nutrient Ham's Mixture F-12
DMSO	Dimethyl sulfoxide
DNA	Deoxyribonucleic acid
DOI	Depth of invasion
DTIC	Dacarbazine
DUTP	Deoxyuridine triphosphate
EGFR	Epidermal growth factor receptor
EMT	Epithelial mesenchymal transition
ENE	Extranodal extension
ER	Endoplasmic reticulum
ERK1/2	Extracellular signal-regulated kinase 1/2
ETC	Electron transport chain
FFPE	Formalin-fixed and paraffin-embedded
FISH	Fluorescence in situ hybridization
FTIRM	Fourier transform infrared microspectroscopy
GC	Gastric cancer
GLUT1	Glucose transporter 1
GSH	Glutathione
GSK-3B	Glycogen-synthase kinase-3β
H_2O_2	Hydrogen peroxide
HCL	Hydrochloric acid
HDI	Human Development Index
HDL	High-density lipoproteins
HEPES	4-(2-hydroxyethyl)-1-piperazineethanesulfonic acid
HF-US	High-frequency ultrasonography
HPV	Human papillomavirus
HRP	Horseradish peroxidase
IARC	International Agency for Research on Cancer
IGG	Immunoglobulin G
IHC	Immunohistochemistry
IL-1	Interleukin-1
IL-6	Interleukin-6
IL-8	Interleukin-8
IR	Infrared
IRE1A	Inositol-requiring transmembrane kinase/endoribonuclease 1α
IRS-1	Insulin receptor substrate-1
JNK	C-Jun N-terminal kinase
KRAS	Kirsten rat sarcoma virus
LAT	Lactonase
LDH	Lactate dehydrogenase
LDL	Low density lipoprotein
LEF	Lymphocyte-enhancer-binding factor
LEF-1	Lymphocyte-enhancer-binding factor 1
LPS	Lipopolysaccharide

MCP-1	Monocyte chemoattractant protein-1
MIRNA	MicroRNA
M-MLV	Moloney Murine Leukemia Virus
MMP2	Matrix metalloproteinase 2
MMP9	Matrix metalloproteinase 9
MMP13	Matrix metalloproteinase 13
MMR	Mismatch repair
MOMP	Mitochondrial outer membrane permeabilization
MRNA	Messenger ribonucleic acid
MS	Mass spectrometry
MT	Metallothionein
MTT	3-(4,5-dimethylthiazol-2-yl)-2,5-diphenyl tetrazolium bromide
N	Normal
N.A.	Not applicable
NACL	Sodium Chloride
NADPH	Nicotinamide adenine dinucleotide phosphate
NBI	Narrow-band imaging
NMSC	Non-melanoma skin cancer
NOTCH1	Notch homolog 1, translocation-associated (Drosophila)
NRAS	Neuroblastoma RAS viral oncogene homolog
NSCLC	Non-small cell lung cancer
OCT	Optical coherence tomography
OS	Oxidative stress
OSCC	Oral squamous cell carcinoma
OXLDL	Oxidized low density lipoprotein
PCR	Polymerase chain reaction
PD	Parkinson’s disease
PD1	Programmed cell death 1
PDCA	Pancreatic ductal adenocarcinoma
PDGF	Platelet-derived growth factor
PDGFR-B	Platelet-derived growth factor receptor-β
PD-L1/2	Programed cell death protein 1 ligand
PERK	Protein kinase R-like endoplasmic reticulum kinase
PI3K	Phosphatidylinositol 3-kinase
PKD	Polycystic kidney disease
PN	Pathological lymph nodes
PNI	Perineural invasion
PON	Paraoxonase
PON1	Paraoxonase 1
PON2	Paraoxonase 2
PON3	Paraoxonase 3
PT	Primary tumor
PTM	Post-translational modification
PUFA	Polyunsaturated fatty acids
PVDF	Polyvinylidene fluoride
QS	Quorum sensing
RB	Retinoblastoma
RCM	Reflectance confocal microscopy

RMN	Nuclear magnetic resonance
RNA	Ribonucleic acid
RNAI	RNA interference
RNS	Reactive nitrogen species
RONS	Reactive oxygen/nitrogen species
ROS	Reactive oxygen species
SALS	Sporadic amyotrophic lateral sclerosis
SCC	Squamous cell carcinoma
SDS-PAGE	Sodium dodecyl sulfate-polyacrylamide gel electrophoresis
SEER	Surveillance, Epidemiology, and End Results
SHRNA	Short hairpin RNA
SMC	Smooth muscle cells
SREBP-2	Sterol regulatory binding protein-2
STAT3	Signal transducer and activator of transcription 3
T	Tumor
TAB1	TGF-beta activated kinase 1 (MAP3K7) binding protein 1
TB	Toluidine blue
TBP	Total-body photography
TBS	Tris-buffered saline
TCF	T-cell factor
TCF4	T-cell factor 4
TF	Tissue factor
TGF-B	Transforming growth factor-β
TME	Tumor microenvironment
TNF-A	Tumor necrosis factor-α
TNM	Tumor-node-metastasis
TP53	Tumor protein P53
TRAF2	TNF receptor-associated factor 2
TS	Thymidylate synthase
UICC	Union for International Cancer Control
UPA	Urokinase plasminogen activator
UPAR	Urokinase plasminogen activator receptor
UPR	Unfolded protein response
UTR	Untranslated region
UV	Ultraviolet
UVA	Ultraviolet A
UVB	Ultraviolet B
UVR	Ultraviolet radiation
VEGF	Vascular endothelial growth factor
VLDL	Very low-density lipoprotein
WHO	World Health Organization
WNT	Wingless-related integration site
WNT3A	Wingless-related integration site 3a
WNT5A	Wingless-related integration site 5a
WTAP	Wilms Tumor 1 Associated Protein
XBP1	X-box binding protein 1

References

(1) Sung H, Ferlay J, Siegel RL, Laversanne M, Soerjomataram I, Jemal A, Bray F. *Global cancer statistics 2020: GLOBOCAN estimates of incidence and mortality worldwide for 36 cancers in 185 countries.* CA Cancer J Clin 2021;71(3):209-249.

(2) Ng JH, Iyer NG, Tan MH, Edgren G. *Changing epidemiology of oral squamous cell carcinoma of the tongue: a global study.* Head Neck 2017;39:297–304.

(3) Farhood Z, Simpson M, Ward GM, Walker RJ, Osazuwa-Peters N. *Does anatomic subsite influence oral cavity cancer mortality? A SEER database analysis.* Laryngoscope 2019;129:1400–6.

(4) Rivera C. *Essentials of oral cancer.* Int J Clin Exp Pathol 2015;8(9):11884-11894.

(5) Rupel K, Ottaviani G, Gobbo M, Poropat A, Zoi V, Zacchigna S, Di Lenarda R, Biasotto M. *Campaign to increase awareness of oral cancer risk factors among preadolescents.* J Cancer Educ 2020;35(3):616-620.

(6) Petti S. *Lifestyle risk factors for oral cancer.* Oral Oncol 2009;45(4–5):340–350.

(7) Li Q, Hu Y, Zhou X, Liu S, Han Q, Cheng L. *Role of oral bacteria in the development of oral squamous cell carcinoma.* Cancers (Basel) 2020;12(10):2797.

(8) Alves A, Diel L, Ramos G, Pinto A, Bernardi L, Yates 3rd J, Lamers M. *Tumor microenvironment and oral squamous cell carcinoma: a crosstalk between the inflammatory state and tumor cell migration*. Oral Oncol 2021;112:105038.

(9) El-Naggar AK, Chan J, Grandis J, Takata T, Slootweg P. *WHO classification of head and neck tumours. 4th ed.;* 2017. p. 105–111.

(10) Almangusha A, Makitiee AA, Triantafylloug A, de Breeh R, Strojani P, Rinaldoj A, Hernandez-Prerak JC, Suarezl C, Kowalskin LP, Ferlitop A, Leivo I. *Staging and grading of oral squamous cell carcinoma: an update.* Oral Oncology 107 2020;104799.

(11) Amin MB, Edge S, Greene F, Byrd DR, Brookland RK, Washington MK, Gershenwald JE, Compton CC, Hess KR et al. *AJCC cancer staging manual. 8th edition*. New York: Springer; 2017.

(12) Brieleyt JD, Gospodarowicz MK, Wittekind C. *TNM classification of malignant tumors, 8th edition.* Willey Blackwell 2017, 272p.

(13) Bagan J, Sarrion G, Jimenez Y. *Oral cancer: clinical features.* Oral Oncol 2010;46(6):414-7.

(14) Romano A, Di Stasio D, Petruzzi M, Fiori F, Lajolo C, Santarelli A, Lucchese A, Serpico R, Contaldo M. *Noninvasive imaging methods to improve the diagnosis of oral carcinoma and its precursors: state of the art and proposal of a three-step diagnostic process.* Cancers (Basel) 2021;13(12):2864.

(15) Cristaldi M, Mauceri R, Di Fede O, Giuliana G, Campisi G, Panzarella V. *Salivary biomarkers for oral squamous cell carcinoma diagnosis and follow-up: current status and perspectives.* Front Physiol 2019;10:1476.

(16) Ferrari E, Pezzi ME, Cassi D, Pertinhez TA, Spisni A, Meleti M. *Salivary cytokines as biomarkers for oral squamous cell carcinoma: a systematic review.* Int J Mol Sci 2021;22(13):6795.

(17) Boztepe T, Castro GR, León IE. *Lipid, polymeric, inorganic-based drug delivery applications for platinum-based anticancer drugs.* Int J Pharm 2021;605:120788.

(18) Kanno Y, Chen CY, Lee HL, Chiou JF, Chen YJ. *Molecular mechanisms of chemotherapy resistance in head and neck cancers.* Front Oncol 2021;11:640392.

(19) Longley DB, Harkin DP, Johnston PG. *5-fluorouracil: mechanisms of action and clinical strategies.* Nat Rev Cancer 2003;3(5):330-8.

(20)Yeeng Chai AWY, Lim KP, Cheong SC. *Translational genomics and recent advances in oral squamous cell carcinoma.* Semin Cancer Biol 2020;61:71-83.
(21)Linares MA, Zakaria A, Nizran P. *Skin cancer.* Prim Care 2015;42(4):645-59.
(22)Gordon R. *Skin cancer: an overview of epidemiology and risk factors.* Semin Oncol Nurs 2013;29(3):160-9.
(23)Davey MG, Miller N, McInerney NM. *A review of epidemiology and cancer biology of malignant melanoma.* Cureus 2021;13(5):e15087.
(24)Kallini JR, Hamed N, Khachemoune A. *Squamous cell carcinoma of the skin: epidemiology, classification, management, and novel trends.* Int J DermatoL 2015;54(2):130-40.
(25)Fitzpatrick TB. *The validity and practicality of sun-reactive skin types I through VI.* Arch Dermatol 1988;124:869–871.
(26)Frank C, Sundquist J, Hemminki A, Hemminki K. *Risk of other cancers in families with melanoma: novel familial links.* Sci Rep 2017;7:42601.
(27)Holly EA, Kelly JW, Shpall SN, Chiu SH. *Number of melanocytic nevi as a major risk factor for malignant melanoma.* J Am Acad Dermatology 1987;17:459–468.
(28)Marçon CR, Maia M. *Albinism: epidemiology, genetics, cutaneous characterization, psychosocial factors.* An Bras Dermatol 2019;94(5):503-520.
(29)Becerril S, Corchado-Cobos R, García-Sancha N, Revelles L, Revilla D, Ugalde T, Román-Curto C, Pérez-Losada J, Cañueto J. *Viruses and skin cancer.* Int J Mol Sci 2021;22(10): 5399.
(30)Scatena C, Murtas D, Tomei S. *Cutaneous melanoma classification: the importance of high-throughput genomic technologies.* Front Oncol 2021;11:635488.
(31)Romano V, Belviso I, Venuta A, Ruocco MR, Masone S, Aliotta F, Fiume G, Montagnani S, Avagliano A, Arcucci A. *Influence of tumor microenvironment and fibroblast population plasticity on melanoma growth, therapy resistance and immunoescape.* Int J Mol Sci 2021;22(10): 5283.
(32)Cameron MC, Lee E, Hibler BP, Barker CA, Mori S, Cordova M, Nehal KS, Rossi AM. *Basal cell carcinoma: epidemiology; pathophysiology; clinical and histological subtypes; and disease associations.* J Am Acad Dermatol 2019;80(2):303-317.
(33)Dika E, Scarfì F, Ferracin M, Broseghini E, Marcelli E, Bortolani B, Campione E, Riefolo M, Ricci C, Lambertini M. *Basal cell carcinoma: a comprehensive review.* Int J Mol Sci 2020;21(15):5572.
(34)Cassarino DS, Derienzo DP, Barr RJ. *Cutaneous squamous cell carcinoma: a comprehensive clinicopathologic classification. Part one.* J Cutan Pathol 2006;33(3):191-206.
(35)Cassarino DS, Derienzo DP, Barr RJ. *Cutaneous squamous cell carcinoma: a comprehensive clinicopathologic classification. Part two.* J Cutan Pathol 2006;33(4):261-79.
(36)Ratushny V, Gober MD, Hick R, Ridky TW, Seykora JT. *From keratinocyte to cancer: the pathogenesis and modeling of cutaneous squamous cell carcinoma.* J Clin Invest 2012;122(2):464-72.
(37)Que SKT, Zwald FO, Schmults CD. *Cutaneous squamous cell carcinoma: incidence, risk factors, diagnosis, and staging.* J Am Acad Dermatol 2018;78(2):237-247.
(38)Gershenwald JE, Scolyer RA, Hess KR, Sondak VK, Long GV, Ross MI, Lazar AJ, Faries MB, Kirkwood JM, McArthur GA, Haydu LE, Eggermont AMM, Flaherty KT, Balch CM, Thompson JF. *Melanoma staging: evidence-based changes in the american joint committee on cancer eighth edition cancer staging manual.* CA Cancer J Clin 2017;67(6): 472–492.
(39)Keohane SG, Proby CM, Newlands C, Motley RJ, Nasr I, Mohd Mustapa MF, Slater DN. *The new 8th edition of TNM staging and its implications for skin cancer: a review by the British Association of Dermatologists and the Royal College of Pathologists, U.K.* Br J Dermatol 2018;179(4):824-828.
(40)Rastrelli M, Tropea S, Rossi CR, Alaibac M. *Melanoma: epidemiology, risk factors, pathogenesis, diagnosis and classification.* In Vivo 2014;28(6):1005-11.
(41)Kato J, Horimoto K, Sato S, Minowa T, Uhara H. *Dermoscopy of melanoma and non-melanoma skin cancers.* Front Med (Lausanne). 2019;6:180.

(42)Hornung A, Steeb T, Wessely A, Brinker TJ, Breakell T, Erdmann M, Berking C, Heppt MV. *The value of total body photography for the early detection of melanoma: a systematic review.* Int J Environ Res Public Health 2021;18(4):1726.
(43)Davis LE, Shalin SC, Tackett AJ. *Current state of melanoma diagnosis and treatment.* Cancer Biol Ther 2019;20(11):1366-1379.
(44)Al-Badr AA, Alodhaib MM. *Dacarbazine.* Profiles Drug Subst Excip Relat Methodol 2016;41:323-77.
(45)Kim DP, Kus KJB, Ruiz E. Basal cell carcinoma review. Hematol Oncol Clin North Am 2019;33(1):13-24.
(46)Mazur A. *An enzyme in animal tissues capable of hydrolysing the phosphorus-fluorine bond of alkyl fluorophosphates.* J Biol Chem 1946;164:271-89.
(47) Aldridge WN. *Serum esterases. I. Two types of esterase (A and B) hydrolysing p-nitrophenyl acetate, propionate and butyrate, and a method for their determination.* Biochem J 1953;53:110–117.
(48)Aldridge WN. *Serum esterases II. An enzyme hydrolysing diethyl p-nitrophenyl acetate (E600) and its identity with the A-esterase of mammalian sera.* Biochem J 1953;53:117–124.
(49)Primo-Parmo SL, Sorenson RC, Teiber J, La Du BN. *The human serum paraoxonase/arylesterase gene (PON1) is one member of a multigene family.* Genomics 1996;33:498–507.
(50)Mackness B, Durrington PN, Mackness MI. *The paraoxonase gene family and coronary heart disease.* Curr Opin Lipidol 2002;13:357–362.
(51)She ZG, Chen HZ, Yan Y, Li H, Liu DP. *The human paraoxonase gene cluster as a target in the treatment of atherosclerosis.* Antioxid Redox Signal 2012;16(6): 597–632.
(52)Draganov DI, La Du BN. *Pharmacogenetics of paraoxonases: a brief review.* Naunyn-Schmiedeberg's Arch Pharmacol 2004;369, 78–88.
(53)Mochizuki H, Scherer SW, Xi T, Nickle DC, Majer M, Huizenga JJ, Tsui LC, Prochazka M. *Human PON2 gene at 7q21.3: cloning, multiple mRNA forms, and missense polymorphisms in the coding sequence.* Gene 1998;213, 149–157.
(54)Harel M, Aharoni A, Gaidukov L, Brumshtein B, Khersonsky O, Meged R, Dvir H, Ravelli RBG, McCarthy A, Toker L, SilMan I, Sussman JL, Tawfik DS. *Structure and evolution of the serum paraoxonase family of detoxifying and anti-atherosclerotic enzymes.* Nat Struct Mol Biol 2004;11, 412–419.
(55)Li XC, Wang C, Mulchandani A, Ge X. *Engineering soluble human paraoxonase 2 for quorum quenching.* ACS Chem Biol 2016;11(11):3122-3131
(56)Carusone TM, Cardiero G, Cerreta M, Mandrich L, Moran O, Porzio E, Catara G, Lacerra G, Manco G. *WTAP and BIRC3 are involved in the posttranscriptional mechanisms that impact on the expression and activity of the human lactonase PON2.* Cell Death Dis 2020;11, 324–327.
(57)Mandrich L, Cerreta M, Manco G. *An engineered version of human PON2 opens the way to understand the role of its post-translational modifications in modulating catalytic activity.* PLoS ONE 2015;10:e0144579.
(58)Akimov V, Barrio-Hernandez I, Hansen SVF, Hallenborg P, Pedersen AK, Bekker-Jensen DB, Puglia M, Christensen SDK, Vanselow JT, Nielsen MM, Kratchmarova I, Kelstrup CD, Olsen JV, Blagoev B. *UbiSite approach for comprehensive mapping of lysine and N-terminal ubiquitination sites.* Nat Struct Mol Biol 2018;25, 631–640.
(59)Bilan V, Selevsek N, Kistemaker HAV, Abplanalp J, Feurer R, Filippov DV, Hottigeret MO. *New quantitative mass spectrometry approaches reveal different ADP-ribosylation phases dependent on the levels of oxidative stress.* Mol Cell Proteom 2017;16, 949–958.
(60)Rajkovic MG, Rumora L, Barisic K. *The paraoxonase 1, 2 and 3 in humans.* Biochemia Medica 2011;21 (2) 122–130.
(61)Manco G, Porzio E, Carusone TM. *Human paraoxonase-2 (PON2): protein functions and modulation.* Antioxidants (Basel) 2021;10(2):256.

(62) DraganoV DI, Teiber JF, Speelman A, Osawa Y, Sunahara R, La Du BN. *Human paraoxonases (PON1, PON2, and PON3) are lactonases with overlapping and distinct substrate specificities.* J Lipid Res 2005;46, 1239–1247.

(63) Yehuda I, Madar Z, Szuchman-Sapir A, Tamir S. *Glabridin, a phytoestrogen fromlicorice root, up-regulates manganese superoxide dismutase, catalase and paraoxonase 2 under glucose stress.* Phytother Res Ptr 2011;25, 659–667.

(64) Morresi C, Cianfruglia L, Sartini D, Cecati M, Fumarola S, Emanuelli M, Armeni T, Ferretti G, Bacchetti T. *Effect of high glucose-induced oxidative stress on paraoxonase 2 expression and activity in Caco-2 cells.* Cells 2019;8:1616.

(65) Yehuda I, Madar Z, Leikin-Frenkel A, Szuchman-Sapir A, Magzal F, Markman G, Tamir S. *Glabridin, an isoflavan from licorice root, upregulates paraoxonase 2 expression under hyperglycemia and protects it from oxidation.* Mol Nutr Food Res 2016;60, 287–299.

(66) Precourt LP, Seidman E, Delvin E, Amre D, Deslandres C, Dominguez M, Sinnett D, Levy E. *Comparative expression analysis reveals differences in the regulation of intestinal paraoxonase family members.* Int J Biochem Cell Biol 2009;41:1628–1637.

(67) Alkhouri RH. *Paraoxonase gene expression in pediatric inflammatory Bowel disease.* J Clin Cell Immunol 2014;5:224.

(68) Rosenblat M, Draganov D, Watson CE, Bisgaier CL, La Du BN, Aviram M. *Mouse macrophage Paraoxonase 2 activity is increased whereas cellular Paraoxonase 3 activity is decreased under oxidative stress.* Arterioscler Thromb Vasc Biol 2003;23:468–474.

(69) Horke S, Witte I, Wilgenbus P, Krüger M, Strand D, Förstermann U. *Paraoxonase-2 reduces oxidative stress in vascular cells and decreases endoplasmic reticulum stress–induced caspase activation.* Circulation 2007;115:2055–2064.

(70) Shiner M, Fuhrman B, Aviram M. *Paraoxonase 2 (PON2) expression is upregulated via a reduced-nicotinamide-adenine-dinucleotide-phosphate (NADPH)-oxidase-dependent mechanism during monocytes differentiation into macrophages.* Free Radic Biol Med 2004;37(12):2052-63.

(71) Shiner M, Fuhrman B, Aviram M. *A biphasic U-shape effect of cellular oxidative stress on the macrophage anti-oxidant paraoxonase 2 (PON2) enzymatic activity.* Biochem Biophys Res Commun 2006;349: 1094–1099.

(72) Fuhrman B, Gantman A, Khateeb J, Volkova N, Horke S, Kiyan J, Dumler I, Aviram M. *Urokinase activates macrophage PON2 gene transcription via the PI3K/ROS/MEK/SREBP-2 signalling cascade mediated by the PDGFR-β.* Cardiovasc Res 2009;84:145–154.

(73) Krüger M, Amort J, Wilgenbus P, Helmstädter JP, Grechowa I, Ebert J, Tenzer S, Moergel M, Witte I, Horke S. *The anti-apoptotic PON2 protein is Wnt/β-catenin-regulated and correlates with radiotherapy resistance in OSCC patients.* Oncotarget 2016;7:51082–51095.

(74) Stoltz DA, Ozer EA, Ng CJ, Yu JM, Reddy ST, Lusis AJ, Bourquard N, Parsek MR, Zabner J, Shih DM. *Paraoxonase-2 deficiency enhances Pseudomonas aeruginosa quorum sensing in murine tracheal epithelia.* Am J Physiol Cell Mol Physiol 2007;292:L852–L860.

(75) Horke S, Witte I, Altenhöfer S, Wilgenbus P, Goldeck M, Förstermann U, Xiao J, Kramer GL, Haines DC, Chowdhary PK, Haley RW, Teiber JF. *Paraoxonase 2 is down-regulated by the Pseudomonas aeruginosa quorumsensing signal N-(3-oxododecanoyl)-L-homoserine lactone and attenuates oxidative stress induced by pyocyanin.* Biochem J 2010;426:73–83.

(76) Schwarzer C, Fu Z, Morita T, Whitt AG, Neely AM, Chi L, Machen TE. *Paraoxonase 2 serves a proapopotic function in mouse and human cells in response to the pseudomonas aeruginosa quorum-sensing molecule N-(3-oxododecanoyl)-homoserine lactone.* J Biol Chem 2015;290:7247–7258.

(77) Zhao G, Neely AM, Schwarzer C, Lu H, Whitt AG, Stivers NS, Burlison JA, White C, Machen TE, Li C. *N-(3-oxo-acyl) homoserine lactone inhibits tumor growth independent of Bcl-2 proteins.* Oncotarget 2016;7:5924–5942.

(78) Witte I, Foerstermann U, Devarajan A, Reddy ST, Horke S. *Protectors or traitors: the roles of PON2 and PON3 in atherosclerosis and cancer.* J Lipids 2012;2012:1–12.
(79) Witte I, Altenhöfer S, Wilgenbus P, Amort J, Clement AM, Pautz A, Li H, Förstermann U, Horke S. *Beyond reduction of atherosclerosis: PON2 provides apoptosis resistance and stabilizes tumor cells.* Cell Death Dis 2011;2:e112.
(80) Ng CJ, Wadleigh DJ, Gangopadhyay A, Hama S, Grijalva VR, Navab M, Fogelman AM, Reddy ST. *Paraoxonase-2 is a ubiquitously expressed protein with antioxidant properties and is capable of preventing cell-mediated oxidative modification of low density lipoprotein.* J Biol Chem 2001;276:44444–44449.
(81) Ng CJ, Bourquard N, Grijalva V, Hama S, Shih DM, Navab M, Fogelman AM, Lusis AJ, Young S, Reddy ST. *Paraoxonase-2 deficiency aggravates atherosclerosis in mice despite lower apolipoprotein-B-containing lipoproteins.* J Biol Chem 2006;281:29491–29500.
(82) Ng CJ, Hama SY, Bourquard N, Navab M, Reddy ST. *Adenovirus mediated expression of human paraoxonase 2 protects against the development of atherosclerosis in apolipoprotein E-deficient mice.* Mol Genet Metab 2006;89:368–373.
(83) Ebert J, Wilgenbus P, Teiber JF, Jurk K, Schwierczek K, Döhrmann M, Xia N, Li H, Spiecker L, Ruf W, Horke S. *Paraoxonase-2 regulates coagulation activation through endothelial tissue factor.* Blood 2018;131:2161–2172.
(84) Xu JH, Lu SJ, Wu P, Kong LC, Ning C, Li HY. *Molecular mechanism whereby paraoxonase-2 regulates coagulation activation through endothelial tissue factor in rat haemorrhagic shock model.* Int Wound J 2020;17:735–741.
(85) Liu D, Yang J, Feng B, Lu W, Zhao C, Li L. *Mendelian randomization analysis identified genes pleiotropically associated with the risk and prognosis of COVID-19.* J Infect 2021;82:126–132.
(86) Bourquard N, Ng CJ, Reddy ST. *Impaired hepatic insulin signalling in PON2-deficient mice: a novel role for the PON2/apoE axis on the macrophage inflammatory response.* Biochem J 2011;436:91–100.
(87) Gagliardi S, Abel K, Bianchi M, Milani P, Bernuzzi S, Corato M, Ceroni M, Cashman JR, Cereda C. *Regulation of FMO and PON detoxication systems in ALS human tissues.* Neurotox Res 2012;23:370–377.
(88) Parsanejad M, Bourquard N, Qu D, Zhang Y, Huang E, Rousseaux MWC, Aleyasin H, Irrcher I, Callaghan S, Vaillant DC, Kim RH, Slack RS, Mak TW, Reddy ST, Figeys D, Park DS. *DJ-1 interacts with and regulates Paraoxonase-2, an enzyme critical for neuronal survival in response to oxidative stress.* PLoS ONE 2014;9:e106601.
(89) Leduc V, Legault V, Dea D, Poirier J. *Normalization of gene expression using SYBR green qPCR: a case for paraoxonase 1 and 2 in Alzheimer's disease brains.* J Neurosci Methods 2011;200:14–19.
(90) Reichert CO, Levy D, Bydlowski SP. *Paraoxonase role in human neurodegenerative diseases.* Antioxidants (Basel) 2020;10(1):11.
(91) Zhao X, Yao H, Li X. *Unearthing of key genes driving the pathogenesis of Alzheimer's disease via bioinformatics.* Front Genet 2021;12:641100.
(92) Shakhparonov MI, Antipova NV, Shender VO, Shnaider PV, Arapidi GP, Pestov NB, Pavlyukov MS. *Expression and intracellular localization of Paraoxonase 2 in different types of malignancies.* Acta Naturae 2018;10(3):92-99.
(93) Zhao G, Neely AM, Schwarzer C, Lu H, Whitt AG, Stivers NS, Burlison JA, White C, Machen TE, Li C. *N-(3-oxo-acyl) homoserine lactone inhibits tumor growth independent of Bcl-2 proteins.* Oncotarget 2016;7(5):5924-42.
(94) Bacchetti T, Sartini D, Pozzi V, Cacciamani T, Ferretti G, Emanuelli M. *Exploring the role of Para-oxonase-2 in bladder cancer: analyses performed on tissue samples, urines and cell cultures.* Oncotarget 2017;8:28785–28795.

(95) Fumarola S, Cecati M, Sartini D, Ferretti G, Milanese G, Galosi AB, Pozzi V, Campagna R, Morresi C, Emanuelli M, Bacchetti T. *Bladder cancer chemosensitivity is affected by Paraoxonase-2 expression.* Antioxidants (Basel) 2020;9(2):175.

(96) Ribarska T, Ingenwerth M, Goering W, Engers R, Schulz WA. *Epigenetic inactivation of the placentally imprinted tumor suppressor gene TFPI2 in prostate carcinoma.* Cancer Genomics Proteomics 2010;7(2):51-60.

(97) Devarajan A, Su F, Grijalva V, Yalamanchi M, Yalamanchi A, Gao F, Trost H, Nwokedi J, Farias-Eisner G, Farias-Eisner R, Fogelman AM, Reddy ST. *Paraoxonase 2 overexpression inhibits tumor development in a mouse model of ovarian cancer.* Cell Death Dis 2018;9(3):392.

(98) Bobin-Dubigeon C, Chauvin A, Brillaud-Meflah V, Boiffard F, Joalland MP, Bard JM. *Liver X receptor (LXR)-regulated genes of cholesterol trafficking and breast cancer severity.* Anticancer Res 2017;37(10):5495-5498.

(99) Précourt LP, Marcil V, Ntimbane T, Taha R, Lavoie JC, Delvin E, Seidman EG, Beaulieu JF, Levy E. *Anti-oxidative properties of paraoxonase 2 in intestinal epithelial cells.* Am J Physiol Liver Physiol 2012;303:G623–G634.

(100) Wang X, Xu G, Zhang J, Wang S, Ji M, Mo L, Zhu M, Li J, Zhou G, Lu J, Chen C. *The clinical and prognostic significance of paraoxonase-2 in gastric cancer patients: immunohistochemical analysis.* Hum Cell 2019;32(4):487-494.

(101) Nagarajan A, Dogra SK, Sun L, Gandotra N, Ho T, Cai G, Cline G, Kumar P, Cowles RA, Wajapeyee N. *Paraoxonase 2 facilitates pancreatic cancer growth and metastasis by stimulating GLUT1-mediated glucose transport.* Mol Cell 2017;67(4):685-701.e6.

(102) Tseng JH, Chen CY, Chen PC, Hsiao SH, Fan CC, Liang YC, Chen CP. *Valproic acid inhibits glioblastoma multiforme cell growth via paraoxonase 2 expression.* Oncotarget 2017;8(9):14666-14679.

(103) Xie F, Li L, Luo Y, Chen R, Mei J. *Long non-coding RNA LINC00488 facilitates thyroid cancer cell progression through miR-376a-3p/PON2.* Biosci Rep 2021;41(3):BSR20201603.

(104) Krüger M, Pabst AM, Al-Nawas B, Horke S, Moergel M. *Paraoxonase-2 (PON2) protects oral squamous cell cancer cells against irradiation-induced apoptosis.* J Cancer Res Clin Oncol 2015;141(10):1757-66.

(105) Bradford MM. *A rapid and sensitive method for the quantitation of microgram quantities of protein utilizing the principle of protein-dye binding.* Anal Biochem 1976;72:248–254.

(106) Laemmli UK. *Cleavage of structural proteins during the assembly of the head of bacteriophage T4.* Nature 1970;227(5259):680-685.

(107) Livak KJ, Schmittgen TD. *Analysis of relative gene expression data using Real-Time Quantitative PCR and the 2−ΔΔCT method.* Methods 2001;25:402-408.

(108) Mosmann T. *Rapid colorimetric assay for cellular growth and survival: application to proliferation and cytotoxicity assays.* Journal of Immunological Methods 1983;65(1-2):55-63.

(109) Strober W. *Trypan blue exclusion test of cell viability.* Curr Protoc Immunol 2015;111:A3.B.1-A3.B.3.

(110) Klaunig JE. *Oxidative stress and cancer.* Curr Pharm Des 2018;24(40):4771-4778.

(111) Gorrini C, Harris IS, Mak TW. *Modulation of oxidative stress as an anticancer strategy.* Nat Rev Drug Discov 2013;12(12):931-47.

(112) Liu C, Jin Y, Fan Z. *The mechanism of Warburg effect-induced chemoresistance in cancer.* Front Oncol 2021;11:698023.

(113) Gul S, Maqbool MF, Maryam A, Khan M, Shakir HA, Irfan M, Ara C, Li Y, Ma T. *Vitamin K: a novel cancer chemosensitizer.* Biotechnol Appl Biochem 2022.

(114) Frank O, Brors B, Fabarius A, Li L, Haak M, Merk S, Schwindel U, Zheng C, Müller MC, Gretz N, Hehlmann R, Hochhaus A, Seifarth W. *Gene expression signature of primary imatinib-resistant chronic myeloid leukemia patients.* Leukemia 2006;20(8):1400-7.

(115) Hui PY, Chen YH, Qin J, Jiang XH. *PON2 blockade overcomes dexamethasone resistance in acute lymphoblastic leukemia.* Hematology 2022;27(1):32-42.